

Fall 2012

Exploitation and exploration of PCR in microfluidic systems with gradient temperature environments

Ilija Pjescic

Follow this and additional works at: <https://digitalcommons.latech.edu/dissertations>

 Part of the [Nanoscience and Nanotechnology Commons](#)

**EXPLOITATION AND EXPLORATION OF PCR IN
MICROFLUIDIC SYSTEMS WITH GRADIENT
TEMPERATURE ENVIRONMENTS**

by

Ilija Pjescic, Dipl. Ing. Mas.

A Dissertation Presented in Partial Fulfillment
of the Requirements of the Degree
Doctor of Philosophy in Engineering

COLLEGE OF ENGINEERING AND SCIENCE
LOUISIANA TECH UNIVERSITY

November 2012

UMI Number: 3534295

All rights reserved

INFORMATION TO ALL USERS

The quality of this reproduction is dependent upon the quality of the copy submitted.

In the unlikely event that the author did not send a complete manuscript and there are missing pages, these will be noted. Also, if material had to be removed, a note will indicate the deletion.

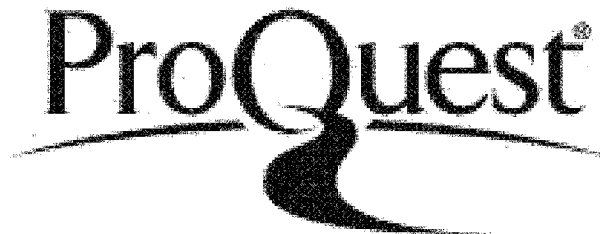


UMI 3534295

Published by ProQuest LLC 2012. Copyright in the Dissertation held by the Author.

Microform Edition © ProQuest LLC.

All rights reserved. This work is protected against unauthorized copying under Title 17, United States Code.



ProQuest LLC
789 East Eisenhower Parkway
P.O. Box 1346
Ann Arbor, MI 48106-1346

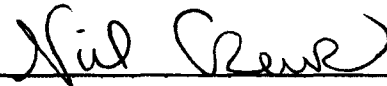
LOUISIANA TECH UNIVERSITY
THE GRADUATE SCHOOL

JULY 12, 2012

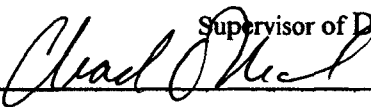
Date

We hereby recommend that the dissertation prepared under our supervision by
Ilija Pjescic, Dipl. Ing. Mas.
entitled “ Exploitation and Exploration of PCR in Microfluidic Systems
with Gradient Temperature Environments”

be accepted in partial fulfillment of the requirements for the Degree of
Doctor of Philosophy in Engineering



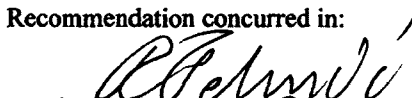
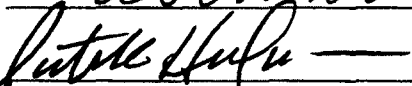
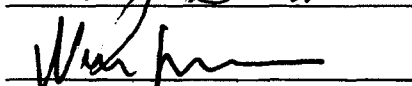
Supervisor of Dissertation Research



Head of Department
Engineering

Department

Recommendation concurred in:



Eric J. Gault


Advisory Committee

Approved:


Director of Graduate Studies

Approved:


Dean of the Graduate School


Dean of the College

ABSTRACT

The main goal of the work was to establish a wholesome picture off all relevant processes for a sample-in, answer out genetic system and to integrate the whole process on a one step device from sample collection to final result. The genetic analysis process consists of ideally three steps: sample preparation, chemical reaction, and analysis. Each of the steps is different and requires a specific environment, where sample preparation might use additives, they might later interfere with the reaction itself or lead to misleading results in the analysis phase. It was found to be quite a challenging process to synchronize the three without compromising each other efficiency.

The design of the devices was a gradual process with an iterative approach. The initial trials were focused on enabling on-chip PCR with spatial melting analysis. In the later work, sample preparation was embedded into the process, though at the cost of reaching the used fabrication method limitations. Apart from the challenges of integrating the process into one complete entity, the gradual enhancement of the system in respect to size and performance consistency was pursued. A range of applications and variations to the devices were fabricated each representing a unique solution to many modern-day problems.

APPROVAL FOR SCHOLARLY DISSEMINATION

The author grants to the Prescott Memorial Library of Louisiana Tech University the right to reproduce, by appropriate methods, upon request, any or all portions of this Dissertation. It is understood that "proper request" consists of the agreement, on the part of the requesting party, that said reproduction is for his personal use and that subsequent reproduction will not occur without written approval of the author of this Dissertation. Further, any portions of the Dissertation used in books, papers, and other works must be appropriately referenced to this Dissertation.

Finally, the author of this Dissertation reserves the right to publish freely, in the literature, at any time, any or all portions of this Dissertation.

Author Jewett Olyza

Date 13th August 2012

DEDICATION

This work is dedicated to my family and all the people I shared hardship, joy, and love with in the last four years at Louisiana Tech University.

TABLE OF CONTENTS

ABSTRACT.....	iii
DEDICATION.....	v
LIST OF FIGURES	x
LIST OF TABLES	xvi
ACKNOWLEDGMENTS	xvii
CHAPTER 1 INTRODUCTION	1
1.1 Genotyping on Chip.....	1
1.1.1 On-chip continuous flow PCR, melting analysis and sample preparation.....	2
1.1.2 Fabrication	5
1.2 Research Goals	7
1.3 Overview.....	8
CHAPTER 2 GLASS-COMPOSITE PROTOTYPING FOR FLOW PCR WITH IN SITU DNA ANALYSIS	10
2.1 Background and Theory.....	10
2.2 Overview.....	10
2.3 Introduction.....	11
2.4 Experimental Setup.....	14
2.5 Microfluidic Device Design and Fabrication.....	14
2.5.1 Temperature control subsystem	17
2.5.2 Optical subsystem	17
2.5.3 Image analysis.....	19

2.5.4	PCR reagents.....	20
2.5.5	Microfluidic PCR and analysis	21
2.5.6	Spatial data quality.....	22
2.6	Results and Discussion	22
2.6.1	Iterative device design and fabrication	22
2.6.2	Thermal control and uniformity	24
2.6.3	Simultaneous amplification and analysis.....	24
2.6.4	Robustness	28
2.6.5	Signal-to-noise ratio.....	30
2.7	Conclusion	32
CHAPTER 3 GENOTYPING FROM SALIVA WITH A ONE-STEP MICRODEVICE		34
3.1	Overview.....	34
3.2	Abstract.....	34
3.3	Introduction.....	35
3.3.1	Full integration.....	36
3.3.2	Sample preparation	36
3.3.3	Assay selection.....	37
3.3.4	Fabrication method	38
3.4	Methods	39
3.4.1	Spatial temperature distribution.....	40
3.4.2	Microfluidic device design and fabrication	40
3.4.3	Microchannel passivation	42
3.4.4	PCR reagents.....	43
3.4.5	Experimental protocol.....	43
3.4.6	Lab on a chip.....	43

3.4.7	Control and validation.....	44
3.5	Results and Discussion	44
3.6	Conclusion	49
CHAPTER 4 SPATIAL MELTING ANALYSIS - APPLICATIONS		51
4.1	Spatial Melting Analysis for Continuous Non-ionizing Damage Detection in DNA Samples.....	51
4.1.1	Methods.....	52
4.1.2	PCR.....	55
4.1.3	Results.....	56
4.2	Fast Spatial DNA Melting Analysis using Surface Modified Capillary Pumping.....	62
4.2.1	Abstract	62
4.2.2	Introduction.....	63
4.2.3	Methods.....	65
4.2.4	Chip design and fabrication	66
4.2.5	Silicone coating of microfluidic devices.....	68
4.2.6	Optical setup	70
4.2.7	Sample reagents	73
4.2.8	Results.....	74
4.3	Conclusions and Future Work	76
CHAPTER 5 ISOFLUX THERMAL GRADIENT IN SOLID STATE HIGH-ASPECT RATIO STRUCTURES		78
5.1	Abstract	78
5.2	Theoretical Analysis	79
5.2.1	Analytical analysis and 1D simulation	79
5.2.2	3D simulation.....	82

5.2.3	2D modeling – isoflux flow in parallel non homogeneous structures	90
5.3	Experimental Design.....	91
5.4	Results.....	94
5.5	Conclusions and Future Work	97
CHAPTER 6 CONCLUSION.....		99
REFERENCES		101

LIST OF FIGURES

- Figure 2-1 By sandwiching a patterned tape between microscope slides, disposable glass-composite cf-PCR devices were fabricated. (a) an exploded diagram of the chip assembly; (b) an image of a fabricated device.[19]..... 15
- Figure 2-2 By placing a microfluidic device in the heating platform, a controlled 1-D temperature gradient develops. (a) shows an IR image of a heated device. The dotted rectangle indicates the location of the cf-PCR microchannel within the device, which corresponds to a 120 x 24 pixel array in the thermal image. (b) shows the average temperatures at the 24 vertical positions. The error bars in the graph indicate the maximum variation of the 120 horizontal temperature values for each vertical position. [19]..... 18
- Figure 2-3 By analyzing one fluorescence image, the entire amplification process can be analyzed. (a) shows a representative image of the microfluidic device after PCR mixture has filled the serpentine channel. The temperature gradient, approximated with the labels to the right of the image, is uniform in the horizontal direction. Fluid flow is from left to right in this image, such that the fluid seen on the far right of the image was in the process of experiencing its 23rd thermal cycle. The increasing fluorescence is shown as a function of cycle number in (b). The decreasing fluorescence as a function of temperature is shown in (c). These spatial melting analyses were performed at multiple cycle locations within the image, as indicated. These curves show the raw fluorescence within each region of interest. [19]..... 25
- Figure 2-4 The melting behavior of the PCR products was imaged while the DNA was undergoing a spatial PCR process. The melting temperatures of both targets were verified on the LS-32. As expected, the 110-bp target was characterized by a single melting regime, while the 181-bp target displayed two melting regimes. Such variations in the melting profile – not just the melting temperature – are sequence-specific characteristics that serve as “fingerprints” of the different PCR targets. Identical processing of both data sets included a 7-fold spatial redundancy and minimal smoothing. [19]..... 27

- Figure 2-5 By pre-treating the microfluidic channel, amplification of the PCR samples occurred immediately. This image shows the air/fluid interface at the front of the flowing PCR mixture. The fluorescence of the sample is indicative of amplification, as is the observable melting transition of the amplifying DNA in the previous cycles. [19] 28
- Figure 2-6 The spatial melting curves at six flow rates are shown in this graph. The maximum melting temperature variation between these 6 curves is about 5 pixels, or 0.15 mm. To accurately compare the shape of the melting transitions, the fluorescence intensities of these 6 curves were normalized with respect to each other. The data shown here has not been smoothed beyond the clustering of adjacent pixel lines. [19]..... 29
- Figure 2-7 Images were taken with exposure times of 125, 250, and 1000 ms. Spatial melting analyses were performed at 5 arbitrary horizontal positions with cycle 22 of these images, and for 7 different pixel line widths. The SNR associated with the spatial melting analysis of a given fluorescence image is a function of both the exposure time and the degree of the spatial redundancy in the image. [19] 31
- Figure 3-1 The microfluidic device (top) was designed with 38 type 1 and four type 2 channel segments as indicated in the inset (bottom left). The type 1 was optimized for rapid PCR, and the type 2 was optimized for fluorescence acquisition of the DNA melting during amplification. The width of the channel as a function of vertical position is shown in the graph (bottom right) for both types. [40] 41
- Figure 3-2 Fluorescent images of the microfluidic channel are shown for the male (left) and the female (right) saliva samples. The images are mirrored for easier visual comparison. The PCR cycle number is indicated below the images, and the approximate temperature is shown between. These images were taken after approximately five mins of continued pumping beyond the filling of the microdevice (18 mins after pumping was initiated). [40] 45
- Figure 3-3 The spatial melting analysis of the images shown in Figure 3-2. The graph on the left shows the melting curves taken from the two images. The graph on the right (the derivative plot) is the negative of the slopes of the melting curves on the left. [40]..... 47
- Figure 3-4 DNA melting analysis of the male and female saliva on the LS-32. The melting curves are shown on the left, and the derivative plots on the right. [40] 48
- Figure 3-5 The effectiveness of the osmotic lysis was evaluated by determining the impact of an additional five minute thermal lysis between sample preparation and the PCR thermocycling. [40] 49

- Figure 4-1 a) The analysis system consists of a syringe and syringe pump, small bore tubing, and the spatial DNA melting analysis subsystem. b) For these experiments, the tubing was inserted into a UV crosslinker so that the flowing DNA sample would experience cumulative radiation damage in the form of photoproducts. c) The microfluidic chip was fabricated by cutting a pattern into double-sided Kapton tape, then sandwiching the film between microscope slides. Polymer ports were attached as interfacing for the small bore tubing. d) The microfluidic device was positioned over aluminum strips, which were independently heated to different temperatures. Once heat flow stabilized, a virtually linear steady-state temperature gradient was present in the vicinity of the microfluidic channel. The melting of the DNA, which occurred across this gradient, was observed in the fluorescence of an intercalating dye.[1] 53
- Figure 4-2 The likelihood of photoproduct formation and the DNA sequence structure based on Douki et al. work.[1] 54
- Figure 4-3 Melting analysis of samples with a constantly increased exposure time. In the image it can be seen that the melting analysis (d) is slowly retracting towards lower temperatures and smaller intensities. This effect is expected, since the radiation should create non-specific bonding, therefore lowering the bonding energy of the strands in between each other. [1] 57
- Figure 4-4 The data acquisition system used allowed a very intense data collection process in which infinitesimal changes in the melting curve could be tracked over a longer period of time. To observe the changes more clearly all the curves were subtracted from the initial one and all-together plotted on one diagram. Due to the excessive line density a shade of gray represents the curves, while an insert is zoomed in. The steady state degradation experiment matches in shape the continuous experiment, though there is a much lesser capability of tracking change over the same period of time. [1] 59
- Figure 4-5 The groups are separated by negative controls, single stranded forward and reverse primers (the 6th and 11th sample). The double stranded oligos (blue=>green) on the left side of the diagram show a consistent deterioration of bonding energy. Likewise, the oligos with damaged reverse (R) and damaged forward (F) segments behaves in a similar fashion. Though it is easily seen in the bottom figure that each of the three cases behaves differently, different curve shapes and heights are achieved at the same exposure times 60

- Figure 4-6 The data shown are three sets of DNA samples that contain an ever increasing Ethidium Bromide concentration. All samples were analysed in doubles. The red samples have the least added EB (far), the light blue samples have a 10-fold of that concentration (middle) and the blue have a 100-fold of the initial concentration (near) 62
- Figure 4-7 Three layers are noticeable, glass (grey), silicone coating (green) and the polyimide adhesive tape (yellow). The fabrication process is in respect to the glass substrate non-invasive. The substrate was initially coated with a silicone layer, and subsequently masked with a polyimide double adhesive layer on top. The mask is pre-patterned and cut prior to placement on top of coating. The top glass slide was machined to enable the loading platform by removing semicircle structures on the channel beginning. The selectively masked silicone coated glass was exposed to air plasma removing the exposed coating. The polyimide layer around the channels was removed and the glass slide was thoroughly cleaned. The two channels top (bottom left) and bottom (bottom right) were assembled and the chip was ready for exploitation 69
- Figure 4-8 The complete experimental setup is presented in the image (left) while a more detailed view of the optical setup is given in the right part. The system is constituted of two subsystems, a heating platform with a control unit representing the thermal subsystem and a compact optical system consisting of filters, a dichromic mirror, a LED light source and a camera. The platform was mounted on a bearing which is mounted on a rail. This allowed axial movement of the platform without compromising the image lighting consistency. The optical cube setup is highly reliable and provides even lighting distribution. This change is a considerable advancement in comparison to previous setups, as in respect to the signal intensity as well as its uniformity 72
- Figure 4-9 A thermal platform with aluminum block and embedded heaters (H1,H2) is used to create a thermal gradient across a microfluidic device. Each of the heaters is coupled with a thermocouple (T1,T2) used as a feedback loop for the control unit. Once the gradient is established, samples are individually loaded manually and the LED (L1) is activated. The light emitted initially propagates through a filter (F1), reflecting from the dichroic mirror (D1) focused on the microfluidic device. The fluorescent dye and DNA present in the sample in interaction with the light emit a lower energy light. The emitted light propagates through the dichroic mirror and the filter F2, separating it from the LED originating light. The images via USB are recorded, visualized and analyzed using a GUI. The platform was mounted on a moving rail (MR1), allowing analysis throughout the whole surface area of the microfluidic chip 73

- Figure 4-10 The top diagram represents a 400 ms exposed sample of PCR product with a very high concentration (top). The background signal is very intense and consumes roughly one third of the acquired signal. In the two images on the bottom, a lighting inconsistency is presented, a problem that made many successful experiments fail in the last instance. The lighting issues as seen the graph are not only in between the channel but also within the channel itself 73
- Figure 4-11 The melt obtained from 1 line of data shows a capable and reliable system for melting analysis. In comparison to previous solutions which had light inconsistency within the channel itself and high background noise, this is a significant advancement. In the bottom image three channels can be seen, though only one is providing a melt. The melt is also obviously distorted and can only provide limited data. The lateral bright spots are samples that due to silicone degradation do not get pumped into the system 76
- Figure 5-1 In this figure a seminifinte solid assessment of the model was achieved. The green line at the beginning shows the actual chip thickness and the speed at which the gradient is formed. Once formed it keeps its shape in an isoflux system and just get heated to a higher temperature 81
- Figure 5-2 In this figure 5 slices of the simulated device are shown, over a 25 s period of time. The two aluminum plates, represented by the thick part show high thermal stability – a constant thermal difference between the plates. The thermal dissipation increases which can be noticed in the increasing color gradient present along the micro-fluidic device length..... 84
- Figure 5-3 The model was modified and 12 points for temperature evaluation over time were added (green). The points were positioned along the measurement channel (bottom 4 nodes), the reference channel (middle 4 nodes) and in the vicinity of the device edge (top 4 nodes)..... 85
- Figure 5-4 All twelve points are simultaneously plotted in one diagram. The temperature differences are small and the systems seem to be linear in its progressive temperature increase 87
- Figure 5-5 The zoomed in analysis of the data shows slight differences between the individual points, that in the selected shown range is maximally 0.5 °C. The temperature difference of two vertical points is of much lesser intensity then the horizontal temperature change. This is understandable since the energy dissipation in the system is provided by the “hanging” surfaces of the microfluidic chip..... 88

- Figure 5-6 The figure illustrates a lateral and horizontal temperature change inside the microfluidic chip. The total horizontal change of temperature for the two most distant points (left) on both the measurement and reference channel are roughly 0.4 °C across a 14 mm distance, resulting in an assumed temperature gradient of 0.0285 °C/mm. The temperature difference across the height was 0.01 °C on a 3 mm distance, resulting in a 0.0033 °C/mm temperature gradient. The two closest points in the center of the structure, for both of the measurement channel and the reference channel the horizontal thermal gradient is 0.01° C/mm and the vertical is 0.0041 °C/mm 89
- Figure 5-7 The temperature distortions shown in a) the measurement channel and b) the reference channel have their origin in the heterogeneous structure in which water with a conductivity of 0.5 W/mK is positioned just next to a polyimide tape layer with 0.15 W/mK thermal conductivity. The intensity of these effects is small leaving only a local effect on the temperature distribution. The adaptation space needed for the temperature to settle to the new value is roughly equivalent to the glass cover slip's thickness 90
- Figure 5-8 In image a we see the whole 2D model in which the heat flux is evaluated. The purpose of this is not to evaluate the amount of energy transferred or to quantify the effect but to see if the boundary conditions and the material heterogeneity affect the temperature distribution within the chip. The top chip has a zero heat flux boundary condition on the lateral edges, while the lower image has convective air cooling. The differences are obvious - the image in b) is the actual total heat flux and we can notice that there is a significant shift of heat flux intensity towards the lateral side. In the model the top is the heater side and the bottom the cooler side 92
- Figure 5-9 This is a schematic of the experimental setup – a thin-film heater is attached to a grounded aluminum plate (left). The glass cover slip in the middle with the thermopile is attached to a voltmeter and in between the two plates. The other plate is attached to the cooling unit which is further attached to a heat sink. The thin layer of PDMS and the coatings are not shown on this image to avoid over complication..... 93
- Figure 5-10 Two diagrams are presented in this image. The thermoelectric signal of a thermopile deposited on polyimide tape (top) shows a very strong response in respect to the directly deposited sensor (bottom). Below each of the two diagrams is the switching protocol 96
- Figure 5-11 The comparison between the two is provided showing a significant difference between the two and their performance (bottom)..... 98

LIST OF TABLES

Table 1-1 Chronology of design and development for integrated one step genotyping systems	6
---	---

ACKNOWLEDGMENTS

This is the one time I can write about people who helped me in my life. It is hard to say who has contributed more or what made my life easier or better. In my eyes there are people I would like to thank, mainly my awesome parents and brother with whom I had my 1 hour chat on skype every weekend. When I arrived I was helped by my aunt and uncle (Irena and Kevin Lombardi) by giving me an introductory course in “how to survive in the USA” with valuable tips and tricks.

Once I arrived in Ruston I was welcomed by Rastko Selmic and Sandra Zivanovic at their house, to stay until I found accommodation of my own. From then on I would be invited for lunch or dinner by both for the rest of my remaining time in Ruston. Rastko is probably the main reason why I came to Louisiana Tech University, for which I am in his debt. Thanks to them, I also met Jadranka and Neven Simicevic. A wonderful couple whose mere attendance brings the occasion to another level, whether through jokes, interesting talk or outstanding culinary skills.

In the four years I spent in my laboratory, my principal adviser, Dr. Niel D Crews, has treated me with respect, understanding and patience. I am not sure could I have had a better adviser from both a professional or personal point of view. I would also like to thank his wife Julie and kids for giving him the energy to deal with us (the whole lab) on a daily basis for such a long period of time. I would also like to thank my awesome girlfriend, Julia for her support in this hectic time of transition. I would also like to thank

my lab partners for being good friends and great colleagues Manasa, Straton, Colin, James, Suvhashis.

In the time of my being here I have met some great people, Divya, Bilal, Talar, Justin, Ishan, Suvhashis, Milap , Bijoya, Mr. Dan, Pavel, Sarah, Ankur...Each of them opened a door or two in my mind and helped me shape myself in what I am today.

Thank you; this accomplishment is not mine alone, it is all of ours.

CHAPTER 1

INTRODUCTION

The dissertation is focused on the efforts to integrate industrially relevant processes within microfluidic devices with a high rate of repeatability. The emphasis was to create stable thermal environments suitable for biochemical reactions and their parallel analysis. The effort of resolving all related issues induced by the intricate multidisciplinary approach required insight into a variety of topics such as: genetics, enzyme kinetics, microfabrication, biochemistry, heat transfer, fluorescence related optics, fluid dynamics and graphic analysis. The following text represents a variety of different approaches, problems and solutions regarding each of the aspects individually or in group.

After careful consideration and experience regarding complicated issues, it is easiest to convey ideas and topics not by explaining the achievements, but by the questions they resolved.

1.1 Genotyping on Chip

In an effort to minimize sample preparation and to keep pace with the semiconductor industry, there is a general tendency to reduce and modernize classical biology approaches with more rapid and economical solutions. This trend is also justified

by a decrease in sample and device size – leading to the inevitable cost reduction in respect to the materials.

If the focus is to be set on the birth of genetic research one could say that the greatest two steps were the development of a thermostable enzyme and subsequently the polymerase chain reaction (PCR). These achievements changed the question from “How can it be done?” to “How little can be used and not compromising the method?” The word “little” refers not only to quantity but to the general cost of an analysis, since its real life relevance gave it prospective industrial value. Though as engineering entered this realm of micro/nano scale science, many seemingly irrelevant factors became influential and of primary consideration for the scientific community.

1.1.1 On-chip continuous flow PCR, melting analysis and sample preparation

The majority of the work presented revolves around the technique used in genetics called Polymerase Chain Reaction (PCR). In this sophisticated chemical reaction a multitude of chemicals engage in maintaining a dynamic equilibrium that results in the continuous increase of double stranded DNA (dsDNA) concentration. Apart from the variety of chemicals present, it is necessary to vary the temperature in the range from approximately 55-60 °C to 93-96 °C. Each of these individual heating and cooling processes represent one PCR cycle (to heat the sample and bring it back to its initial temperature is considered one cycle). During each cycle the amount of dsDNA ideally doubles. This cyclical heating/cooling reaction is repeated until the dsDNA structure is present in a quantity where the bulk reagent starts asserting properties of the multiplied DNA strand, and therefore starts behaving as one as well. As well as the temperature range, the duty cycle of the thermal variations (the speed at which the temperature of the

sample changed from minimum to maximum temperature and back) is of essential importance to the quality of the reaction. The inadequate performance of heating and cooling will cause nonspecific dsDNA formation (nonspecific relates to a sequence of DNA that was not the intended target and is present in either small amounts or dominates the final mixture composition).

In short PCR is a thermally induced biochemical reaction where two major factors affecting the reaction quality can be singled out: the capabilities of the thermal environment to rapidly and reliably change and the biochemical composition of the initial mixture itself.

In the efforts to integrate this reaction onto a small microfluidic chip issues like a somewhat less conventional approach has been taken to resolve the thermal issues as well as microfabrication of the device itself. The profound difference is that the chose method inverted the process from temperature variation of the samples by heating and cooling the whole device, to moving the samples by the means of flow on a steady thermal field. The integration of this reaction in an on-chip continuous flow PCR is generally not a novel concept [2]. Though many unresolved issues were present and had to be addressed before this device can be a competitive technology to the classical PCR thermal cycling devices. Initially, these fields were formed of blocks that would create temperature zones at a certain distance from each other. Though this left an uncertainty about the temperatures the reagents would experience in the region between the two thermal fields (as previously mentioned, this is of importance to the quality of the reaction) making the reaction kinetics unreliable and inconsistent. In the later development stages of the method, an

enhancement was made in the form of a thermal gradient stretching itself from high to low temperatures and replacing the locally enabled temperature block system.

Another step towards a functional system of scientific relevance was the integration of an analysis capable of qualitative and quantitative DNA analysis within the device. Since there was a thermal field present on the device itself, and the sample was within the channel along which the thermal field is spreading, it was most convenient to introduce a technique called melting analysis. Melting analysis is a method in genetics where the interaction of dsDNA and fluorescent dyes results in a unique interaction in respect to temperature changes of the environment. This means that with increase of temperature the sample fluorescence emitted will decrease. The reaction relies on the weak hydrogen bonds, between each of the DNA molecules, giving in to the thermal energy increase and resulting in the disassociation of the two strands. The integration of melting analysis within the PCR was directed towards minimizing the time needed for sample analysis since the same thermal field is simultaneously used for both. Also a significant simplification is achieved since no additional functions or control systems needed to be added.

The last hurdle for a system with the capability to perform complete analysis within the system was sample preparation. The issue represents a great challenge since the samples have various forms (saliva, blood, sperm, tissue) and a multitude of biochemical compounds present in them some of which inhibit PCR significantly. Also the genetic material is encapsulated within the cell itself making it less accessible for the PCR reaction. Therefore two challenges had to be simultaneously overcome: the extraction of the genetic material from within the cell (lysing) and the inactivation of

PCR inhibition chemicals. The most simple and straight forward solution was found to be human saliva. One of the reasons is the non-intrusive extraction method.

The question in this section is, “how to reconcile three different processes onto one single chip?” For the melting analysis and the PCR, it was the formation of the thermal gradient – the chemicals would vary in temperature as they would progress through the temperature field, allowing the reaction to take place, and at the same time the quasi-linear temperature gradient present would allow the acquisition of a fluorescence signature, a spatial DNA melt. Now the question became, “how to allow access to the genomic DNA of the cell for the process without compromising the previous achievements?” The attempt to create a general solution for all sample types would be an idea worth pursuing, though this was not the objective of this thesis. Additionally, it was also emphasized that non-invasive methods have advantages for commercial applications making skilled labor and technicians obsolete and potentially allowing the patient to perform the test himself. All these factors led to the solution by using the same thermal energy that allows the PCR and melting analysis Table 1-1.

1.1.2 Fabrication

One of the challenges of the microfluidic society is to rapidly design and fabricate novel concepts to a proof-of-concept level. In microfluidics the used of hot embossing is popular, though the limitation in respect to throughput time and limited thermal and optical properties do not make it the most suitable approach. The classical semiconductor approaches of etching are efficient though high maintenance since they have a need for a cleanroom environment. Due to the high structural stability of glass it is necessary to use

extremely aggressive chemicals such as hydrofluoric acid (which has an MSDS health risk hazard level of 4 on a scale of 0 to 4).

Table 1-1 Chronology of design and development for integrated one step genotyping systems

	Lab on a Chip*, 2008, 6: 919-924 [3]	Lab on a Chip*, 2008, 8: 1922- 1929 [4]	Biomedical Microdevices, 2010, 12(2): 333- 343 [5]	Lab on a Chip, 2012. [6]
Fabrication technique	Photolithography	Xurography	Xurography	Xurography
Number of cycles	30	1	22	42
Template type	Human genomic DNA	PCR amplicon	Bacterial phage, ph174	Saliva (Human genomic DNA)
Template concentration	5 ng/ μ l	Unknown	10 ⁸ copies/ μ l	Varies
Template pretreatment	Purified DNA	PCR	Purified DNA	NONE
Clinically relevant genetic targets	DYZ1, CYP2C9-2 and CYP2C9-3	N/A	NO	DYZ1
CF-PCR	YES	NONE	YES	YES
Spatial Melting Analysis	YES**	YES	YES	YES
On chip sample preparation	NONE	NONE	NONE	YES
Total time needed for process		N/A	14 min	18 min

* the publications presented were published by Crews et al.

** Although the spatial melt was provided for all products, comparative data represented in the manuscript between the obtained products, was analyzed using a commercial system HR-1 (Idaho Technologies, Utah)

To avoid using dangerous chemicals or imposing a significant financial burden, a simple rapid prototyping technology was used to fabricate all tested devices – xurography. Briefly the technique is a simple cut and paste method where a double-sided adhesive tape is joined in between two glass slides. Prior to assembly, the tape was cut in channel like patterns, and subsequently they were removed leaving empty space for the fluid to propagate. The glass slides were predrilled with adequately positioned holes, with PDMS ports attached to them. It can be said that providing glass slides and the tape, an iteration from idea to chip would take less than 2 h of work.

Generally, this technique has its drawbacks in terms of quality since its results are strongly influenced by the technician's experience and skill set. In return, this technique requires no clean-room, cheap materials and allows rapid design adaptation, all good prerequisites for a flexible attitude in the fast expanding and ever-changing field of microfluidics. If the benefits glass microscope slides bring with them, are considered, both in respect of optical and thermal properties, this technology is shown to be superior to any available solution.

In Table 1-1 the chronological advancements in respect to a multitude of relevant factors is presented. The table contains previous works of my adviser Dr. Crews and the most recent joint achievements.

1.2 Research Goals

The main goal of the work was to assess the fragile balance between thermal environments and the corresponding biochemical reactions. The emphasis is set on creating a functional device while in parallel addressing all issues to the extent of needed for reliable functionality of the system.

The design of the devices was a gradual process with an iterative approach. The initial trials were focused on enabling on-chip PCR with spatial melting analysis. In the later work, sample preparation was embedded into the process, though at the cost of reaching the used fabrication method limitations. Apart from the challenges of integrating the process into one complete entity, a side endeavor was the gradual enhancement of the system in respect to size and performance consistency. A range of applications and variations to the devices were fabricated each representing a unique solution to many of the problems of today.

1.3 Overview

In the first part, an introductory text is given with a steady progression of answers and questions during the process. In the second chapter a detailed description of a proof of concept solution was presented. The device, fabricated in the absence of a clean room environment, proved to be capable of continuously performing PCR on the chip as well as allowed a spatial melting analysis for qualitative sample analysis. Though the initial sample tested was at a relatively high concentration and valid for proof of concept situations, it lacked capability for a complete genomic analysis and sample preparation.

In the third chapter the proof of concept design was expanded to the extent where raw saliva samples could be tested. Two saliva samples, male and female by origin, were mixed with the reagents and immediately loaded onto the system. The two samples as expected showed a difference in the spatial melt form and were clearly distinguishable. The system was a single channel that integrated sample preparation, the polymerase chain reaction and sample analysis in one continuous process.

In the fourth chapter multiple variations of spatial melting analysis application are presented. One, focusing on continuous screening of DNA for non-ionizing radiation damage, genotoxin detection and damaged DNA annealing; the second, a capillary loading method by means of surface modification applied on spatial melting analysis. Both systems although with no great scientific relevance represent technical innovations with creative solutions to relevant problems.

In the fifth chapter a gradient thermal environment, similar to what is used in the fluorescence sensing was present as a viable option for possible thermoelectric measurements. A detailed study of the theoretical concepts, simulations and an experimental setup were shown. The results suggest that the system is capable of performing rapid thermal changes for potential use on biochemical reaction kinetics evaluation using thermoelectric measurements.

CHAPTER 2

GLASS-COMPOSITE PROTOTYPING FOR FLOW PCR WITH IN SITU DNA ANALYSIS

2.1 Background and Theory

In this chapter a complete literature review, introduction, methods and experimental setup are given for continuous flow PCR using prototyping technologies. The capability and limitations of such an approach were experimentally tested and subsequently evaluated. Some sections of this chapter were published in a paper written by the author of the thesis as “Glass-composite prototyping for flow PCR with *in situ* DNA analysis”, in *Biomedical Microdevices*, Volume 12, Number 2 (2010), p333-343 [5].

2.2 Overview

Low cost microfluidic devices have been presented as a solution for simultaneous amplification and analysis of DNA. Temperature gradient flow PCR was performed, during which the unique fluorescence signature of the amplifying product was determined. The devices were fabricated using xurography, a fast and highly flexible prototype manufacturing method. Each complete iterative design cycle, from concept to prototype, was completed in less than 1 h. The resulting devices were of a 96% glass composition, thereby possessing a high thermal stability during continuous-flow PCR.

Volumetric flow rates up to 4 $\mu\text{l}/\text{min}$ induced no measurable change in the temperature distribution within the microchannel. By incorporating a preliminary channel passivation protocol, even the first microliters through the system exhibited a high amplification efficiency, thereby demonstrating the biocompatibility of this fabrication technique for DNA amplification microfluidics. The serpentine microchannel induced 23 temperature gradient cycles in 15 min at a 2 $\mu\text{l}/\text{min}$ flow rate. Fluorescent images of the device were acquired while and/or after the PCR mixture filled the microchannel. Because of the relatively high initial concentration of the DNA template, images taken after 10 min (less than 15 PCR cycles) could be used to positively identify the PCR product. A single fluorescent image of a full device provided the amplification curve for the entire reaction as well as multiple high resolution melting curves of the amplifying sample. PCR template for these experiments was a phage DNA (plasmid - ΦX174), with primers targeting either a 110-bp or a 181-bp segment. In addition, the signal-to-noise ratio associated with the spatial fluorescence was characterized as a function of spatial redundancy and acquisition time.

2.3 Introduction

Continuous-flow PCR (cf-PCR) is the microfluidic DNA amplification technique that reverts the polymerase chain reaction (PCR) into a steady-state process [2]. By maintaining the device at a single thermal and flow profile over time, simpler controls and faster analysis times result [7]. In addition, massively serial DNA testing can be achieved with no cross-contamination between successively amplified samples [8]. Two significant limitations to the versatility of cf-PCR have recently been resolved in the literature. Since the number of thermal cycles is designed into the microfluidic structure,

it had not been possible to select the number of PCR cycles for a given sample prior to its subsequent analysis. Obeid et al. responded by designing a cf-PCR device with multiple outlets spaced at intervals along the microfluidic channel, thereby allowing for the PCR product to be removed for analysis after 20, 25, 30, 35, or 40 amplification cycles [9]. Another challenge associated with cf-PCR, as well as other micro-PCR technologies, involves the integration of analysis subsystems for characterization of the PCR product. Nakayama et al. demonstrated an *in situ* fluorescence technique to confirm that amplification was occurring during cf-PCR [10], although product verification was not attempted. In the past, product verification could only be achieved through a post-PCR analysis. Recently, however, Crews et al. showed that the DNA target can be analyzed while it is amplifying, rather than afterwards [3]. This was achieved by performing cf-PCR within a stable thermal gradient, during which the fluorescence of the PCR mixture was imaged. The cyclic melting of the amplifying DNA was characterized and used to identify the DNA product. This spatial melting analysis is analogous to a time-domain DNA melting analysis [11], and has recently been shown capable of even single nucleotide polymorphism (SNP) genotyping [12].

The specific fabrication techniques used for cf-PCR micro-devices greatly determine their expense and complexity. Glass [2, 7, 9] and glass/silicon [13] microfluidic devices have been made using conventional micromanufacturing methods. Such devices are chemically robust and possess optimum thermal characteristics for flow PCR. However, low production volumes of these devices usually require a significant investment of time and financial resources, as well as the support of a dedicated laboratory infrastructure. Cf-PCR devices have also been fabricated from polymers [14],

such as polycarbonate (PC) [15], polydimethylsiloxane (PDMS) [16], and polymethylmethacrylate (PMMA) [8]. Although polymers are more susceptible to flow-induced thermal variations [4, 15], the transition of cf-PCR microfluidics to these materials has resulted in a reduction in long-term fabrication costs. However, there is typically a significant initial investment to create the original master, mold, or cast required for polymer fabrication. A notable “master-less” method for polymer fabrication involves the laser ablation of thin films [17]. However, this technique possesses unique operational complexities and can require a significant equipment expense. Therefore, when considering iterative device design and development, the conventional polymer, glass, and silicon fabrication techniques are equally impractical.

A recently developed rapid prototyping technique, xurography, is characterized by a low startup cost in addition to a reduction in the long-term investment of time and resources [16]. Greer et al. estimated that xurographic microfluidic devices can be fabricated for less than \$0.40 USD for materials or for less than \$7.00 USD for labor and materials [18]. In addition, the initial investment for the xurography equipment is less than \$2000 USD, and no part of the fabrication protocol requires exposure to hazardous chemicals (HF, HNO₃, etc.) or cleanroom processing. This technique involves the patterning of double-sided tape with a precision-guided cutting blade, after which the thin patterned film is sandwiched between blanks of a thicker substrate material [19]. This rapid prototyping technique has been used to fabricate microfluidic devices capable of time-domain DNA melting analysis [18, 19] and spatial DNA melting analysis [12]. While short-term contact with the exposed adhesive layers does not interfere with DNA

melting analysis, Erill et al. found that the adhesive in acrylic tape “induces an acute inhibition of PCR” [20].

This current chapter describes the manufacture and use of cf-PCR microdevices fabricated with the xurography technique. Thin films with a silicone adhesive were used to enhance PCR biocompatibility, and glass substrates were used to enhance the thermal performance of the prototype devices.

2.4 Experimental Setup

The experimental system consisted of a microfluidic chip, a syringe and syringe pump (KDS100, KD Scientific, MA, USA), a heating subsystem, and an optical subsystem. A computer was used to store and analyze the images acquired by the optical subsystem. The microfluidic chip had a serpentine channel through which a PCR mixture was pumped. A stable temperature gradient was generated across the chip, such that the flowing fluid would experience the cyclic heating and cooling for PCR to occur. A syringe containing the PCR sample was attached through 1.58 mm tubing (Upchurch Scientific, WA, USA) to the chip inlet. The chip outlet was connected to a waste reservoir. Periodically during the PCR, the fluorescence of the intercalating dye (LC Green Plus, Idaho Technology, UT, USA) in the PCR mixture was imaged. Both the amplification curve and characteristic melting curves of the DNA were obtained from each image.

2.5 Microfluidic Device Design and Fabrication

Microfluidic devices fabricated with the xurography technique were comprised of a patterned adhesive tape between two blank substrates (see Figure 2-1), along with the appropriate fluidic interfaces. The choice of substrate material was based primarily on

performance and cost. Since the extent of undesired temperature shift within microfluidic flow channels is inversely proportional to the thermal conductivity (k) of the bulk material [4], glass ($k = 1.1 \text{ W/mK}$) microscope slides rather than polymer ($k = 0.1 - 0.2 \text{ W/mK}$) substrates were used. Aminosilane-coated slides (S4615, Sigma-Aldrich, MO, USA) were used rather than plain glass slides in order to reduce adsorption of the PCR reagents onto the microchannel walls. A $100 \mu\text{m}$ thick, double-sided polyimide tape (PPTDE 1 ½, Kaptontape.com, CA, USA) was patterned using a sign cutter (CE 5000-40-CRP, Graphtec, Yokohama, Japan), a previously documented technique [12].

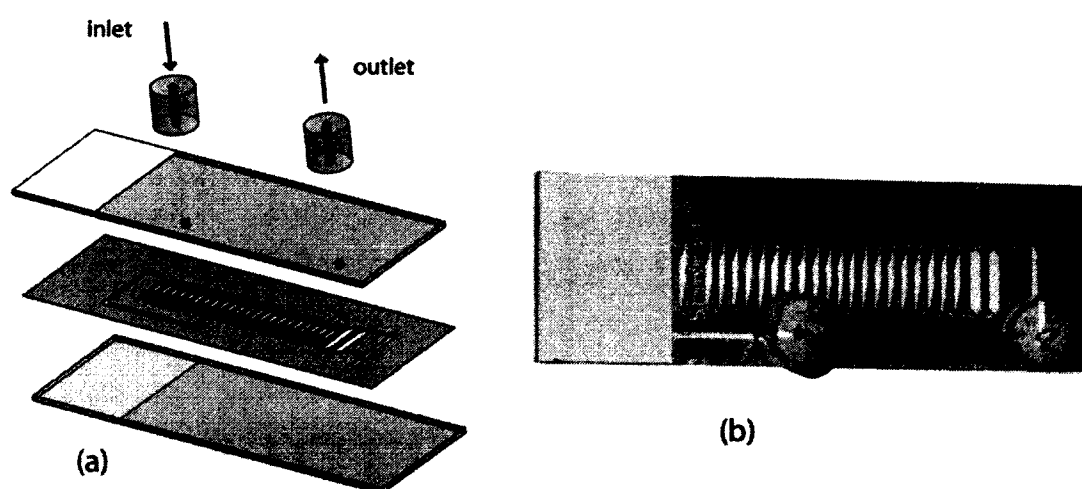


Figure 2-1 By sandwiching a patterned tape between microscope slides, disposable glass-composite cf-PCR devices were fabricated. (a) an exploded diagram of the chip assembly; (b) an image of a fabricated device.[5]

This tape was selected in part for its high temperature rating and for its silicone adhesive (thereby avoiding acrylic [20]). Prior to the assembly of the composite device, access holes were mechanically drilled (850-010C, NTI, Kahla, Germany) through the glass slides, over which improvised fluidic interfaces were attached. These cylindrical

ports (diameter of ~ 1 cm) were punched (6122A26, McMaster-Carr, IL, USA) out of an 8 mm thick sheet of PDMS (Sylgard 184, Dow Corning, MI, USA). A 1.5 mm hole was then punched (33-31A, Miltex, PA, USA) in the port (see Figure 2-1) to create a compression fit interface for the tubing. The PDMS ports were then bonded to the glass over the pre-drilled hole positions. This was done by exposing both mating surfaces to ionized air for 2 min at a pressure of 250 mTorr (Harrick Plasma, NY, USA), and then positioning and pressing them together. To prevent the plasma treatment from damaging the aminosilane coating, polyimide tape was used to temporarily mask the opposite side of the glass, where the microchannels would be located. All cleaning of the glass pieces during the assembly process was done by rinsing with a 1% solution of detergent (Alconox, NY, USA), then distilled water, and then manually blowing the material dry with compressed nitrogen.

Within the microfluidic channel, one thermal heating and cooling cycle was performed as the molecules in the fluid moved from the middle of the chip to its hottest periphery, then to its coolest periphery, then back to the middle. The product extension by thermostable DNA polymerase, which occurred at low to intermediate heating temperatures, was considered the only time-dependent aspect of PCR kinetics [21]. While this rate of reaction restricted the maximum heating rate of the PCR mixture, only physical limitations dictated the maximum cooling ramp rate from the denaturing to the annealing temperature. For this reason, wide heating sections (decreasing mixture velocity) and narrow cooling sections (increasing mixture velocity) were characteristic of every tested design. The channel geometries for the iterative design and fabrication were created in Adobe Illustrator (Adobe Systems, CA, USA). At least one microfluidic device

of each design was fabricated and tested. Several criteria were used to optimize the design, such as the propensity to form or trap air bubbles, ease of fabrication, the maximum number of channels that would fit on a device, the ramping ratio between heating and cooling sections, and the quality as well as quantity (i.e. spatial redundancy) of fluorescent data.

2.5.1 Temperature control subsystem

The temperature control subsystem was designed to generate a stable, controllable temperature gradient within the device that would be virtually linear in the vicinity of the microchannel. The uniformity of the thermal gradient would ensure a reliable thermocycling protocol for the PCR as well as a precise DNA melting analysis of the product during its amplification. The thermal subsystem was comprised of a heating platform and a closed-loop temperature controller. A 3D model of the heating platform, along with further assembly and circuitry details about the temperature control subsystem are provided as Supplementary Material. An infrared (IR) camera (A230, FLIR, OR, USA) was used during the development of the temperature control subsystem to characterize the spatial temperature distribution across the glass substrate Figure 2-2.

2.5.2 Optical subsystem

The optical subsystem consisted of a diffuse LED light source and a CCD camera, designed to excite and detect the spatial emission of the fluorescent dye that would bind to the DNA as it was amplifying. LC Green Plus absorbs light between 440-470 nm and, when double-stranded DNA is present, strongly emits light between 470-520 nm. Therefore, the LED source (HPLS-Dragon, LightSpeed Technologies, CA, USA) was filtered to a 50 nm wide band between 425-475 nm (HQ450/50x, Chroma, VT, USA).16-

bit images of the microfluidic device were acquired with the 0.3 megapixel monochrome camera (LU075, Lumenera, ON, Canada) fitted with a 50 mm macro lens (Canon EF 50 mm f/2.5, Canon, Tokyo, Japan) that was filtered to block out all wavelengths below 485 nm (HQ485LP, Chroma, VT, USA). The field of view for this camera covered approximately 10 PCR cycles. When examination of more cycles was desired, the heating platform and microfluidic device were shifted beneath the stationary optics, so that multiple regions of the chip could be imaged in quick succession. These images were merged together using an automated function in Adobe Photoshop (Adobe Systems, CA, USA), resulting in a single image of the entire channel length.

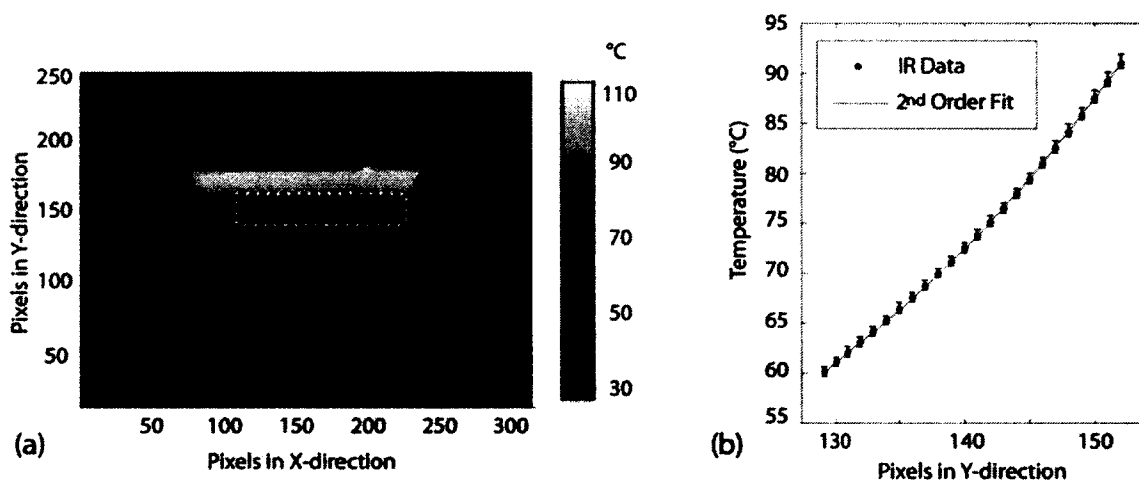


Figure 2-2 By placing a microfluidic device in the heating platform, a controlled 1-D temperature gradient develops. (a) shows an IR image of a heated device. The dotted rectangle indicates the location of the cf-PCR microchannel within the device, which corresponds to a 120 x 24 pixel array in the thermal image. (b) shows the average temperatures at the 24 vertical positions. The error bars in the graph indicate the maximum variation of the 120 horizontal temperature values for each vertical position. [5]

2.5.3 Image analysis

A software program was used to obtain DNA amplification and melting data from the fluorescent images. These in-house graphical user interfaces (GUIs) were developed in MATLAB (MathWorks, MA, USA), based partially on algorithms that have been previously described [8]. The program allowed for the user to interactively orient each image and indicate the regions of interest for the analysis.

Fluorescence was measured as a function of cycle number and of temperature in order to generate an amplification curve and one or more DNA melting curves for each image. In the amplification curve GUI, it was important to minimize the effect of any spatial variations in the excitation light. Therefore, the background fluorescence in each cycle was subtracted from the measured signal before the amplification curve was obtained. The fluorescence intensity was average within a 10 x 10 pixel region of interest within each section to obtain these values. The melting analysis GUI allowed for the user to select any PCR cycle or multiple cycles in which to examine the amplifying DNA. The analysis algorithm took advantage of the spatial redundancy which was inherent in the 2-D fluorescence distribution. In channel sections that were oriented parallel to the 1-D temperature gradient, it was assumed that adjacent pixel lines would exhibit virtually identical fluorescence, differing only by the effects of the optical and electrical noise in the system. By grouping these parallel data lines together for combined analysis, it was hypothesized that the signal-to-noise ratio (SNR) of the data would increase. Therefore, the GUI allowed the user to select the pixel width of the data subset for the spatial DNA melting curve analysis.

2.5.4 PCR reagents

An identical PCR mixture was used for all of the experiments conducted as part of this work. Unless otherwise noted, all reagents were purchased from Sigma-Aldrich (MO, USA). The mixture contained 10^8 copies/ μl of a viral phage DNA template (plasmid ΦX174 , New England Biolabs, MA, USA), $0.5 \mu\text{M}$ of each of the forward and reverse primers, $200 \mu\text{M}$ of each deoxynucleotide triphosphate (dNTP), $0.04 \text{ U}/\mu\text{l}$ of KlenTaq1 polymerase (AB Peptides, MO, USA), 2 mM MgCl_2 , 2.5 mg/ml BSA, and 1X LCGreen Plus in a 30 mM Tris (pH 8.3) buffer. One of two primer sets¹ were used to target either a 110-bp or a 181-bp segment of the template DNA[7]. The concentration of the DNA template used in these tests was approximately 1,000 times higher than is used in clinical applications with human genomic DNA [3]. This was done to reduce the number of cycles by ten that would result in a measurable fluorescence signal (10 cycles $\sim 2^{10}$ increase).

Positive and negative controls for each batch of PCR mixture were amplified and analyzed on a commercial system (LS-32, Idaho Technology, UT, USA). The amplification protocol for the LS-32 consisted of a 1 min initial denaturation at 95°C , followed by 30 cycles of 95°C for 1 s, 60°C for 1 s, and 75°C for 3 s. All temperature ramping during PCR was at a rate of 5°C/s . At the conclusion of the PCR, a high resolution melting analysis of each amplified sample was performed serially, by monitoring the fluorescence during a steady ramp of 0.3°C/s from 60 to 90°C .

Previous work indicated that reactants in the mixture can adhere to the glass walls of the cf-PCR channels, thereby inhibiting initial amplification [3]. To reduce this effect

¹ 110-bp (5' – GGTTTCGTC AAGGACTGGTTT – 3', 5' – TTGAACAGCATCGGACTCAG – 3')
181-bp (5' – GCTTCCATGACGCAGAAGTT – 3', 5' – GCGAAAGGTCGCAAAGTAAG – 3')

in the current system, the microchannel was passivated prior to its first use with a solution identical to the PCR reaction mixture, minus the nucleic acids and Taq polymerase. Then 40 μl of this passivation mixture was passed through the device at a flow rate of 2 $\mu\text{l}/\text{min}$, and PCR testing was initiated shortly after the microchannel was emptied.

2.5.5 Microfluidic PCR and analysis

To prepare each device for testing, a microfluidic chip was placed in the heating platform and the heating protocol was initiated. While the gradient was equilibrating, the passivation mixture was passed through the channel and the PCR mixture was loaded into a syringe. At the conclusion of the pre-treatment, the sample was injected into the channel at a constant flow rate of 2 $\mu\text{l}/\text{min}$. The device was periodically imaged while the microchannel was filling. Upon filling, all thermal and flow conditions were maintained. Fluorescence images continued to be taken at intervals, in order to observe any change in the behavior of the system over time. This experiment was repeated multiple times, with different chips, and with each of the target-specific primer sets.

Experiments were also conducted to evaluate the thermal stability of the temperature distribution within the glass-polymer-glass microfluidic devices. The melting of the PCR product was used as the metric, such that a shifting or a distortion of the observable fluorescence transition would be indicative of flow-induced temperature drift. Volumetric flow rates up to 4 $\mu\text{l}/\text{min}$ were examined. For these tests, a microfluidic device was filled with pre-amplified PCR product of 110-bp in size. When the chip reached thermal equilibrium, the flow rate was set to a value, and 60 s (± 5 s) elapsed

before the device was imaged and the flow rate was changed. This was repeated for all of the flow rates of interest.

2.5.6 Spatial data quality

The effect of spatial redundancy and of camera exposure time on the data quality obtained from the CCD images was investigated by measuring the SNR of the spatial DNA melting curves. These calculations were performed by importing the GUI-generated melting curves into an analysis software (MeltingWizard, University of Utah, UT, USA). A representative amplification of the 110-bp plasmid target was examined for this evaluation. With a full chip, under steady-state flow and thermal conditions, three images of the fluorescence were taken with exposure times of 125, 250, and 1000 ms. The MATLAB GUI was used to perform spatial melting analyses on each of these images at five arbitrary positions within the 22nd PCR cycle. Line clusters from 1 to 13 pixels wide were evaluated, and the corresponding SNRs of these curves were examined as a function of exposure time and pixel line width.

2.6 Results and Discussion

2.6.1 Iterative device design and fabrication

Microfluidic chips were fabricated according to the aforementioned protocol. The final microchannel design, as shown in Figure 2-1, contained 23 PCR cycles. During the design development process, device variations were quickly applied and tested. The fabrication of each iterative design was achieved by one person in less than one hour, beginning with the initial concept idea and ending with an experiment-ready prototype. Since material costs for the devices were negligible, labor was the only significant expense. The fabrication yield with this technique was approximately 80% when all

geometric features were at least 200 μm in size. The occasional unusable prototypes were characterized by wrinkles in the tape leading to leaking, shifting of the serpentine pattern in the tape resulting in channel blockage, and/or leaking around the PDMS ports. Mishandling of the components and inadequate cleaning during fabrication have been identified as the leading causes of these failures.

The channel sections where sample cooling would occur were designed to be as narrow as possible. Channel widths below 150 μm , however, proved challenging to fabricate consistently, due to the difficulty associated with manually removing the material on the interior of the cut channel outline. In the final design, the widths for the cooling channels were 200 μm . In addition, abrupt width changes resulted in more frequent formation of bubbles, and were avoided in the later design iterations. To maximize the extension time for a given volumetric flow rate, gradually increasing widths, up to a maximum of 1.0 mm in the middle of the chip, were selected for the final device design. In the optimized design, the two final heating channel sections were particularly wide: 1.5 mm. During the analyses of the fluorescence images, these two channels were the ones most commonly used for the spatial melting analysis, and therefore designed for maximum spatial data redundancy. The resulting microfluidic devices had a footprint of approximately 75 mm x 25 mm, and a total thickness of 2.3 mm. Excluding the PDMS ports, whose thermal properties were considered inconsequential, the chip was approximately 96% glass when considering the bulk materials. The sidewalls of the microfluidic channel itself were between 80-90% glass, depending on the specific geometry used.

2.6.2 Thermal control and uniformity

By heating a microfluidic device from room temperature with the heating platform and controller, a stable temperature gradient would develop within 5 min, as determined by the IR images of the system. Figure 2-2 shows an IR image after thermal equilibrium was achieved. The gradient is oriented vertically in this image, with the cooler edge along the bottom of the chip. The dotted rectangle overlaid on the image in Figure 2-2 indicates the position within the microfluidic device of the serpentine channel. As is shown in Figure 2-2, the gradient within this rectangular region encompassed the entire temperature range within which PCR can be achieved. The error bars in the graph show the temperature uniformity across the rectangular region indicated in Figure 2-7, with a maximum temperature variation of less than 1 °C at the lower temperatures, and of approximately 1.4 °C at the higher temperatures.

2.6.3 Simultaneous amplification and analysis

The microfluidic PCR was performed and the device was imaged, with the reaction proceeding at full speed. Figure 2-3 shows a representative fluorescence image taken shortly after the PCR mixture filled the channel, such that there was PCR mixture simultaneously in every stage of the amplification process. The orientation of the gradient in Figure 2-3 is the same as that shown in Figure 2-2. The flow rate of the PCR mixture was 2 µl/min from left to right, such that the fluid observed in the left-most section in the image was experiencing its 2nd thermal cycle and the fluid observed in the right-most section was experiencing its 23rd thermal cycle. The fluorescence in the cooler regions of the channel increased with cycle number, first observable around cycle 12 and reaching a plateau near cycle 20.

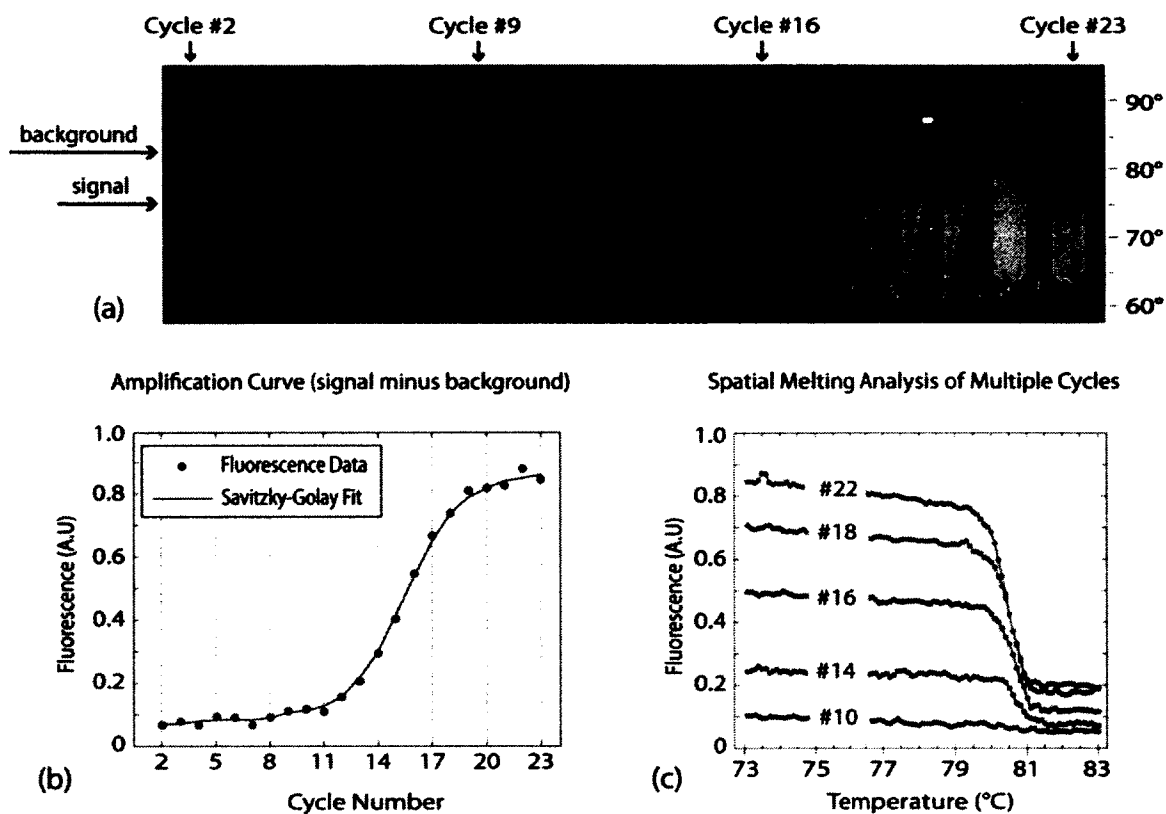


Figure 2-3 By analyzing one fluorescence image, the entire amplification process can be analyzed. (a) shows a representative image of the microfluidic device after PCR mixture has filled the serpentine channel. The temperature gradient, approximated with the labels to the right of the image, is uniform in the horizontal direction. Fluid flow is from left to right in this image, such that the fluid seen on the far right of the image was in the process of experiencing its 23rd thermal cycle. The increasing fluorescence is shown as a function of cycle number in (b). The decreasing fluorescence as a function of temperature is shown in (c). These spatial melting analyses were performed at multiple cycle locations within the image, as indicated. These curves show the raw fluorescence within each region of interest. [5]

This indicated that that amplification was occurring, and agreed qualitatively with the real-time data obtained on the LS-32. Within the higher cycle channels, the strong fluorescence that was observed at lower temperatures abruptly disappeared at a specific and consistent vertical position. This transition signaled the denaturation of the specific

PCR product. An amplification curve and multiple DNA melting curves were extracted from the acquired images.

The amplification curve, as shown in Figure 2-3, included one data point for each cycle. Each data point was obtained by averaging the intensity of a pair of 10 x 10 pixel squares, one at a vertical position where the product was double-stranded (labeled “signal” in the figure), and the other at a vertical position where the product was single-stranded (labeled “background” in the figure). The difference between these two values (signal minus background) was used as the data point in the amplification curve shown in Figure 2-3. A first order Savitzky-Golay filter was also used to obtain a best-fit line through the data points. The resulting curve is also shown in the figure.

Spatial melting curves, shown in Figure 2-3, were obtained from cycles 10, 14, 16, 18, and 22 of the image shown in Figure 2-3. Using the GUI, a 13 pixel wide vertical line of fluorescence intensity was used produce the DNA melting curves shown. Although a single vertical pixel line could be used to characterize the melting within a channel section, this 13-fold spatial redundancy resulted in a significant increase in the SNR, which approached 200 for higher cycle melts. The curves shown in Figure 2-3 constitute the raw fluorescence data, as no additional smoothing was performed.

The amplification of both the 181 bp and the 110 bp targets were examined with this spatial analysis technique. Figure 2-4 compares the DNA melting curves and derivative plots for these two PCR targets. Both data sets consist of a 7 pixel wide line cluster, minimally smoothed using a first order Savitzky-Golay filter. The variation between the melting temperatures and melting profiles of the two products agrees

qualitatively with the control amplification and analysis experiments performed on the LS-32.

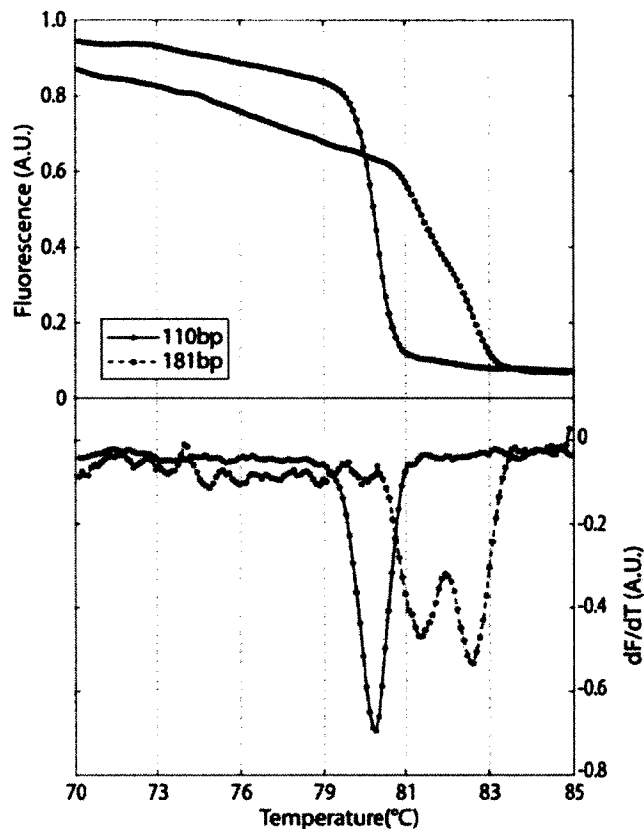


Figure 2-4 The melting behavior of the PCR products was imaged while the DNA was undergoing a spatial PCR process. The melting temperatures of both targets were verified on the LS-32. As expected, the 110-bp target was characterized by a single melting regime, while the 181-bp target displayed two melting regimes. Such variations in the melting profile – not just the melting temperature – are sequence-specific characteristics that serve as “fingerprints” of the different PCR targets. Identical processing of both data sets included a 7-fold spatial redundancy and minimal smoothing. [5]

While comparison between spatial melt curves has been used to genotype SNPs [12], the extent of the product analysis that was performed with the homozygous samples from this current study concluded that the process did in fact amplify the desired

sequence, and that *only* the desired target was amplified. For all experiments, images such as that shown in Figure 2-3 were analyzed to confirm the specificity of the spatial PCR, differentiate the products, and to obtain qualitative efficiencies for the respective experiments.

2.6.4 Robustness

The combination of aminosilane-coated glass and the surface passivation step were expected to reduce the reagent adsorption that can prevent initial amplification of the PCR mixture [3]. By monitoring the fluorescence of the PCR mixture as it filled the microchannel, the effect of this surface passivation protocol was examined. The air/liquid interface at the leading front of the PCR mixture can be seen in Figure 2-5.

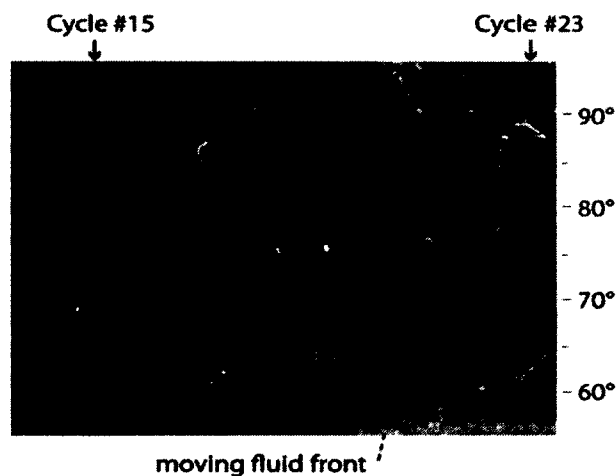


Figure 2-5 By pre-treating the microfluidic channel, amplification of the PCR samples occurred immediately. This image shows the air/fluid interface at the front of the flowing PCR mixture. The fluorescence of the sample is indicative of amplification, as is the observable melting transition of the amplifying DNA in the previous cycles. [5]

The melting transitions are clearly observable in these leading microliters, thereby confirming the initial PCR biocompatibility of the microchannel. The extended

biocompatibility of the system was also evaluated by identifying any change in the amplicon melting within a selected heating region over time. DNA melting curves from cycle 22 were measured after 10, 40, and 80 μl of the PCR mixture had been amplified. No statistical change in the melting curves was observed (data not shown). The thermal robustness of the glass-composite device was examined by quantifying changes in the spatial melting as a function of volumetric flow rate. Figure 2-6 shows the fluorescence, normalized in intensity only, for flow rates between 0.5 and 4.0 $\mu\text{l}/\text{min}$.

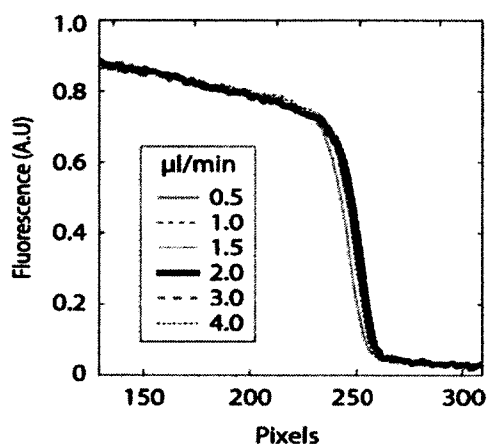


Figure 2-6 The spatial melting curves at six flow rates are shown in this graph. The maximum melting temperature variation between these 6 curves is about 5 pixels, or 0.15 mm. To accurately compare the shape of the melting transitions, the fluorescence intensities of these 6 curves were normalized with respect to each other. The data shown here has not been smoothed beyond the clustering of adjacent pixel lines. [5]

The shapes of the 6 melt curves are virtually identical. The minute shifting in position of the melting transitions are random rather than proportional to the flow rate. The maximum variation between the melting positions for these 6 curves is approximately 5 pixels, or 150 μm of channel length. Since very slight shifting of the optics or of the microfluidic device is anticipated, the differences between the melt curves

at the 6 flow rates are within the uncertainty range of the optical and thermal subsystems. From this, it can be concluded that no significant temperature drifting is occurring within this range of flows. In contrast, numerical and experimental work with continuous-flow polymer microfluidics records significant thermal perturbations with flow rates even as low as $0.45 \mu\text{l}/\text{min}$ [4, 15]. The superior thermal robustness of these glass-composite cf-PCR devices is attributed to the nearly 10-fold higher thermal conductivity of glass over polymer substrates.

2.6.5 Signal-to-noise ratio

A representative image was used to qualitatively evaluate the effect of spatial redundancy and camera exposure time on data quality. Figure 2-7 displays this dependence, as calculated from cycle #22 within a representative image acquired during PCR. The error bars in the graph indicate the maximum variation of the SNR for the 5 values that were collected for each data point. The SNR increased with exposure time. In addition, the irregularity in the SNR also increased with exposure time.

This has been attributed to non-electrical irregularities in the fluorescent signal which would vary with position, such as small bubbles or precipitates within the microchannel, as well as external contaminants such as dust on the surface of the device. The positive effect of increased spatial redundancy is most pronounced for low values, approximately doubling the SNR when a single line is coupled with both its immediate neighbors. It is valuable to note that this inclusion of adjacent pixel lines in the spatial melting analysis – in contrast to averaging in the direction of the gradient – only strengthens the melting signal, and has a clarifying effect, rather than a smudging effect

on the data. This benefit is a product of the spatial redundancy naturally inherent in such systems, and is independent of the time of the experiment.

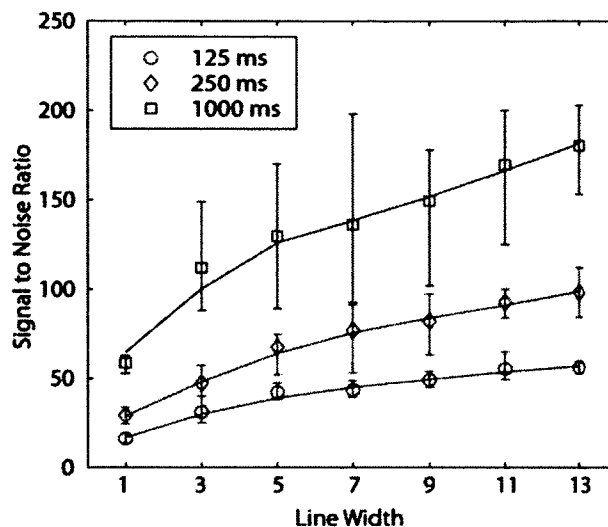


Figure 2-7 Images were taken with exposure times of 125, 250, and 1000 ms. Spatial melting analyses were performed at 5 arbitrary horizontal positions with cycle 22 of these images, and for 7 different pixel line widths. The SNR associated with the spatial melting analysis of a given fluorescence image is a function of both the exposure time and the degree of the spatial redundancy in the image. [5]

The relatively high SNR obtained with this system is very promising, given the grade of the CCD camera used for this work. By upgrading the optical system with a larger CCD pixel array, or by cooling the CCD chip, it is anticipated that the SNR would increase substantially. Even without these improvements, however, the current version of this system can achieve a SNR with a one second exposure time that exceeds the SNR obtained by some commercial systems after an hour long DNA melting analysis[22].

2.7 Conclusion

A low cost microfluidic device for simultaneous DNA amplification and identification was fabricated using a rapid prototyping technique. An iterative design, testing, and re-design process was achieved with minimal time and expense. The microfluidic device was comprised of a patterned polymer film adhered between two unpatterned microscope slides. The final product was a composite structure of approximately 96% glass, thereby maintaining essentially the same thermal and biocompatibility properties of glass. By inducing a steady-state thermal gradient in the substrate through which the PCR mixture was steadily pumped, temperature cycling was performed and efficient, specific amplification was achieved. A 23-cycle PCR was achieved on the device within 15 min, during which the amplifying plasmid target was detected and positively identified. This was done by quantifying the spatial fluorescence distribution produced by an intercalating dye in the mixture. Signal-to-noise ratios on the order of 200 were achieved with an entry-level CCD camera by evaluating areas of fluorescence rather than lines of fluorescence.

With the fabrication technique used in this work, the necessary expense of cf-PCR development and testing is significantly reduced. The virtually unmatched ease of iterative design is coupled with lower cost materials and equipment, while preserving much of the functional advantages of glass microfluidics. The experimental technique presented in this chapter incorporates the analytical features of real-time PCR into the cf-PCR platform. In addition, the PCR becomes the final process of a genetic test, with the DNA being characterized while within the cf-PCR channels themselves. The *in situ* melting analysis of the PCR product can be achieved by analyzing data obtained before

the reaction is even completed, without interrupting the amplification process. By incorporating such optical analysis, cf-PCR now achieves a significant versatility, which is a welcome companion to its already proven speed and simplicity.

CHAPTER 3

GENOTYPING FROM SALIVA WITH A ONE-STEP MICRODEVICE

3.1 Overview

In this chapter a genotyping system is represented using a thermal gradient field for three separate processes: sample preparation, PCR and melting analysis. All three processes are simultaneous and result in a functional process within the microfluidic chip. Some sections of this chapter were published in a paper written by the author of the dissertation as “*Genotyping from saliva with a one-step microdevice*”, in *Lab Chip*, (2012), p2514-2519 [6].

3.2 Abstract

This chapter presents a disposable microfluidic device for on-chip lysing, PCR and analysis in one continuous-flow process. Male-female sex determination was performed with human saliva in less than 20 min from spit to finish, and requiring only seconds of manual sample handling. This genetic analysis was based on the amplification and detection of the DYZ1 repeat region unique to the Y-chromosome. The flow-through microfluidic chip consisted of a single serpentine channel designed to guide samples through 42 heating and cooling cycles. Cycling was performed by matching the local channel geometry to a steady-state temperature gradient established across the

microfluidic chip. Thirty-eight channel segments were designed for rapid low volume PCR, and four were optimized for spatial DNA melting analysis. Fluorescence detection was used to monitor the amplification and to capture the melting signature of the amplicon was performed with a basic 8-bit CCD camera. The microfluidic device itself was fabricated from microscope slides and a double-sided tape. The simplicity of the system and its robust performance combine for elegant solution for lab-on-a-chip genetic analysis.

3.3 Introduction

Genetic analysis commonly involves three processing stages: 1) sample preparation, 2) DNA amplification by PCR, and 3) subsequent analysis of the amplified product. Researchers have worked toward the miniaturization and integration of these processes into lab-on-a-chip systems. This has been done by creating physically separate modules that interface together [23], as well as by creating monolithic devices that perform the separate processing stages at different locations on the chip [24, 25]. With raw engineering force, the required array of pumps, valves, and feedback sensors neatly orchestrate the precise movement, washing, mixing, thermal cycling, and eventual analysis of each sample. While such a design methodology is functional and versatile, the result is a significantly intricate system requiring elaborate external sensing and control. This complexity has contributed to the current challenges of such systems for widespread adoption [26]. In this chapter, a microfluidic device is presented which performs complete processing and analysis of human saliva samples in a single channel, and under unchanging operating conditions.

3.3.1 Full integration

A partial response to this integration need was demonstrated previously [3], but did not combine the sample pre-processing steps. In the previous work, Crews et al. created a microfluidic system on which human genomic DNA was amplified (30 PCR cycles) and analysed (spatial DNA melting analysis) in approximately ten minutes. This was achieved by performing both processes simultaneously within a single continuous flow microchannel, under steady-state flow and thermal conditions [7]. While this represented a significant stride beyond existing devices, only purified and highly concentrated DNA samples could be used. This required the additional preprocessing of each sample, which took well over an hour using conventional DNA extraction protocols and laboratory equipment. Therefore, without the additional microfluidic integration of the sample preparation steps, the combination of PCR and melting curve analysis (MCA) into a single step represented only a marginal improvement of the complete genetic analysis process. In this chapter, the successful integration of the sample processing is finally achieved, effectively liberating the entire microfluidic analysis procedure from the final macro-scale bottleneck. The overarching objective of this work was to do so with the least possible increase in the physical or functional complexity of the system itself.

3.3.2 Sample preparation

Solid phase extraction is particularly popular in microfluidic systems because this method lacks the long incubations and manual sample handling used in conventional techniques. These microscale DNA extraction processes typically require three successive reagent flows across a solid support to successively bind, wash, and elute the DNA which is then conducted to the next stage of processing [27]. However, researchers

have developed techniques to bypass this multi-step extraction process and perform PCR directly, by inactivating the inhibitors in the sample. Chomczynski et al. [28] developed an alkaline lysis buffer that allows direct PCR from culture cells, tissues, and whole blood. Inhibitors were inactivated after simply incubating the sample and buffer at room temperature for 15 min prior to the PCR. Park et al. [29] have demonstrated a similar performance using a commercially-available buffer that also requires a 15 min incubation period prior to direct PCR. Kermekchiev et al. [30] have made strides toward reducing or eliminating this incubation period by genetically modifying the Taq polymerase enzyme for greater resistance to the inhibitors. These researchers demonstrated direct PCR from blood without incubation. However, this method exhibits poorer performance within flow systems, since any agitation or mixing of PCR mixture containing whole blood can completely halt the amplification process. For the flow-through system presented in this chapter, this inhibitor-resistant Taq mutant was used in the mixture, but saliva rather than blood was used for the biological sample. Saliva has been identified as a quality, noninvasive source of human [31, 32] and microbial [33, 34] DNA for PCR-based genetic testing. With significantly lower concentrations of PCR inhibitors than whole blood, saliva has been used for direct PCR on conventional laboratory-based PCR systems [35].

3.3.3 Assay selection

The DNA target that has been amplified for the validation of this current device is a 108-bp segment of the DYZ1 region within the human genome. Since the DYZ1 sequences are located only on the Y-chromosome, PCR amplifications of the DYZ1 have been used for gender determination in forensics [36], athletics, and even *in utero*. An

added advantage is that the 3.4 kb DYZ1 sequence is repeated between 800 and 5,000 times within each copy of the genome [37]. This partially offsets the low template DNA concentration that is expected in dilute saliva samples. Targeting such a repeat sequence circumvents the compromise between pre-PCR sample concentration and a high cycle number amplification protocol.

3.3.4 Fabrication method

In addition to functional simplicity, a focus in this work has been the application of the xurographic fabrication method [16] to high-cycle PCR microfluidics. xurography, which is an adhesive laminating process for glass microfluidic devices, has been demonstrated for less exacting microchannel geometries [12, 38, 39]. However, in this present work, the technique is being used to generate a feature size and density that approaches conventional bulk microfabrication standards. Aside from its ease and low cost, xurography remains the fabrication method of choice for the current application due to its superior performance over more common polymer and glass techniques. Since the current device is a flowing thermal system, a glass substrate will reduce the thermal distortion due to advective effects by approximately 80% over polymer alternatives [4]. In addition, the optical properties of xurographic microfluidics are unmatched. This is because fluorescence imaging occurs through virgin glass surfaces, untouched by chemical etchants, mechanical grinders, or thermal annealing processes that all introduce optical aberrations. Because of these advantages that xurography provides, this current work serves to extend its utility by refining the dimensional constraints associated with this fabrication method.

3.4 Methods

The basic operating principle of the system is as follows: Saliva is collected into medical grade water to initiate osmotic lysis of the cells. A portion of this diluted sample is immediately combined with the PCR reagents and thermocycled through 42 amplification cycles. Complete lysis of the cells is expected within the first heating cycles. With an intercalating dye included in the PCR mixture, fluorescence imaging of the sample during thermocycling will reveal amplification. As the mixture experiences its final heating and cooling cycles, fluorescence imaging will be used to determine the melting behavior of the amplifying sample during the temperature induced transition between its double-stranded and single stranded DNA configuration. This DNA melting analysis will be used to identify the gender of the saliva donor. Since the sample is analysed during its amplification, no post-PCR processing is required. In the device presented in this chapter, the thermocycling required for this experimental procedure was performed by continuously flowing the sample through a stable temperature gradient [7]. The microfluidic device was heated such that a one-dimensional temperature gradient formed within the substrate containing a serpentine microchannel. The flowing sample was heated and cooled by heat transfer between the fluid and the microchannel walls. The three-fold advantage of this cycling protocol is: 1) the accelerated cycling achieved by reducing the thermal mass to just that of the PCR mixture [2], 2) the reduced system complexity associated with steady heating and steady flow, and 3) with the entire reaction spread spatially instead of over time, a single fluorescence image can provide the cycle-dependent fluorescence (analogous to quantitative PCR) and the temperature-dependent fluorescence (i.e. DNA melting analysis) of the complete process at once [39].

3.4.1 Spatial temperature distribution

A quasi-linear temperature gradient was formed across the microfluidic device by maintaining two parallel edges of the substrate at different temperatures. Depending solely on the two set-point temperatures, which were each held constant using independent closed-loop control, an unchanging temperature distribution would develop within the microdevice. Infrared thermometry was used to map the surface temperatures, and fundamental heat transfer theory was used to extrapolate the temperatures at the channel depth, as detailed previously [7]. In this way, the temperature at all points within the microfluidic channel was approximated with an accuracy of ± 1 °C. This accuracy is strictly applied to the no-flow condition, rather than when the sample is being pumped through the device. The perturbation of temperature fields due to flow-induced thermal advection is well documented. To minimize this effect, fluid flow rates were kept within the limits previously established for this type of system. After initial calibration of the system with an infrared camera, the user-controlled set points alone were used to infer the temperature distribution throughout the entire microsystem.

3.4.2 Microfluidic device design and fabrication

The microfluidic channel consisted of 42 serpentine passes, 38 of which were optimized for PCR and the remaining four optimized for spatial melting analysis. The geometry of channel is shown in Figure 3-1. The type 1 geometry was designed to minimize volume and optimize the heating and cooling rates according to known reaction kinetics [40]. Since the channel width is inversely proportional to the heating rate experienced by the flowing fluid, the widest section (600 μm) of the channel was

designed to be at approximately 70 °C, where the DNA polymerase approaches maximum activity. The width then decreased linearly to 250 μm at 95 °C.

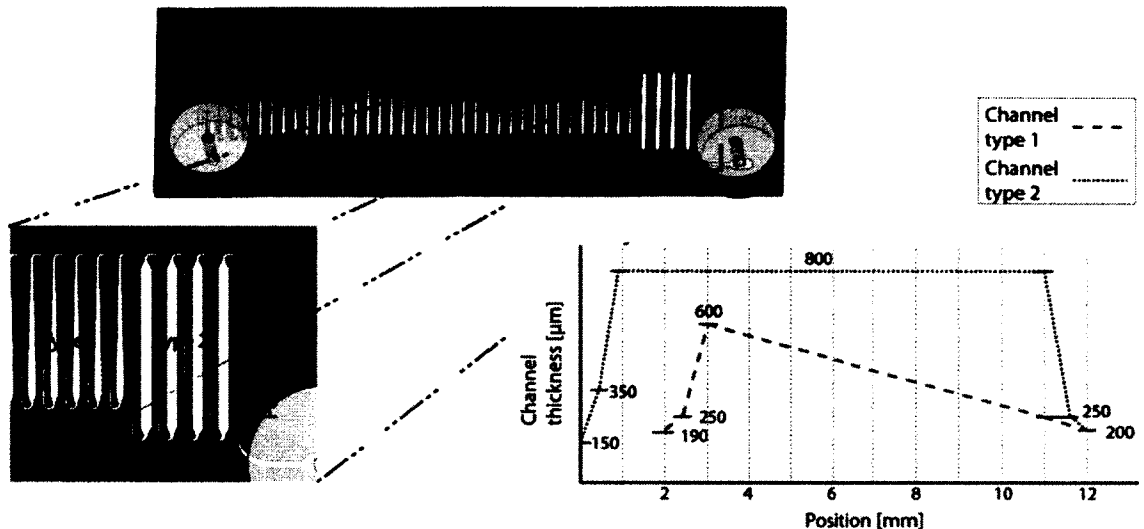


Figure 3-1 The microfluidic device (top) was designed with 38 type 1 and four type 2 channel segments as indicated in the inset (bottom left). The type 1 was optimized for rapid PCR, and the type 2 was optimized for fluorescence acquisition of the DNA melting during amplification. The width of the channel as a function of vertical position is shown in the graph (bottom right) for both types. [6]

The channel segment corresponding to the cooling of the sample from its denaturation to its annealing temperature is 150 μm wide, which was found to be the minimum reliable feature size for the specific polymer film used in this fabrication technique. The ratio of the heating and cooling rates for the type 1 geometry is 3.32. The type 2 geometry used for the final four thermal cycles, was a uniform 800 μm and 150 μm wide for the heating and cooling sections, respectively. Since the spatial melting analysis would be performed from a fluorescence image of the final heating sections, the constant width would allow for increased spatial redundancy. The type 2 geometry was

also extended to lower temperatures to maximize the temperature span of the analysis. The fabrication technology has been described in detail previously. Briefly, a thin double-sided tape (100 μm thick, including the polyimide film and silicone adhesive) was patterned by cutting out the desired channel shape. The tape was then sandwiched between two passivated microscope slides, forming a microfluidic channel with a rectangular cross section and sidewalls of both tape and glass. The width of the cross section was determined by the pattern in the tape, and the height of the channel was formed by the thickness of the tape. With the channel dimensions described above, the surface area in contact with the PCR reagents was roughly 75% glass and 25% polyimide/silicone, having a total surface to volume ratio of approximately 27 mm^{-1} .

3.4.3 Microchannel passivation

Passivation of the microfluidic channel was particularly critical due to the unrefined nature of the saliva PCR mixture. In the previous work, only a dynamic BSA passivation scheme was employed [4]. This contributed significantly to the need of that system for only pre-purified and pre-concentrated DNA template. Biocompatibility of the microchannel surfaces was achieved with a two-part passivation process, one before and one after device assembly. The pre-assembly passivation protocol has been described previously [38]. Briefly, the glass was silanized with a dimethyldichlorosilane (DDMS) monolayer that was formed using a liquid-phase deposition process. After device assembly, 60 μl of a buffered dye mixture was injected through the microfluidic channel, as detailed previously [38]. The mixture consisted of 6 mM MgCl_2 (Sigma-Aldrich, MO, USA), 0.5 ml/ml Tween 20 (Sigma-Aldrich, MO, USA), and 2X LCGreen (Idaho Technology, UT, USA) in a 50 mM Tris (pH 8.3) buffer.

3.4.4 PCR reagents

A master PCR mixture was prepared, containing all reagents with the exception of the template DNA. The mixture contained 0.5 μM of each of the forward and reverse primers (Integrated DNA Technologies, IA, USA), 200 μM of each deoxynucleotide triphosphate (dNTP) (Sigma-Aldrich, MO, USA), 0.08 U/ μl of KlenTaq1 polymerase (AB Peptides, MO, USA), 1.2 U/ μl of Anti-Taq monoclonal antibodies (eEnzyme, MD, USA), 6 mM MgCl_2 , 0.125 mg/ml BSA (Sigma-Aldrich, MO, USA) and 2X LCGreen in a 50 mM Tris (pH 8.3) buffer. The primers used in this experiment define a 108-bp long section of the DYZ1 sequence. The primer sequences used for this work are those validated previously by Lo et al. Diluted saliva samples were added to this mixture immediately prior to thermocycling. Saliva samples were obtained from male and female volunteers. Immediately after a volunteer would expectorate saliva into a specimen cup, 20 μl of the saliva was diluted into 80 μl of medical grade water, and shaken for approximately three seconds. A portion of this dilution was then combined with the PCR reagent mixture to a final saliva concentration of 2%.

3.4.5 Experimental protocol

To validate the functionality of the prototype device, the PCR solution was divided immediately after preparation. A portion was loaded in a syringe for direct analysis on the lab-on-a-chip, and a portion was loaded into capillaries for analysis on a commercial real-time PCR instrument (LS-32, Idaho Technology, UT, USA).

3.4.6 Lab on a chip

The general optical and thermal setup for the lab-on-a-chip testing has been described previously [39]. Since a stable temperature gradient would form within

approximately five minutes after powering up the thermal control system, heating of the device was initiated shortly before the collection of the saliva. Once the PCR mixture was prepared, it was injected by syringe pump through the microchannel at a constant flow rate of 2 $\mu\text{l}/\text{min}$. When the mixture filled the entire microchannel, the chip was illuminated with a diffuse and filtered LED [1]. The sample undergoing the final few heating and cooling cycles was imaged (800 ms exposure, gain 0.88) with an uncooled 8-bit monochrome CCD camera (PL-B953U, PixeLink, Ottawa, Canada). The image was imported into a MATLAB (MathWorks, MA, USA) graphical user interface (GUI) that was developed by the authors for spatial melting analysis. The GUI provided interactive selection of the channel(s) for analysis, as well as analysis parameters such as width, position, and degree of smoothing [39]. For some experiments, images were acquired before and after the sample first filled the microchannel in order to monitor the progress and stability of the reaction.

3.4.7 Control and validation

The samples analyzed on the LS-32 were evaluated as controls in order to validate the performance of the microfluidic system. The LS-32 amplification protocol consisted of 32 cycles of 3 s at 96 °C, 3 s at 65 °C and 3 s at 72 °C with a 5 °C/s ramp rate between temperatures. After PCR, the LS-32 performed a DNA melting analysis with a heating rate of 0.3 °C/s during which fluorescence was continuously acquired.

3.5 Results and Discussion

PCR mixture filled the microfluidic device approximately 13 min after the pumping was initiated. Prior to filling the channel, as the sample approached cycle 38, fluorescence was already detectable (in the male saliva experiments only). This

fluorescence lagged slightly behind the fluid front, such that the fluid was at cycle 38, but no fluorescence was observable above cycle 36. Right as the chip filled, the fluorescence had not yet reached the final cycle, but continued to advance as pumping continued. After approximately 15 min, fluorescence was detectable in the 42nd channel. The intensity of the fluorescence continued to increase until it reached a stable appearance approximately 18 min after pumping was initiated (see Figure 3-2). Although 18 min was required for the fluorescence signature of each sample to completely stabilize, distinctly different fluorescence intensities (for male versus female saliva donors) were present much sooner in the microdevice. The observed lag of the fluorescence behind the flowing fluid front was attributed to an imperfect passivation of the microchannel during the device assembly. In such a case, reagents in the flowing fluid would adsorb onto the channel walls, thereby depleting their solution concentration.

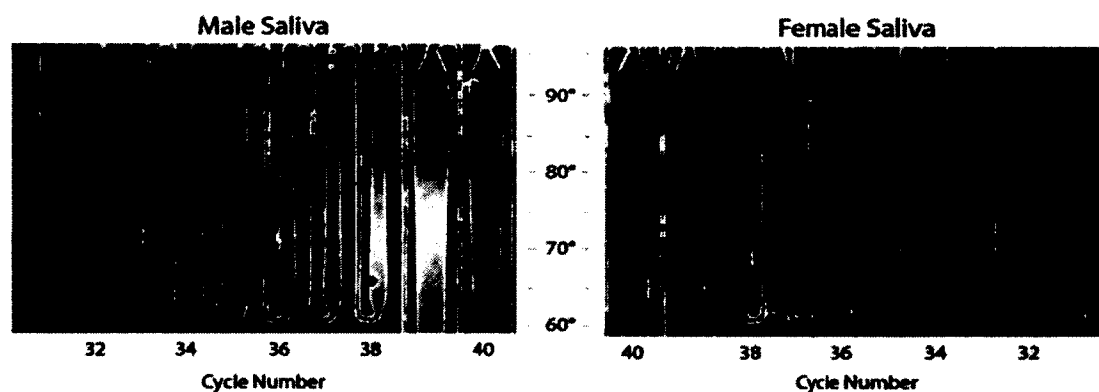


Figure 3-2 Fluorescent images of the microfluidic channel are shown for the male (left) and the female (right) saliva samples. The images are mirrored for easier visual comparison. The PCR cycle number is indicated below the images, and the approximate temperature is shown between. These images were taken after approximately five minutes of continued pumping beyond the filling of the microdevice (18 min after pumping was initiated). [6]

The principal suspect in these experiments was the intercalating dye, since PCR of the foremost solution was detected (using saliva from a male donor) by adding additional LC Green to the first elution of the microdevice and performing a DNA melting analysis on the LS-32 (data not shown). Amplification of the saliva from male donors resulted in a strong fluorescence signature. Cooler temperature fluorescence was observed to appear late in the PCR and increase to a high level in the final cycles. In addition, the distinct quenching of the fluorescence was visible at a specific horizontal location (i.e. temperature) within the device. This indicated a concentrated PCR product with high specificity. In contrast, direct PCR from saliva from female donors resulted in only a faint fluorescence in the final cycles, lacking a sharp temperature-dependent fluorescence transition. This was indicative of non-specific amplification, thereby verifying that the DNA sequence amplified from the male DNA was not present in that of a female. Using the MATLAB GUI, the images were analyzed in order to generate DNA melting curves and derivative plots for the amplifying samples. Melting curves (fluorescence versus pixel) and derivative plots (the negative slopes of the melting curves) for the images in Figure 3-2 are shown in Figure 3-3. For the melting curves for both the male and the female DNA, the fluorescence decreases to the left of pixel 275. This is attributed to the non-uniformity of the light source, which can also be seen visually in Figure 3-2. This gradual fading with the weakening excitation light is markedly different from the sharp quenching that begins near pixel 400. This latter fluorescent signature indicates the melting of the DNA. The derivative plot of the male sample gives a strong single peak at that location, while the female sample shows several small erratic peaks on the same scale as the background noise.

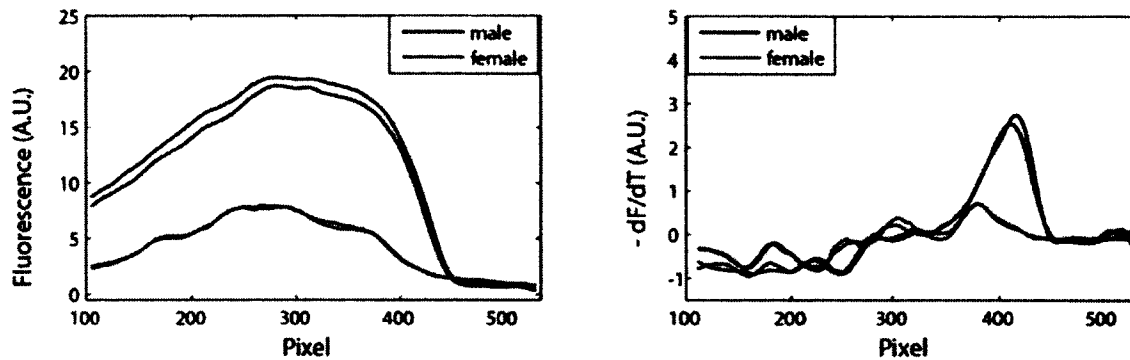


Figure 3-3 The spatial melting analysis of the images shown in Figure 3-2. The graph on the left shows the melting curves taken from the two images. The graph on the right (the derivative plot) is the negative of the slopes of the melting curves on the left. [6]

These lab-on-a-chip results were compared with the direct PCR and subsequent melting analysis performed on the commercial instrument. The DNA melting curves and derivative plots for the LS-32 control experiments are shown in Figure 3-4. As in the microdevice, the male and female samples can be clearly differentiated. PCR product from male saliva results in a strong fluorescence with a single melting temperature at approximately 81 °C. The female PCR only provides minor nonspecific products. In addition, the amplified sample from the male saliva has been verified as 108-bp in size using gel electrophoresis (data not shown).

The lysis approach used in this work was a combination technique: bursting of the cell membrane through osmotic shock, followed by thermal cycling. The osmotic lysis was induced by diluting the saliva into pure water so that the cells would swell to bursting. No pause was made to ensure complete lysis, but rather the PCR mixture was quickly prepared and subsequently thermocycled for amplification.

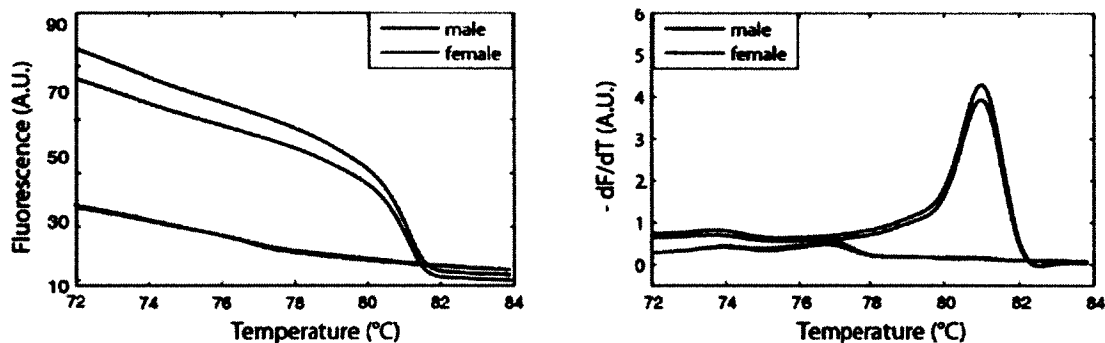


Figure 3-4 DNA melting analysis of the male and female saliva on the LS-32. The melting curves are shown on the left, and the derivative plots on the right. [6]

The PCR protocols for both the lab-on-a-chip and the LS-32 did not incorporate an initial hold at high temperature before cycling. Rather, rapid heating and cooling through the PCR temperatures was initiated immediately. It was hypothesized that this cycling would complete the cell lysis process within the first due to the exponential nature of PCR.

Such an analysis was applied to the protocol presented in this chapter. If satisfactory lysis required multiple heating and cooling cycles, then the PCR would be delayed significantly. On the other hand, if DNA was released completely during the osmotic lysis, then no delay in PCR would result. To determine the effectiveness of the osmotic lysis, PCR and melting analysis was performed on the LS-32 with samples prepared as explained above. For the control reaction, the PCR mixture was held at 95° C for 5 min before the PCR cycling was performed (which is a standard technique to ensure that the cells are completely lysed prior to thermocycling). Results of these tests were compared with PCR experiments where thermocycling was initiated immediately after the mixtures were prepared. Representative amplification curves from these tests are shown in Figure 3-5.

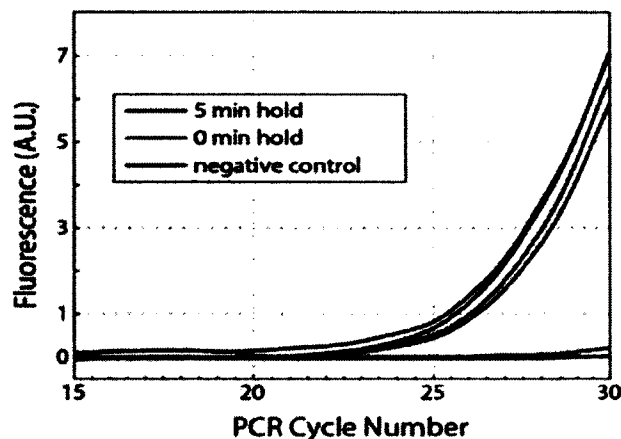


Figure 3-5 The effectiveness of the osmotic lysis was evaluated by determining the impact of an additional five minute thermal lysis between sample preparation and the PCR thermocycling.[6]

Only a minor delay in the PCR was observed when the five minute hold was not instituted, calculated as 0.49 ± 0.033 cycles. This indicated that a high percentage of the cells were adequately ruptured either from the osmotic lysis alone, or promptly within the first denaturation step of the PCR cycling. It was thus concluded that the quickness of the PCR sample preparation did not delay the PCR amplification.

3.6 Conclusion

The experimental microfluidic device was able to perform gender determination directly from saliva. Forty-two PCR cycles were completed in less than 15 min, during which the fluorescence signatures of the amplifying DNA were analyzed. A DNA melting analysis was used to identify the distinct differences between PCR product from the male and female samples. This differentiation was due to the PCR target chosen for these tests, which was a portion of the DYZ1 repeated sequence found only on the Y-chromosome of the human genome. No extended lysis of the cells in the saliva was

necessary, since the saliva was first diluted into pure water for several seconds before being added to the other PCR reagents. No purification of the DNA from the other biological material remaining after lysis was needed. This was because an inhibitor-resistant DNA polymerase enzyme was used for the PCR. Since thermal cycling of the PCR mixture was performed by passing the fluid through a serpentine microchannel embedded within a stable temperature gradient, precision PCR was performed at a rate of approximately 20 sec per cycle. This was done under steady-state thermal and flow conditions characterized by low power consumption and minimal feedback control. The analysis of the PCR-amplified saliva samples occurred during amplification, from within the PCR microchannel. Therefore, all processes to perform this genetic analysis of raw saliva samples was performed in a single flow channel, under uniform conditions, in an elegant one-step process.

CHAPTER 4

SPATIAL MELTING ANALYSIS - APPLICATIONS

In this chapter two different applications for spatial melting analysis are represented. In the first application, melting analysis and spatial melting analysis are used for quantitative and qualitative description of non-ionizing radiation damage. Some images and captions in the following chapter regarding continuous non-ionizing radiation effects on DNA were published in a paper written by the author of the dissertation as “Real-time damage monitoring of irradiated DNA”, in *Integrative Biology*, Volume 3, (2011), p937-947 [1]. In the second part a conjunction of capillary induced forces and spatial melting analysis is used to create a system in which there are no fluidic components apart from the device itself. By performing passive pumping using nano-silane layers the system was simplified and brought down to only heating and optical subsystem.

4.1 Spatial Melting Analysis for Continuous Non-ionizing Damage Detection in DNA Samples

The goal of this project was to track intermolecular behavior of DNA in real time and its possible distortions due to radiation, particularly DNA deformations called photoproducts. Spatial melting analysis showed to be a very convenient method for real

time phenomena tracking due to its very practical isoflux nature; in the course of the process a constant amount of heat is provided to the system over time, enabling a suitable environment for all fluid flowing through to be analyzed. Once the fluid enters the chip due to its very small and finite volume it assimilates to the thermal distribution of the system. Therefore if the microfluidic device has a steady change of temperature present throughout its volume, so will the samples have the same thermal distribution. This phenomenon is valid until a certain flowrate of the fluid is reached, after which the incoming and outgoing fluid would locally cool the system inducing temperature distortions. Since the thermal properties are consistent it would be assumed that if change of the fluorescence signature appears it would be due to intramolecular changes within the DNA itself.

4.1.1 Methods

As shown in the image below Figure 4-1, a very rudimentary but efficient setup was assembled consisting of a UV-C radiation source for sample irradiation, one pump to push the fluid through the system, one microfluidic chip on a heating platform to enable the suitable thermal environment for sample analysis and a camera and lighting to acquire the images continually. The microfluidic chip was designed to have a few serpentine channels to allow analysis redundancy since the chip fabrication method, although economical, is very prone to bubble nucleation due to the laminar-composite nature of the device.

The DNA sequence analysed was 110 bp long originating from an E. Coli bacterial phage. The structure of this sequence is of great importance since the UV radiation provides only a specific deformation called photoproduct.

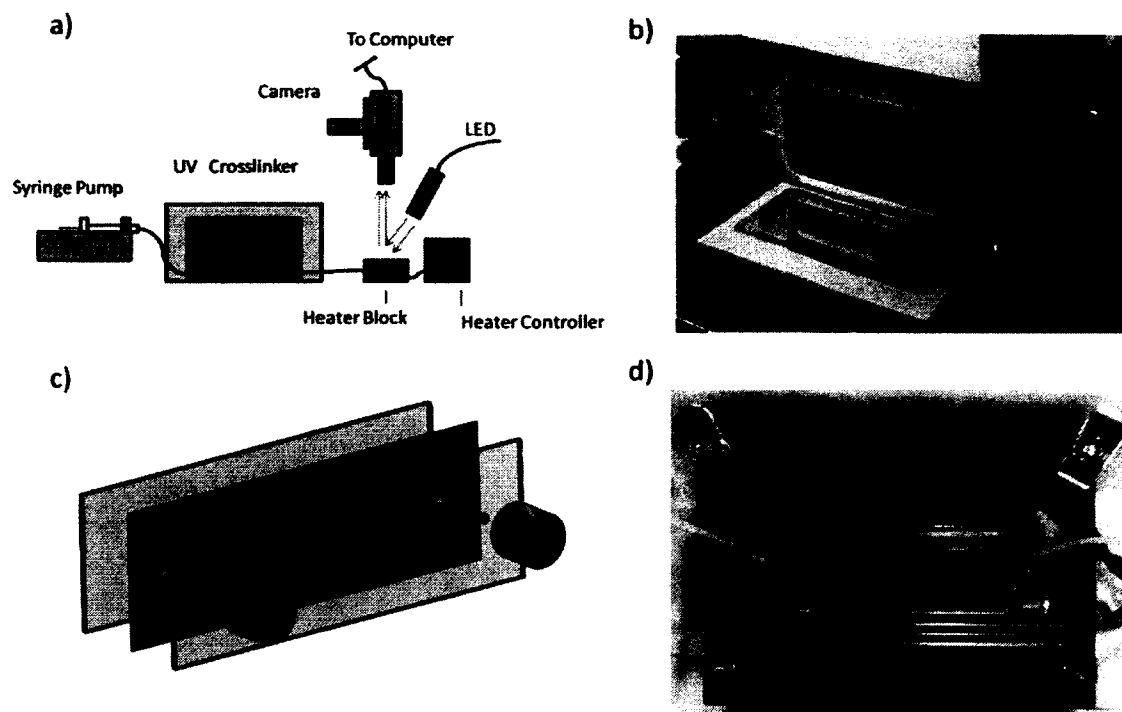


Figure 4-1 a) The analysis system consists of a syringe and syringe pump, small bore tubing, and the spatial DNA melting analysis subsystem. b) For these experiments, the tubing was inserted into a UV crosslinker so that the flowing DNA sample would experience cumulative radiation damage in the form of photoproducts. c) The microfluidic chip was fabricated by cutting a pattern into double-sided Kapton tape, then sandwiching the film between microscope slides. Polymer ports were attached as interfacing for the small bore tubing. d) The microfluidic device was positioned over aluminum strips, which were independently heated to different temperatures. Once heat flow stabilized, a virtually linear steady-state temperature gradient was present in the vicinity of the microfluidic channel. The melting of the DNA, which occurred across this gradient, was observed in the fluorescence of an intercalating dye.[1]

These molecular interactions happen between adjacent pyruvic nucleic bases in form of covalent bonds. Based on previous work of Cadet et al. [41] a visual correlation between the likelihood of photoproduct formation and the DNA sequence structure was created: the higher the bar in between the two nucleic bases the higher the likelihood for the photoproduct formation is present in Figure 4-2. The experimental protocol consisted

of fluid propagating through a longer piece of tubing within the radiation source, immediately after which it went into the microfluidic device for subsequent analysis. The microfluidic device was illuminated with an adequate wavelength light which caused the sample to fluoresce along the thermal field in the chip. A camera, positioned immediately above the setup, acquired continuous images in 5 s increments.

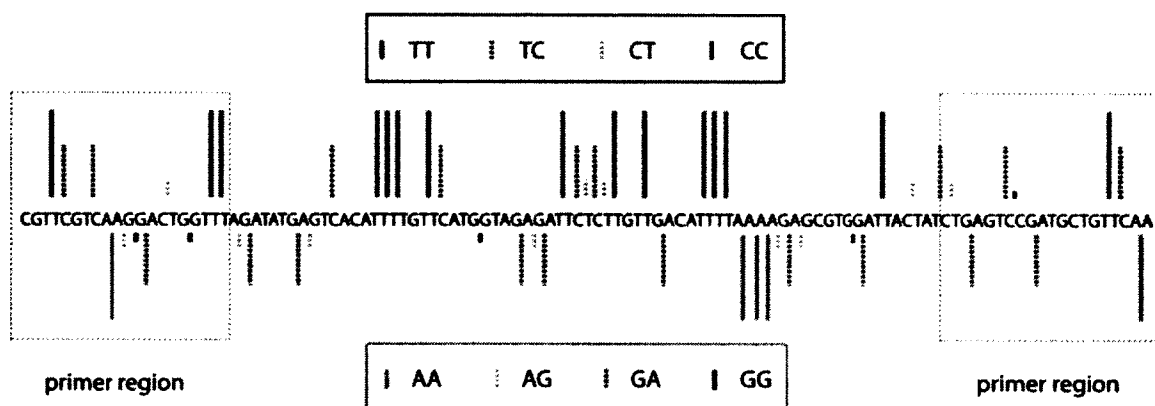


Figure 4-2 The likelihood of photoproduct formation and the DNA sequence structure based on Douki et al. work.[1]

A separate experiment was performed in which the individual strands were exposed to the radiation and subsequently analyzed on a commercial device LS-32 (Idaho Technologies, Utah, USA) using high resolution melting analysis. The purpose of this experiment is to determine whether damage of one DNA strand will be able to cause complete dsDNA disassociation. If so, PCR would not be possible and the primer sequences would have to be designed in respect to the content of adjacent pyrimidic bases. If the primers do anneal, the resulting non functionality of PCR would originate from the inability of the enzyme to perform for one or another reason. Excluding either of the two would provide an important insight in the direction of the future course of action. Using

the same method Ethidium-Bromide (a known carcinogen) was tested to observe changes in the sample fluorescent signature.

4.1.2 PCR

The continuous radiation effect observation consisted of a PCR product using in a previous project presented by Pjescic et al. [38]. The only deviation in respect to the mixture is the concentration of the fluorescing dye present in the mixture for signal enhancement.

In the second part of the experiment, the protocol consisted of making a 2 X LCGreen, 60 mM MgCl₂ in 50 mM Triz buffer premix. Single forward oligonucleotides (a synthetic short DNA sequence), single reverse oligos² and combined forward and reverse oligos were mixed added in the mixture above so that the final yield for all of them is 3 μM. Each batch was heated at 95° C for 2 min in warm water, and subsequently five samples out of each batch was taken and placed in capillaries. The duplex oligos are 10 μl each while the single strands are 9 μl each. After exposing the samples in capillaries to UV-B light incrementally in 100 s intervals (0 – 100 – 200 – 300 – 400 s), in the single strand capillaries 1 μl of the opposing healthy strand would be added. The capillaries would be spun up and down 3 times each and vortexed to achieve homogeneity. Prior to analysis (both standard and high resolution melting analysis performed on the commercial device) a 2 min 95 °C denaturing step was added.

The third section of this experiment involved evaluation of genotoxins and their interaction with DNA. The initial hypothesis is that genotoxins interact directly with DNA, thereby lowering or increasing their binding energy. This would cause the

² 5'-AATCCACGCTCTTTTAAAATGTCAACAAGAGAATCTCTACCACGAACAAAATGTGACTCA -3'
5'-TGAGTCACATTTTGTTCATGGTAGAGATTCCTTGTGACATTTTAAAAGAGCGTGGAITT-3'

gene/sequence to be either unavailable or too available for gene expression. If this assumption is valid for DNA-DNA interaction, it should also hold validity for genotoxin-DNA interaction as well. The most known and easily obtainable chemical in a genetics laboratory that is known to be carcinogenic is ethidium bromide (EtBr). The protocol sample preparation was the same as described for the single stranded DNA radiation test, including the analysis protocol. The hope is to analyze and observe fluorescence changes due to the effects of EtBr. The EtBr concentrations used are 0.1 mg/ml, 0.01 mg/ml and 0.001 mg/ml in the final mixture (the initial EtBr concentration is 10mg/ml); 1 mM oligos were diluted 30 times in DI water to obtain approximately 3 μ M of oligo duplex in the final mixture.

Optical considerations had to be made for this experiment since there is a presence of two dyes, each with its own excitation and emission spectrum. The excitation wavelength of the LS-32 is 470 nm and the excitation profile for EB and the emission for LCGreen is 530 nm coincide. The emission of EB is in the range of 550 nm so it is not in the range of the commercial device sensor.

4.1.3 Results

For the continuous observation of radiation effects on DNA, in the course of the experiment, both the steady state and continuous flow experiment were evaluated yielding similar results of the same nature. In the steady state experiment for double stranded DNA, a gradual retraction of the melting curve can be observed. For easier observation of the phenomena, the first derivative of the melting curve was observed, yielding in a function with a single peak that represents the slope intensity change for each of the melting curves. Two main parameters that are the most obvious and could be

analyzed were the peak position and the peak height (insert figure cross-reference). Both of the parameters showed a consistent change, the melting temperature (peak position) decreased linearly, while the peak height had a non-linear intensity reduction. In the continuous flow experiment, the spatial melting analysis Figure 4-3 yielded a consistent transient change that was able to detect even minuscule changes in time.

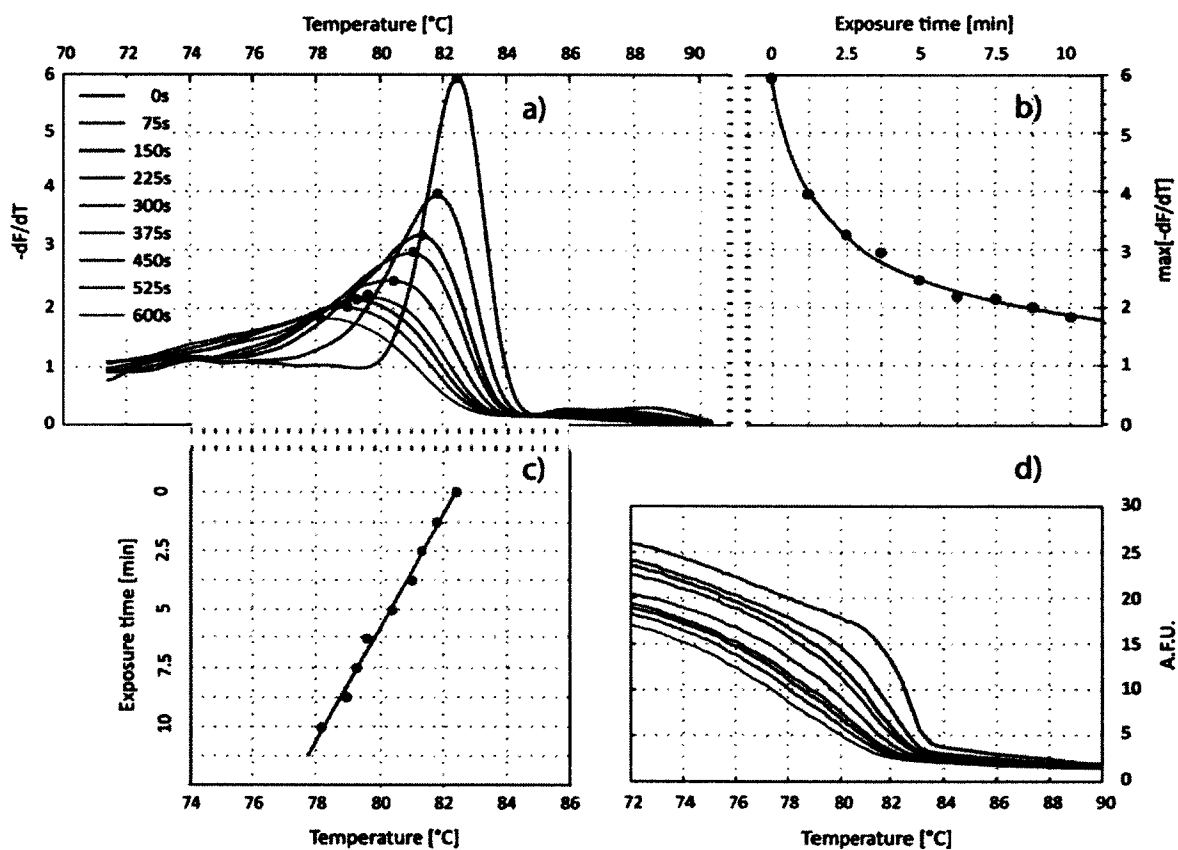


Figure 4-3 Melting analysis of samples with a constantly increased exposure time. In the image it can be seen that the melting analysis (d) is slowly retracting towards lower temperatures and smaller intensities. This effect is expected, since the radiation should create non-specific bonding, therefore lowering the bonding energy of the strands in between each other. [1]

To easily observe the change, the first derivative curves were subtracted from the initial one, creating a diagram that shows only differences and their progressive change. Since the data acquisition system gathered a vast amount of similar curves, for the sake of graphical representation, a grayscale was created where the starting and ending curve are of the same black color, while all in between represent a gradient. To explain the data precision, a segment was selected from the image and enhanced showing more than 20 curves within a much confined space.

In the double stranded DNA disassociation experiment, where single stranded DNA was exposed to radiation and subsequently annealed with its healthy complementary strand, the single DNA had no fluorescence reading but the usual background due to dye presence. This data showed that the single strand DNA, damaged and undamaged, does not create fluorescence signals of comparable intensity as dsDNA. This was an indicator that our observations of fluorescence change would probably be only of double stranded DNA interaction in Figure 4-4.

A significant change in the melting peaks is noticeable, yet the continuous presence of one indicates that no matter what the damage is and how intensive it might be, the complementary strands will anneal with the damaged one. The results regarding the individual oligo stands exposed show a significant shift of the derivative curve for all three cases, forward damaged, reverse damaged, and both damaged (insert figure cross reference). Negative controls, individual strands of reverse and forward oligos melted, were analyzed and no signal was observable, excluding the possibility that any of the acquired data is the strand interacting with itself. In the data analysis they are samples 6 and 11 on Figure 4-5.

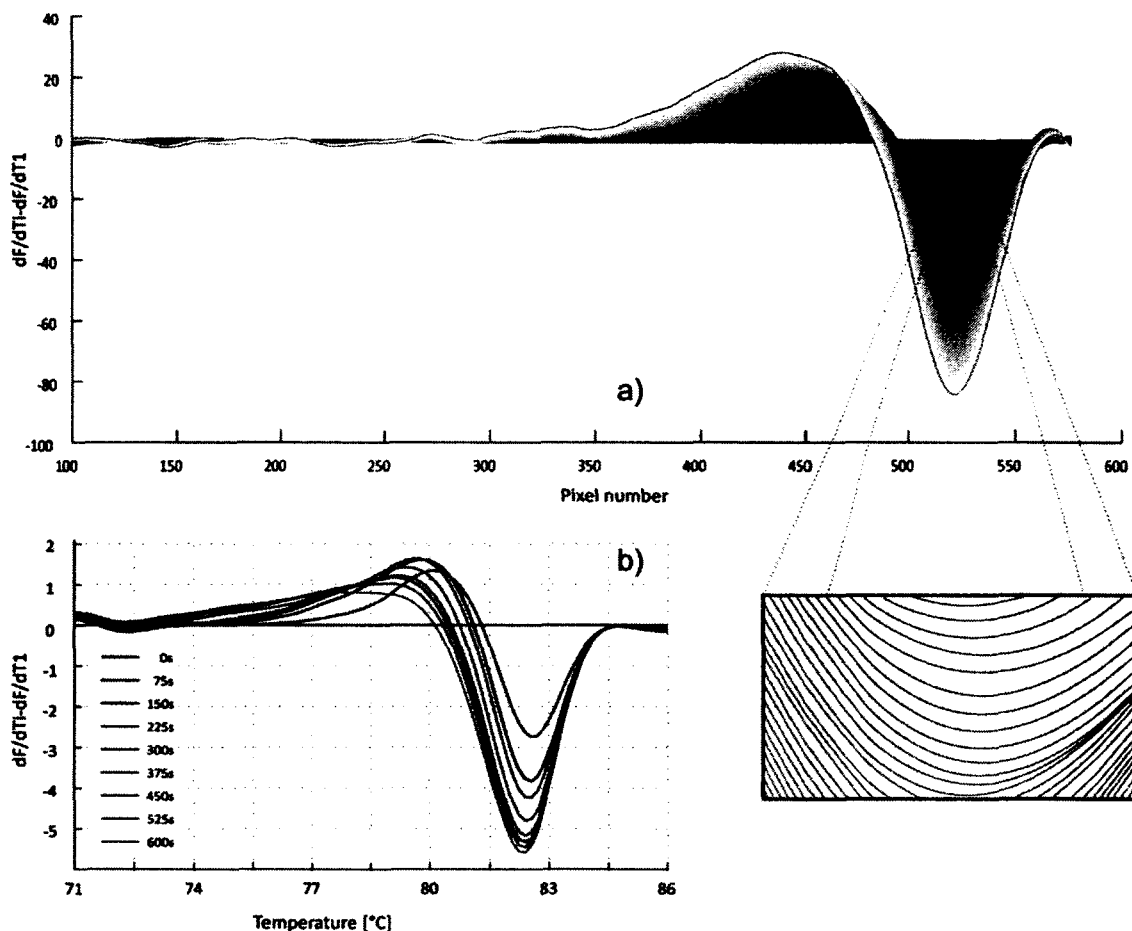


Figure 4-4 The data acquisition system used allowed a very intense data collection process in which infinitesimal changes in the melting curve could be tracked over a longer period of time. To observe the changes more clearly all the curves were subtracted from the initial one and all-together plotted on one diagram. Due to the excessive line density a shade of gray represents the curves, while an insert is zoomed in. The steady state degradation experiment matches in shape the continuous experiment, though there is a much lesser capability of tracking change over the same period of time. [1]

The double stranded oligos (blue=>green) on the left side of the diagram show a consistent deterioration of bonding energy. Likewise, the oligos with damaged reverse (R) and damaged forward (F) segments behave in a similar fashion. Though it is easily seen in the bottom figure that each of the three cases behaves differently, different curve

shapes and heights are achieved at the same exposure times. The gradual intramolecular bonding energy of increasingly exposed samples is significantly altered.

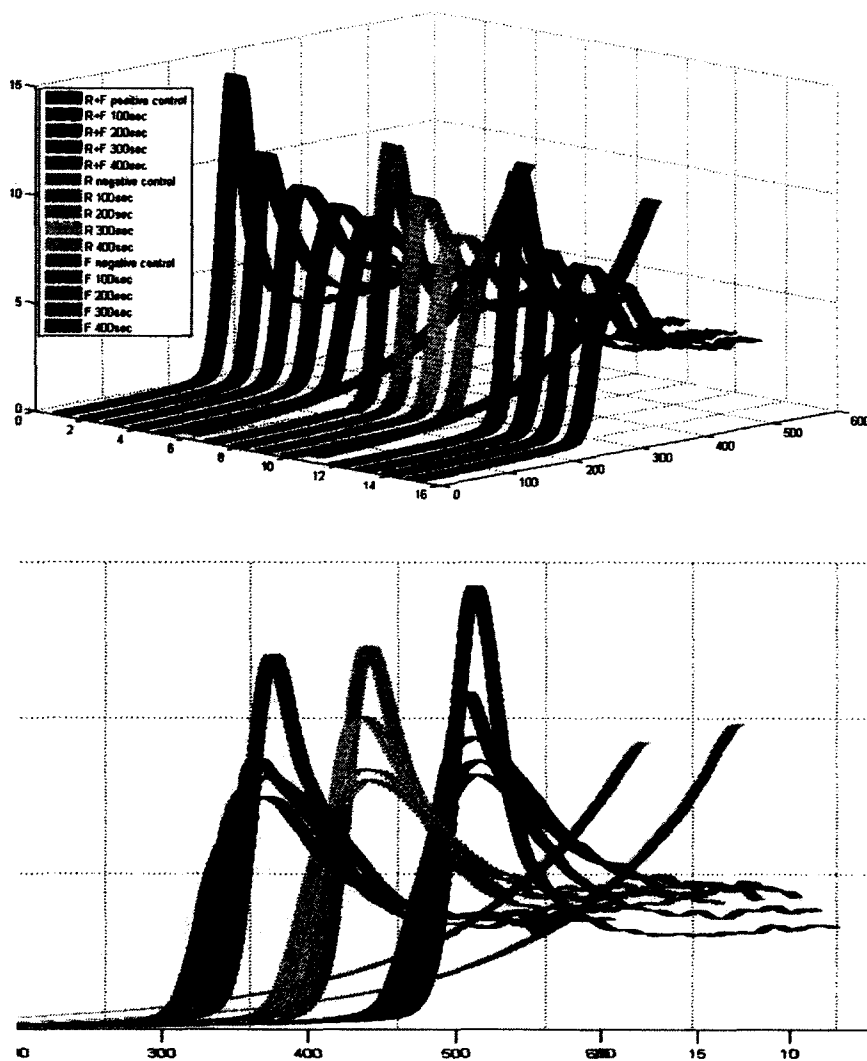


Figure 4-5 The groups are separated by negative controls, single stranded forward and reverse primers (the 6th and 11th sample). The double stranded oligos (blue=>green) on the left side of the diagram show a consistent deterioration of bonding energy. Likewise, the oligos with damaged reverse (R) and damaged forward (F) segments behaves in a similar fashion. Though it is easily seen in the bottom figure that each of the three cases behaves differently, different curve shapes and heights are achieved at the same exposure times.

These exposure times (the UV-B lamps used provide 40 watts of power) are very significant time increments and yet DNA seems to bond to its complementary strand relentlessly. Though this observation was only made on short oligo sequences whereas the genome interaction would be presumably much more complex to analyze and quantify. The genotoxin ethidium-bromide was studied in the third part of this experimental series. The interaction between the double stranded DNA and Ethidium Bromide was evaluated by the means of melting analysis Figure 4-6. The results obtained from this experiment show a consistency in the melting temperature with the rise of EB concentration.

The change is not insignificant, increasing from 78 °C to 92 °C. A similar behavior was noticed (data not shown) with the LCGreen Plus used in all the experiments, a gradual increase of the melting temperature with an increase of relative dye concentration.

This observed behavior indicates that direct genotoxin-DNA interaction can possibly be observed by means of melting analysis. Even if the genotoxin does not interfere with the DNA *per se*, at least that option can be excluded or confirmed.

The backdrop of the applied method, is the use of two fluorescent dyes simultaneously as well as the susceptibility of the LCGreen Plus dye to interactions with alternate compounds. The interaction of the dye and the tested material would have to be run before any further testing to avoid obtaining false positives. Though considering the level of sophistication of PCR and the vast amount of sensitive reagents present in the system, we can say that the LCGreen Plus dye has some inherent neutrality and redundancy in respect to chemical interaction.

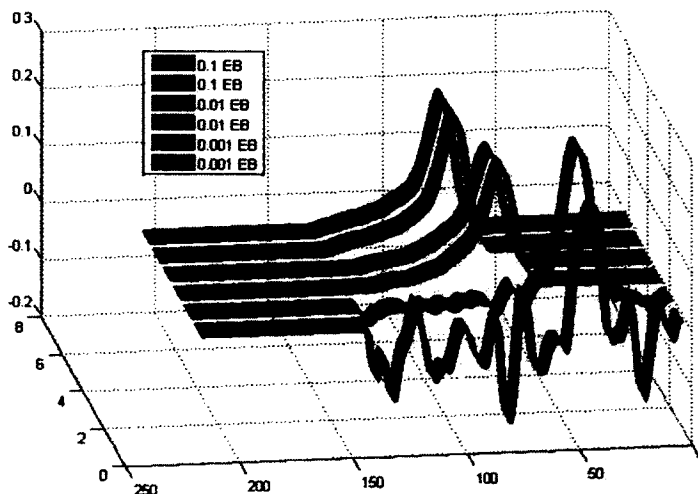


Figure 4-6 The data shown are three sets of DNA samples that contain an ever increasing Ethidium Bromide concentration. All samples were analysed in doubles. The red samples have the least added EB (far), the light blue samples have a 10-fold of that concentration (middle) and the blue have a 100-fold of the initial concentration (near).

4.2 Fast Spatial DNA Melting Analysis using Surface Modified Capillary Pumping

4.2.1 Abstract

The herein presented system has the capability to perform spatial melting analysis of DNA samples on a microfluidic device. The design concept is to passively pump fluid into a microfluidic chip by modifying the substrate surface in a pattern of the hydrophobic and hydrophilic regions. The system apart from the optical and heating subsystems had no fluidic components but the microfluidic chip itself. The chip consisted of two hydrophobic coated glass slides, with a polyimide double sided adhesive layer, acting as a spacer in between. The hydrophobic surfaces were selectively etched to create hydrophilic channel structures, along which the fluid would flow by means of capillary forces. While the pumping was provided by the hydrophilic nature of glass-fluid

interaction, the surrounding residual hydrophobic coating provided directional fluid movement, allowing spatial melting analysis and minimizing the amount of volume needed. Each of the samples loaded would contain 10 μl of fluid volume. Once the system was heated, the analysis for each sample from the loading point of time to the final result was less than three seconds. The fabrication method was non-invasive and did not need any etching or dangerous chemical usage in the fabrication process. The sample loading pads were spaced from each other in such a manner to accommodate an 8-tip pipetter to allow multiple simultaneous sample injections, although potential for more was present.

4.2.2 Introduction

One of the approaches to distinguish between different structured, possibly same length PCR products and gain insight in to the intermolecular structure is melting analysis, a gradual decrease of fluorescence due to temperature increase. Two concepts developed to perform melting analysis from microliter volumes are: the standard thermal cycling, in which by thermally ramping the sample a continuous fluorescence signature is acquired [42], the spatial melting analysis, the loading of samples on a linear thermal gradient and acquiring a spatial change of fluorescence along a microfluidic channel [12]. The approach of the thermal gradient in a continuous-flow system allowed the quantitative observation of the PCR product and a simultaneous qualitative analysis [5]. The advantage of a spatial melting approach was the ability to immediately analyze the sample. A system for spatial melting analysis [1] requires, apart from the optical and thermal subsystems, equipment for the sample manipulation in forms of ports and pumps. An alternative approach to the standard fluid management that is based on pressure

driven flow, with a major reduction in the number of cumbersome external fluid elements, was presented by Man et al. [43], in the form of capillary passive pumping and stop valves. The capillary pumping effect was coupled with a capillary valve that used geometry change along the channel, to increase the air-liquid surface disproportionately thereby creating a negative pressure which would the further fluid propagation. Man et al. [43] also presented the theoretical background of the designed elements.

Though capillary action can provide fluid motion based on the contact angle, surface modifying additives commonly used in PCR as reaction enhancers [44], whether deliberately present or not, could strongly influence surface properties. Therefore, any geometry induced fluid motion control would be compromised due to change of the contact angle. Lu et al. [45] showed that the functionality of a capillary system is partially or totally inhibited by the presence of surfactants, and resolved the problem by creating a superhydrophobic pattern. Though this is a viable solution to the problem, Cuband et al. [46] showed that hydrophilic channels have a greater flow consistency in two phase pressure driven flows than hydrophobic channels. The residual air along the channel would inhibit the melting analysis, resulting in a reduction of spatial redundancy and data quality, thereby compromising the obtained melting curve.

Using opposite wettability in substrates is not a novelty in microfluidics. Lu et al. [47] have presented a method for modifying paper using its inherent capillary capabilities by creating sealed regions around hydrophilic geometry which would provide capillary induced fluid motion. The material used as paper matrix sealant was wax, making it cheap and feasible. A similar solution was later proposed by Martinez et al. [48] as a solution for cheap on site diagnostics. Though both systems use paper as substrate which

is very economical, the material does not have thermal or optical properties suitable for spatial melting analysis.

A rapid capillary loading system for fast DNA analysis is presented, using spatial melting analysis. The proposed system was capable of quantitative and qualitative sample evaluation from microliter volumes, redirecting all fluid manipulation to capillary induced effects. The microfluidic device had no side walls as was solely relying on the surface properties provided by the native substrate and the deposited silane. Additionally, the system was designed to be functionally invariant in respect to applied protein blockers potentially present in samples.

4.2.3 Methods

A microfluidic chip with 8 individual channels for spatial melting DNA analysis is positioned on a heating platform presented with a schematic in Figure 4-7. The microfluidic device acted as a thermal bridge between two heaters at different temperatures, inducing a quasi-linear thermal gradient along its width. Fluid sample manipulation was performed by capillary action of hydrophilic surfaces, native to the glass substrate and hydrophobic surfaces of the silicon thin film layer. The hydrophilic surfaces were in the shape of a straight 15 mm long and 1 mm wide channel, with a semicircular loading zone on the channel beginning, while the surrounding surfaces were hydrophobic. Once the sample was loaded, using a standard pippeter, the pumping was instant and directed along the designed hydrophilic pattern. The chip was observed by a CCD camera in real time while being illuminated with a LED, both equipped with adequate filters in respect to the fluorescing dye present in the sample. For each of the samples, the heating platform would be manually moved along a rail until the loading

channel position was immediately under the imaging system within the field of view of the camera. The acquired images of the sample fluorescence on the microfluidic chip would show a gradual decrease of signal intensity along the thermal gradient, resulting in a recognizable spatial melt. The image was further processed on a GUI designed in MATLAB and the extracted data was compared with a commercially available system (LS-32, Idaho Technologies, Utah).

4.2.4 Chip design and fabrication

The fabrication process consisted of coating two glass slides with a hydrophobic silane layer, masking the same with a polyimide tape and removing a specific predefined pattern for each channel. After the mask was pasted on the coated glass slides, parts of the pattern were removed manually defining future hydrophobic surfaces for active capillary pumping. To create the same capillary effects at both fluid-substrate interfaces, the oppositely positioned glass slides were masked with the same symmetric pattern. A hydrophilic loading zone was created at each channel beginning by removing semicircular pieces of the masking tape that was further defined as the loading zone. The channel was 1.1 mm wide along its whole length. To facilitate the pipette approach and sample deposition, a machine tool was used to remove small semicircles of the substrate corresponding to the mask pattern from the top slide. For the alignment of the two mirror image patterns, a pair of positioning rectangles was designed in the corners of the chip. Once the chip was fabricated, in the exploitation process, the chip was oriented on the heaters in such a way that the loading zones would be positioned on the lower temperature to avoid sample boiling.

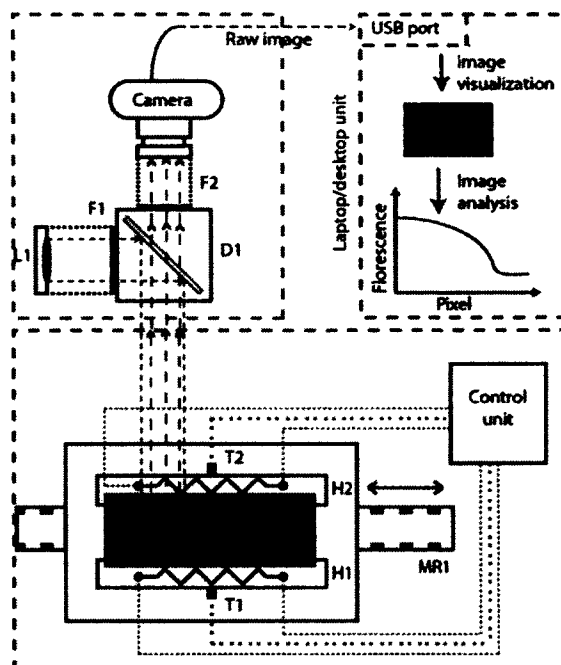


Figure 4-7 A thermal platform with aluminum block and embedded heaters (H1,H2) is used to create a thermal gradient across a microfluidic device. Each of the heaters is coupled with a thermocouple (T1,T2) used as a feedback loop for the control unit. Once the gradient is established, samples are individually loaded manually and the LED (L1) is activated. The light emitted initially propagates through a filter (F1), reflecting from the dichroic mirror (D1) focused on the microfluidic device. The fluorescent dye and DNA present in the sample in interaction with the light emit a lower energy light. The emitted light propagates through the dichroic mirror and the filter F2, separating it from the LED originating light. The images via USB are recorded, visualized and analyzed using a GUI. The platform was mounted on a moving rail (MR1), allowing analysis throughout the whole surface area of the microfluidic chip.

Flaws in the fabrication process were almost always due to glass slide misalignment. Although markers were designed to guide the alignment process, imperfection on such small scales is humanly inherent due to limited hand-eye coordination precision. Additionally, with the coating being translucent, alignment was only performed based on the markers present.

In the fabrication process two different affinity surfaces were induced on the same glass substrate. Hydrophobicity is where water repelling would limit the direction of fluid motion and hydrophilicity would provide capillary induced pumping. Once the fluid sample was positioned on the loading zone, the capillary action of the hydrophilic channel would provide the passive pumping, while the surrounding hydrophobic region would direct the fluid movement minimizing the sample uptake. The design allowed the sample fluid to be only in contact with the patterned glass leading to a reduced surface to volume ratio and reagent adsorption. On the sides the fluid would be exposed to air, possibly regulating possible air-bubble nucleation.

4.2.5 Silicone coating of microfluidic devices

The microfluidic device designed consists of two silicone coated glass slides (Gelest Aquaphobe CM, Gelest, USA). The chosen coating was described by the vendor to be molecular in thickness with a very low critical surface tension in comparison to untreated glass. The coatings were applied in a nitrogen inert environment on a previously cleaned glass slide. The cleaning protocol consisted of detailed removal of possible contaminants, first manually with a detergent solution in RO water and RO water rinsing, secondly by exposing the glass slides for 2 h at 120 mTorr and “High” in a oxygen plasma cleaner (Harrick plasma cleaner, USA). The slides were placed in a nitrogen glove box where a 10 μ L solution of 8% CM silicone in Toluene was applied and the glass slides were left to cure for 24 h at room temperature. The glass slides were additionally baked for 2 h at 100 °C and thoroughly cleaned again.

Chips coated in the graphically explained protocol Figure 4-8 would retain their hydrophobic nature over a long period of time. The removal of the coating from the glass

substrate was performed by plasma cleaning the coated glass slides in the same device as previously used.

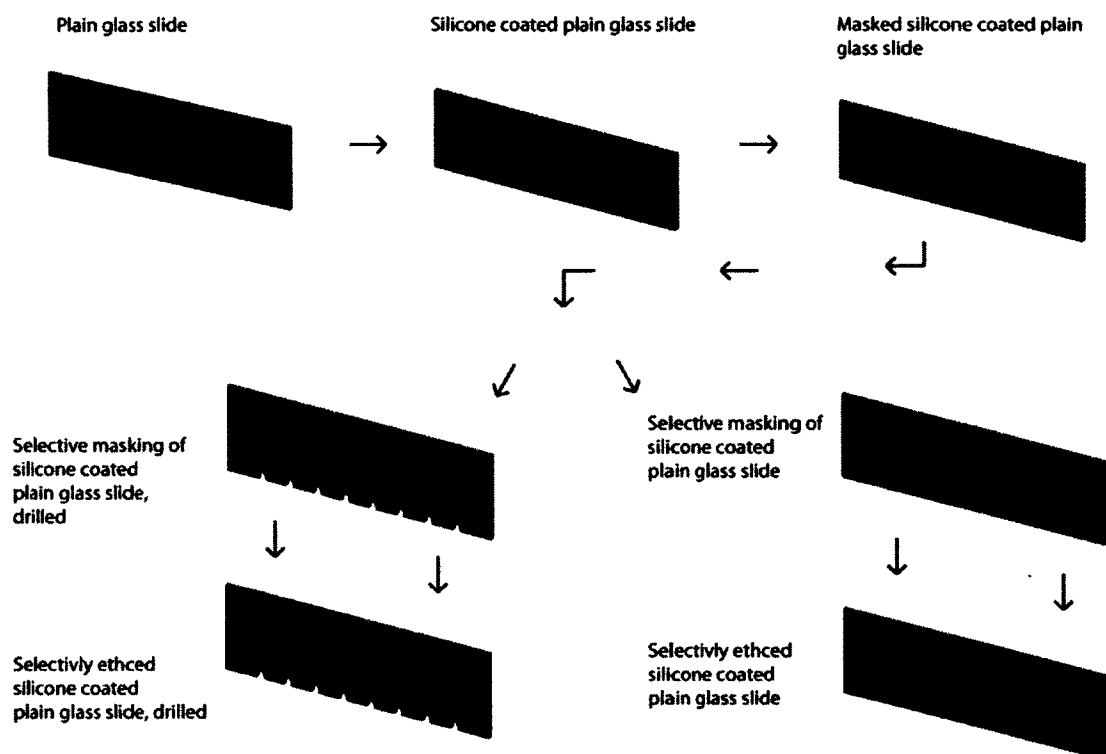


Figure 4-8 Three layers are noticeable, glass (grey), silicone coating (green) and the polyimide adhesive tape (yellow). The fabrication process is in respect to the glass substrate non-invasive. The substrate was initially coated with a silicone layer, and subsequently masked with a polyimide double adhesive layer on top. The mask is pre-patterned and cut prior to placement on top of coating. The top glass slide was machined to enable the loading platform by removing semicircle structures on the channel beginning. The selectively masked silicone coated glass was exposed to air plasma removing the exposed coating. The polyimide layer around the channels was removed and the glass slide was thoroughly cleaned. The two channels top (bottom left) and bottom (bottom right) were assembled and the chip was ready for exploitation.

Since Bhattacharya et al. [49] showed PDMS surface properties change with an increase oxygen plasma exposure, later tending to retain their initial hydrophobic state, a sufficient long etching time period had to be used. All the channels were therefore etched for 20 min at 250 mTorr on “high”, and subsequently cleaned and rinsed with water.

No residues or changes of the substrate surface properties were noticed before the mask was applied and after its removal. Study of long term effects of the surface properties were not performed in this experiment, although similar behavior like PDMS is expected.

4.2.6 Optical setup

The primary goal of the optical setup was to create a reliable consistent lighting distribution along the microfluidic chip area. Emphasis was also set on lowering the exposure time of the samples and increase the system’s acquisition sensitivity. The optical setup consists of a CCD camera (PL-B957U, PixeLink, USA) an LED light and adequate filter set (49013, Chroma, USA) all centrally integrated around a beam splitter cube. The selection of the optical setup and the synchronization of each element was performed. The light system consists of three different functional entities: the filter set, optical subsystem for focusing and the lighting system Figure 4-9.

The light source was a pre-mounted set of three LED diodes (LXML-PR01-0500, Luxeon®Star, USA) on a base (Saber 20mm Tri-Star MCPCB base, Luxeon®Star, USA). The light was powered by a LED driver (3021-D-E-700, Luxeon®Star, USA) and focused using a lens array (Carclo 10570 lens, Luxeon®Star, USA). The LED system was mounted on a pre-machined lens tube cap (SM1CP2M, Thorlabs, USA), and connected onto the cube with a lens tube (SM1L10, Thorlabs, USA).

The same lens tube contains one of the three filters from the filter set with the excitation filter (ET445/30x, Chroma, USA) mounted within. The light, after getting filtered into the specific narrow bandwidth, is reflected by the longpass dichroic mirror (T470Lpxr, Chroma, USA) onto the chip with the sample containing fluorescent dye. The fluorescence caused by the incoming light emitted by the dye passes through the longpass filter and is further filtered by the emission filter (ET500/40m Chroma, USA).

After the light passes the excitation filter, a low magnification video lens (HF25HA-1B, Fujinon, USA) focuses the light onto the CCD chip of the camera. The lighting of the LED was shown to be consistent (data not shown) within a radius sufficient for the spatial melting analysis. Additionally, the camera was chosen as an upgrade from the previous version in respect to individual pixel size. By increasing this feature a 4-fold and keeping the resolution the same, significantly lower exposure times can be achieved. This combination of a strong light source, sensitive camera and dye-specific filter set provides a reliable set for sensitive fluorescence signature acquisition over a 20 mm radius area.

The design of the optical system was facilitated by the target geometry, the microfluidic chip. With its flat structure and small channel depth ($\sim 150 \mu\text{m}$), long exposure times were possible at maximum $f\#$ of the lens system without compromising the resolution. The relatively large pixel pitch (distance between two adjacent pixels) and CCD chip size made sure that there are no geometrical aberrations of the lens even on the image outlines.



Figure 4-9 The complete experimental setup is presented in the image (left) while a more detailed view of the optical setup is given in the right part. The system is constituted of two subsystems, a heating platform with a control unit representing the thermal subsystem and a compact optical system consisting of filters, a dichromatic mirror, a LED light source and a camera. The platform was mounted on a bearing which is mounted on a rail. This allowed axial movement of the platform without compromising the image lighting consistency. The optical cube setup is highly reliable and provides even lighting distribution. This change is a considerable advancement in comparison to previous setups, as in respect to the signal intensity as well as its uniformity.

The possible spectral aberrations due to the different refraction indices of different wavelength light were conveniently addressed by the narrow light spectrum and allowed to reach the chip due to the light filtering. In contrast to the previous system this represents a significant improvement in every aspect (previous lighting conditions are presented in Figure 4-10).

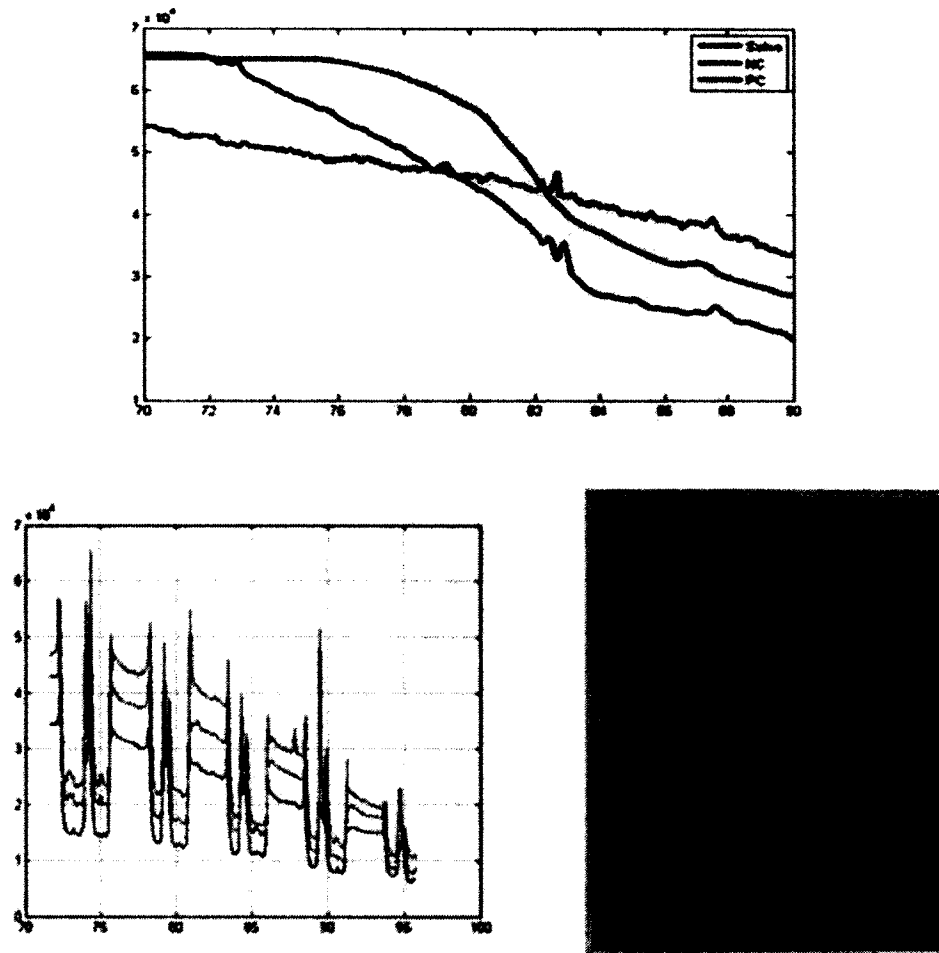


Figure 4-10 The top diagram represents a 400 ms exposed sample of PCR product with a very high concentration (top). The background signal is very intense and consumes roughly one third of the acquired signal. In the two images on the bottom, a lighting inconsistency is presented, a problem that made many successful experiments fail in the last instance. The lighting issues as seen the graph are not only in between the channel but also within the channel itself.

4.2.7 Sample reagents

Tests performed with the goal of determining the detection threshold by using various DNA concentrations, had DNA oligo-nucleotides (IDT, USA) in a 50mM Triz buffer solution with 3 mM MgCl₂ (Sigma, USA) and 2X LCGreen (Idaho Technologies,

Utah, USA). The DNA was a 60 bp long predesigned sequence³, originally present on the *E.Coli* bacterial phage Φ X174. As was previously mentioned capillary systems are susceptible to surface modifying agents commonly present in PCR products, as well as their substrate optical properties. To address these issues and to confirm functionality of the capillary action driven pumping and spatial melting analysis, multiple samples with different agents were analyzed. The two reagents chosen are BSA (0.25 mg/ml) and Tween20 (0.5 %) as additives to the oligonucleotide mixture. Quantitative and qualitative comparison of melting analysis was performed for all samples on the LS-32 (Idaho Technologies, Utah, USA) at a ramp rate of 0.05° C/s.

4.2.8 Results

While sample loading was performed onto the chip, no significant surface temperature changes were noticed, although the loading would be instant. This thermal redundancy of the system can be attributed to the very small thermal mass of the loaded sample that merely represents 0.5 % of the total device volume (under the assumption that the tape is 200 μ m high and the 5 μ l sample is completely taken up in the channel). Though this observation might be misleading since local temperature changes can occur masked behind the relatively large thermal capacity of glass and the thermal dissipation.

The silicone coating based on which the fluid propagates through the channel has been shown practically to be susceptible to degradation over time. Though it is unclear whether the silane degrades or it is hydrophilicity, it is for sure that this represents a significant barrier to this technology being applied in real-life applications. The microfluidic device was not initially susceptible to even great amounts of surfactants

³ 5'-AATCCACGCTCTTTTAAAATGTCAACAAGAGAATCTCTACCACGAACAAAATGTGACTCA -3'
5'-TGAGTCACATTTTGTTCATGGTAGAGATTCTCTTGTGACATTTTAAAAGAGCGTGGATT-3'

present in the fluid, but at a later “degraded” stage, the fluid would propagate between the two glass slides in all directions. The system exposure time was set at 100 ms resulting in the signal reaching the maximum at a 3.3 μM concentration Figure 4-11. In comparison to previous optical system this solution is adopted from a widely used approach in microscopy, though represents a significant improvement in many aspects, especially in reliability and near object homogeneous light distribution. The light source is a three LED system with a collimating lens without a diffuser (that was previously present). By using a lens and not a diffuser to create uniform lighting, the light loss that was associated to the diffuser has been eliminated. Also, the surface area on which the light source is focused, at the given distance on image Figure 4-11, is roughly 20 mm in diameter. Also, the small distance of the system to the chip has contributed to the light being high intensity. The filter set was also changed.

Whereas in the previous setup only two filters were present, now have three filters present, two bandpass filters and a longpass dichroic mirror. The aluminum in the background is not as big a problem as it was in the previous setup, where the presence of the same would cause the sample fluorescence signal to interfere with the strong aluminum fluorescence crippling the analysis. In addition, the light source, and the camera are at a constant spacing and angle in respect to each other. Since the new camera has an increased pixel size and chip size and the camera is in the immediate vicinity of the object observed, a long focal length lens was chosen. The 10 mm channel took one half of the screen width, resulting in a 500 pixel distribution along its length or roughly 50 pixel/mm.

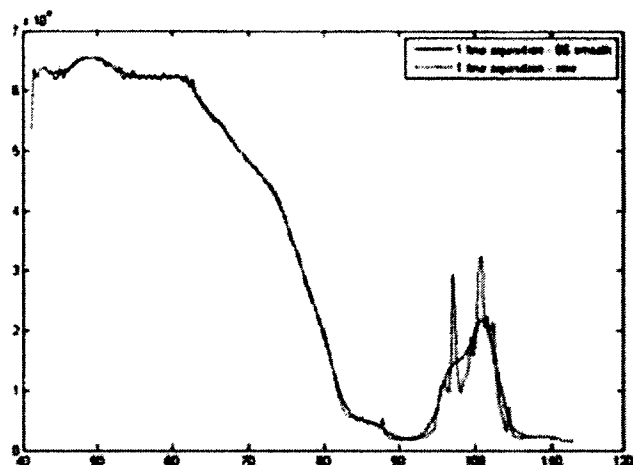


Figure 4-11 The melt obtained from 1 line of data shows a capable and reliable system for melting analysis. In comparison to previous solutions which had light inconsistency within the channel itself and high background noise, this is a significant advancement. In the bottom image three channels can be seen, though only one is providing a melt. The melt is also obviously distorted and can only provide limited data. The lateral bright spots are samples that due to silicone degradation do not get pumped into the system.

4.3 Conclusions and Future Work

In the process of melting analysis, after observing both changes, there was an increase and a decrease of dissociation energy of double stranded DNA. In the process of the cell replication, there are a multitude of stages throughout in which damage is

possible due to one or another occurrence. It is inductive to think that other types of DNA deformations could be observed using the same technique like: double-stranded breaks, a nucleotide loss, several nucleotide loss, the sugar-phosphate bond being incomplete and cross-link.

One consideration is to use this method to aid the study of cell repair pathways by studying protein bindings to damaged DNA using melting analysis. The proteins present (ATR kinase) for damage detection have a hard time to find pyrimidine dimers that account most of the UV caused damage but are relatively efficient in detection of 6-4 photoproducts. The current process of detecting this interaction of damaged DNA and the protein is as follows: radiolabeled oligonucleotides would be added with the ATF protein, further crosslinking it using UV-C radiation source, separating the products on a SDS/PAGE, which was then analyzed by silver staining and radiography. After the process explanation, the mere possibility of simply melting the whole DNA protein mixture and observing the change the dissociation energy is tempting, because it is simple and because the amount of data feedback would be much greater than just a positive or negative answer.

CHAPTER 5

ISOFLUX THERMAL GRADIENT IN SOLID STATE HIGH-ASPECT RATIO STRUCTURES

5.1 Abstract

In this chapter high as isoflux approach is taken to thermal management of high aspect structures. The approach is an offshoot of the gradient used in the previous chapters where high thermal consistency is achieved. To measure the thermal stability of the field within the gradient a planar thermoelectric sensor (thermopile) was used. The experimental setup was assembled with a non-conventional low cost approach where the same sensing element is the most expensive part of the whole experiment. The experimental setup managed to transition the sensing element temperature from 18° C up to 110 °C with a maximum deviation of 1.5 mV from the signal baseline. Additional theoretical explanations and simulations are provided with insight into possible problems and solutions regarding many aspects of the problem.

The conceptual idea is to create an environment with a high degree of thermal consistency whether it be in a steady or dynamic work regime. For this purpose high aspect ratio structures are chosen, since they have a preferable z-axis dimension that prevents thermal dissipation in directions orthogonal to the z axis. This geometry induced thermal bottle neck is used to maintain the thermal energy within the structure so that the

heat travels only across the shortest distance of the high aspect ratio structure (in this case along the z-axis). To measure such an event a thermoelectric planar measurement sensor attached to a microscope cover slip #1, is sandwiched between two thermoelectric heating/cooling devices. The stability of the thermal field is reflected in a low temperature fluctuation in transitional stages of the system (heating and cooling). This stability is inherent to conductive systems, while natural or forced convection due to fluid motion and complicated boundary layer issues at fluid-solid interfaces are hard to resolve and evaluate. Also, fluids (especially gases) are much more susceptible to environmental changes like pressure or humidity, as well as possible fluid control issues related to flow consistency due to geometry inconsistency.

5.2 Theoretical Analysis

5.2.1 Analytical analysis and 1D simulation

The theory behind the thermal stability of the systems is initially reduced to the study of a transient one-dimensional conduction problem. This approach is necessary to gain understanding into the transient changes and the individual properties that guide them. The propagation of heat through a disproportionately dimensioned structure like the previously presented chip (the exposed chip surface was 25.4 x 25.4 x 0.36 mm) can be assessed as a one-dimensional transient heat propagation. In our case that would be the z-axis direction or normal to the largest surface of the microscope cover

$$\frac{\partial^2 T}{\partial x^2} = \frac{1}{\alpha} \cdot \frac{\partial T}{\partial t} \quad (5.1)$$

where T is temperature along the slab, x is the position along the slab, t is the time, and α is the thermal diffusivity of the material,

$$\alpha = \frac{k}{c_p \rho} \quad (5.2)$$

where k is the thermal conductivity, c_p is the specific heat capacity and ρ is the material density.

Although the above equation is the basic approach, a pre-solved model was used to assess initial system behavior. In this model we assume that all heat generated by the heat source at the boundary of the system is in full transferred through the material, and no losses occurred. Also, the heat source boundary conditions are set to *boundary conditions of second order – constant flux*. The reason for this approach was that *first order boundary conditions* assume that a heat source maintains the wall temperatures constant. This is not an adequate representation since in practice heaters provide a power output in Watts which further influences the system temperature accordingly. In this simplified simulation, we are observing a system that only has a heater and a semi-infinite solid body. The semi-infinite body approach makes the second boundary condition obsolete, therefore simplifying the setup. The model is as follows:

$$T(x, t) - T_i = \frac{2 \cdot q_0 \cdot \sqrt{\frac{at}{\pi}}}{k} \cdot e^{\left(\frac{-x^2}{4at}\right)} - \frac{q_0 x}{k} \cdot \operatorname{erfc}\left(\frac{x}{2\sqrt{at}}\right) \quad (5.3)$$

where *erfc* is the complementary function of the Gaussian error function *erf* defined as

$$\operatorname{erfc}\left(\frac{x}{2\sqrt{at}}\right) = 1 - \operatorname{erf}\left(\frac{x}{2\sqrt{at}}\right) = 1 - \frac{2}{\pi} \int_0^{\left(\frac{x}{2\sqrt{at}}\right)} e^{-v^2} dv. \quad (5.4)$$

In the obtained results in Figure 5-1 we can see the process of heating in respect to a 10 s time interval. Since the applied heater strength was very low, the maximum total temperature change was a mere 0.005 °C (Figure 5-1). Even though immediately upon starting the process, a thermal gradient is established in the needed region dotted with the thick green line. The additional time intervals, and thermal energy provided, show no change in the temperature slope but only in the absolute temperature values in the material. This form of thermal redundancy and short response times is of great value since the thermoelectric measurements are very sensitive and thereby susceptible to even miniscule temperature differences.

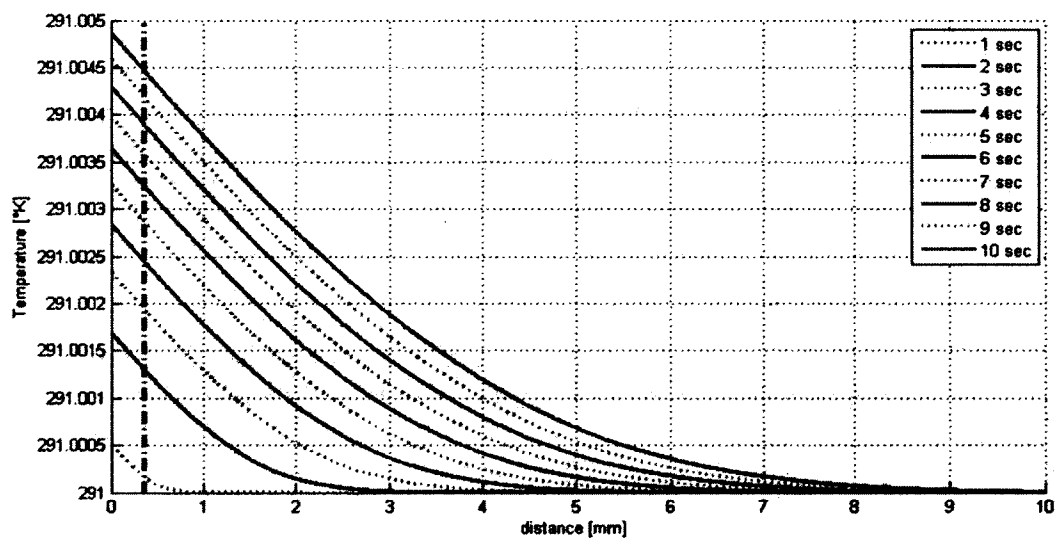


Figure 5-1 In this figure a seminifinte solid assessment of the model was achieved. The green line at the beginning shows the actual chip thickness and the speed at which the gradient is formed. Once formed it keeps its shape in an isoflux system and just get heated to a higher temperature.

5.2.2 3D simulation

Though this model gives insight into the physical basics of conductive heating, which was the initial intent, it is not capable of introducing other aspects of the model limiting its use. To alleviate this issue a numerical approach was taken. In the numerical approach a software (in this case COMSOL Multiphysics) uses a partial differential equation, approximates it with a linear algebraic equation and solves the system for the unknown values. In this process each one equation represents one node of a structure called a “mesh”. The mesh is a set of points and correlations in space, and therefore a direct dependency between the mesh refinement and the number of equation is present. Mathematically, all the equations are represented with a banded matrix that contains a main diagonal and values that correspond to relations of adjacent nodes and are proportional to their distance. The matrix is solved using iterative numerical methods until a previously set convergence criterion is met. The convergence criterion is compared with the difference between two consecutive iterative solutions, and the process is terminated once the difference is greater than the set value. In summary, a numerical solution approach is a balance between *feasibility* in respect to time and *precision* in respect to node number and distribution.

In the process of the model design, a high aspect ratio structure represents a great challenge. In this case, the model has a 100 μm tape covering a 76.2 x 25.4 mm surface resulting in an aspect ratio (the ratio of the largest and smallest dimension of the device) of 762. One of the approaches to reduce this immense ratio is to introduce two axes of symmetry by using a symmetry boundary condition.

The principle idea was to substitute a bulk surface with a boundary condition of similar behavior, reducing the model size. The symmetry boundary condition means no heat will move across that boundary since the temperatures across the axis are mirror images resulting in a zero gradient. Once the two boundaries were applied the total volume was reduced four times and the aspect ratio by two times. A further simplification of the model was performed by shortening the coverslip by 15 mm on the side and applying an outflow boundary condition on the truncated surface. The outflow boundary condition assumes a steady gradient allowing the heat to dissipate across the boundary into an infinite heat sink. The resulting ratio was reduced to a third of the initial and a reduction of the high aspect ratio volumes is to one sixth of its original size.

The heating provided by the heater was 10 W/in^2 which in SI unit system is $15,500 \text{ W/m}^2$. To simulate the device performance, 50% of the applied power on the Peltie was assumed to be heating the system while 5% of is assumed to be consumed by the cooling of the same. The remaining geometry of the device was set to be convectively cooled by $5 \text{ W/m}^2\text{K}$ at 293.15 K ambient temperature.

During the process the thermal gradient present in the device should be consistent along its thickness with minimal or ideally no temperature variation. In Figure 5-2 the system was heated for a period of 25 s. To quantify the system's behavior we have extracted several point temperature values during the time intervals. A total of 12 points were chosen, all positioned in between the two glass cover slips, exactly at the same distance from each other.

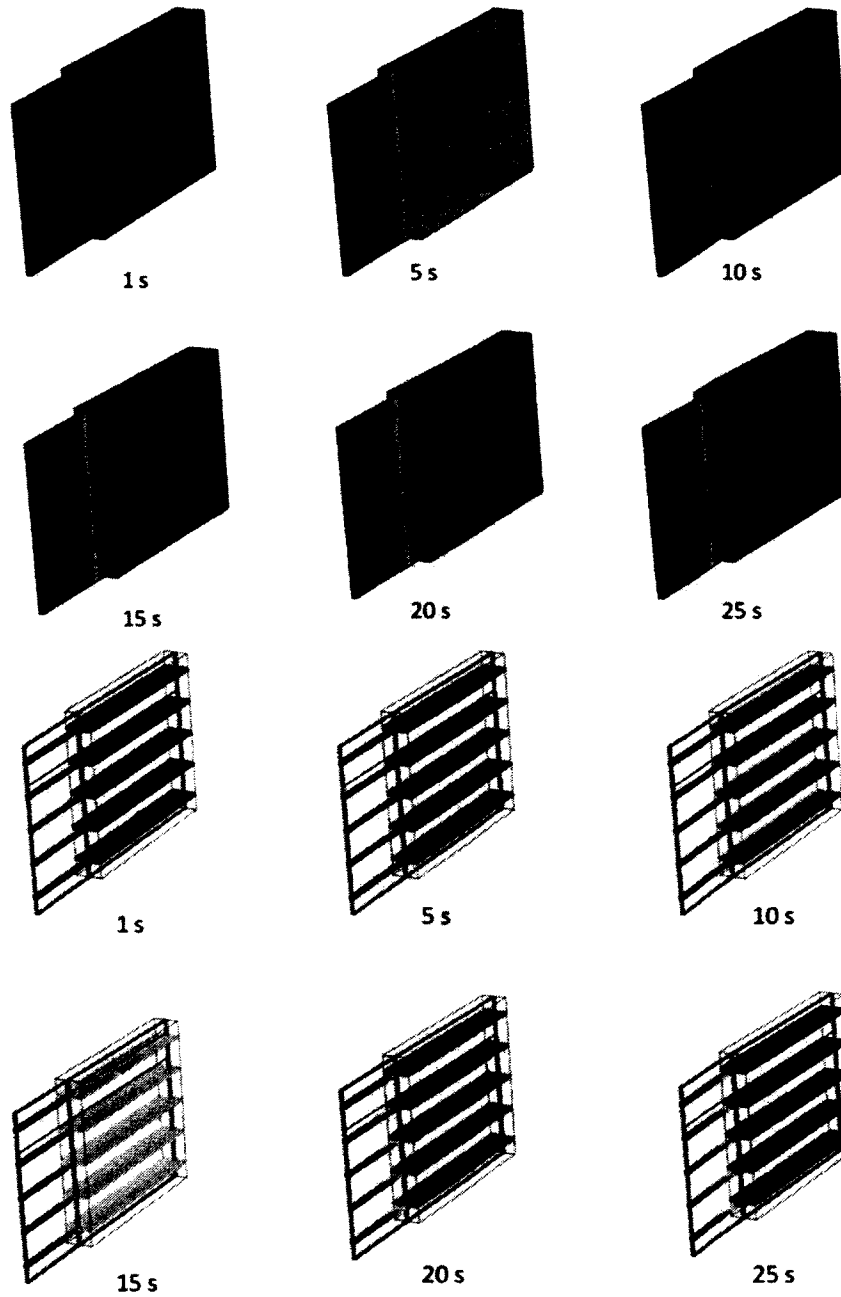


Figure 5-2 In this figure 5 slices of the simulated device are shown, over a 25 s period of time. The two aluminum plates, represented by the thick part show high thermal stability – a constant thermal difference between the plates. The thermal dissipation increases which can be noticed in the increasing color gradient present along the micro-fluidic device length.

The points are divided into three groups: the first group is positioned close to the symmetry boundary, the second at a fixed distance from the first row and the third close to the top edge of the device. Points of each of the three groups were distanced 2, 7, 12, and 16 mm from the vertical axis of symmetry respectfully as shown in Figure 5-3. The twelve points show a linear response increasing their temperatures in a linear state.

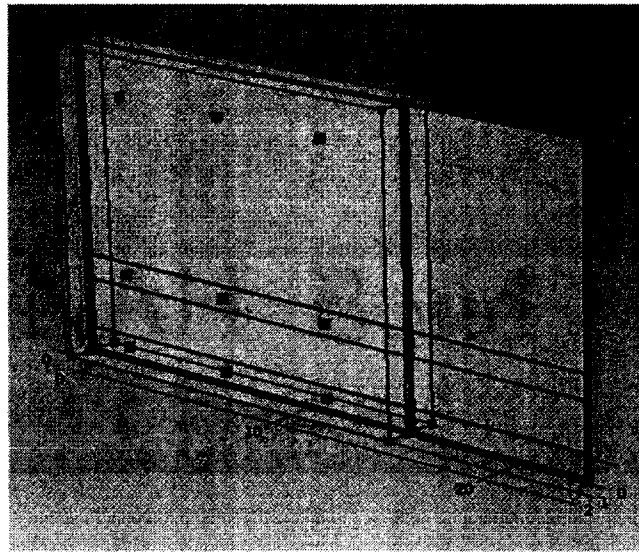


Figure 5-3 The model was modified and 12 points for temperature evaluation over time were added (green). The points were positioned along the measurement channel (bottom 4 nodes), the reference channel (middle 4 nodes) and in the vicinity of the device edge (top 4 nodes).

In Figure 5-4 it can be seen that all the curves are linearly increasing their temperature in time. It seems as though that all the points follow the same pattern. In the following Figure 5-5 we can observe a zoomed view of the same diagram for the time range of 5 to 6 s and to thereby corresponding ranges of 24 to 26 °C. It can be noticed that the temperatures are not the same for each of the nodes and they defer for the given time frame maximally 0.6 °C. If the same data is analyzed from a lateral and horizontal

temperature change, we can observe from Figure 5-5 that the total horizontal change of temperature for the two most distant points on both the measurement and reference channel are roughly $0.4\text{ }^{\circ}\text{C}$ across a 14 mm distance, resulting in an assumed temperature gradient of $0.0285\text{ }^{\circ}\text{C}/\text{mm}$. The temperature difference across the height was $0.01\text{ }^{\circ}\text{C}$ on a 3 mm distance, resulting in a $0.0033\text{ }^{\circ}\text{C}/\text{mm}$ temperature gradient. The two closest points in the center of the structure, for both of the measurement channel and the reference channel the horizontal thermal gradient is $0.01\text{ }^{\circ}\text{C}/\text{mm}$ and the vertical is $0.0041\text{ }^{\circ}\text{C}/\text{mm}$ Figure 5-6.

The outcome was partially expected since the oversized chip cannot completely fit in between the aluminum plates, the “hanging parts” work as cooling fins. The horizontal gradient is an order of magnitude greater in comparison to the vertical gradient. These gradients are essential to the base level signal of the thermopile. The thermopile is a planar structure of a multitude of consecutive measurement and reference junctions that are directional.

To avoid a strong baseline reading in the system, after evaluating the gradient intensities, it is recommendable that the thermopile is positioned along the greater gradient, therefore horizontal. Also, it can be noticed that the gradient increases over distance, leading to the suggestion that the closer the thermopile is to the center of the device, the smaller base reading will be observed.

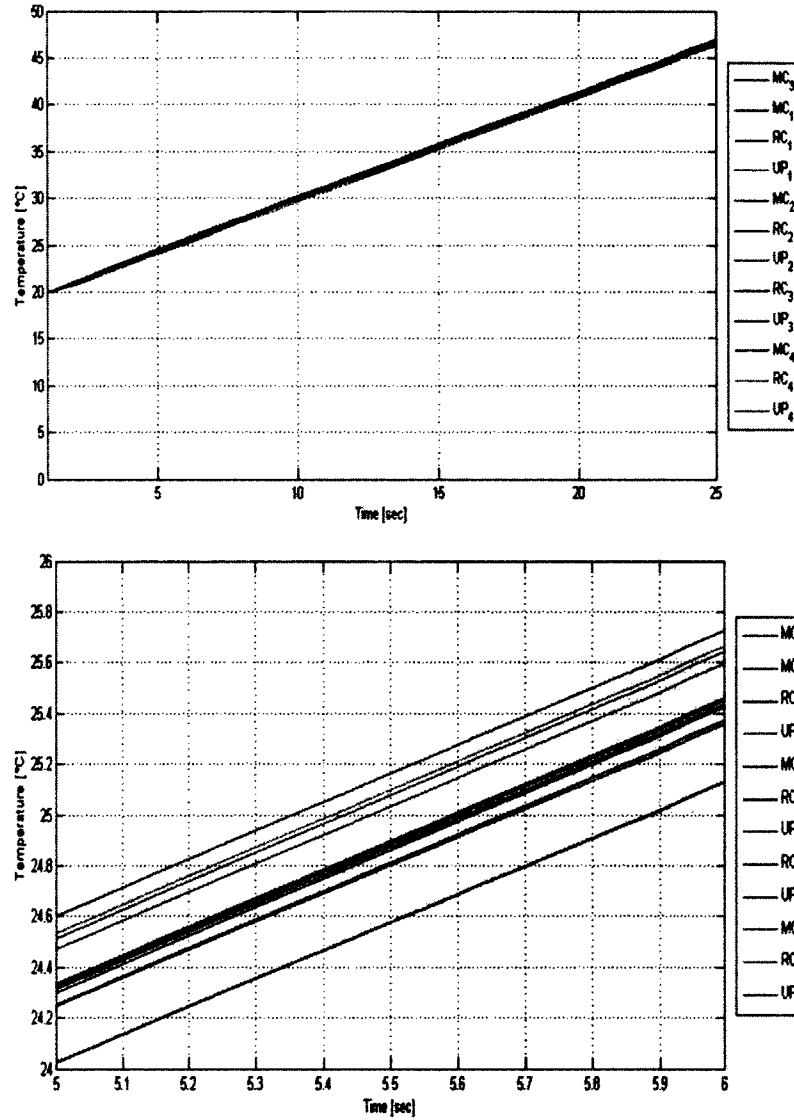


Figure 5-4 All twelve points are simultaneously plotted in one diagram. The temperature differences are small and the systems seem to be linear in its progressive temperature increase.

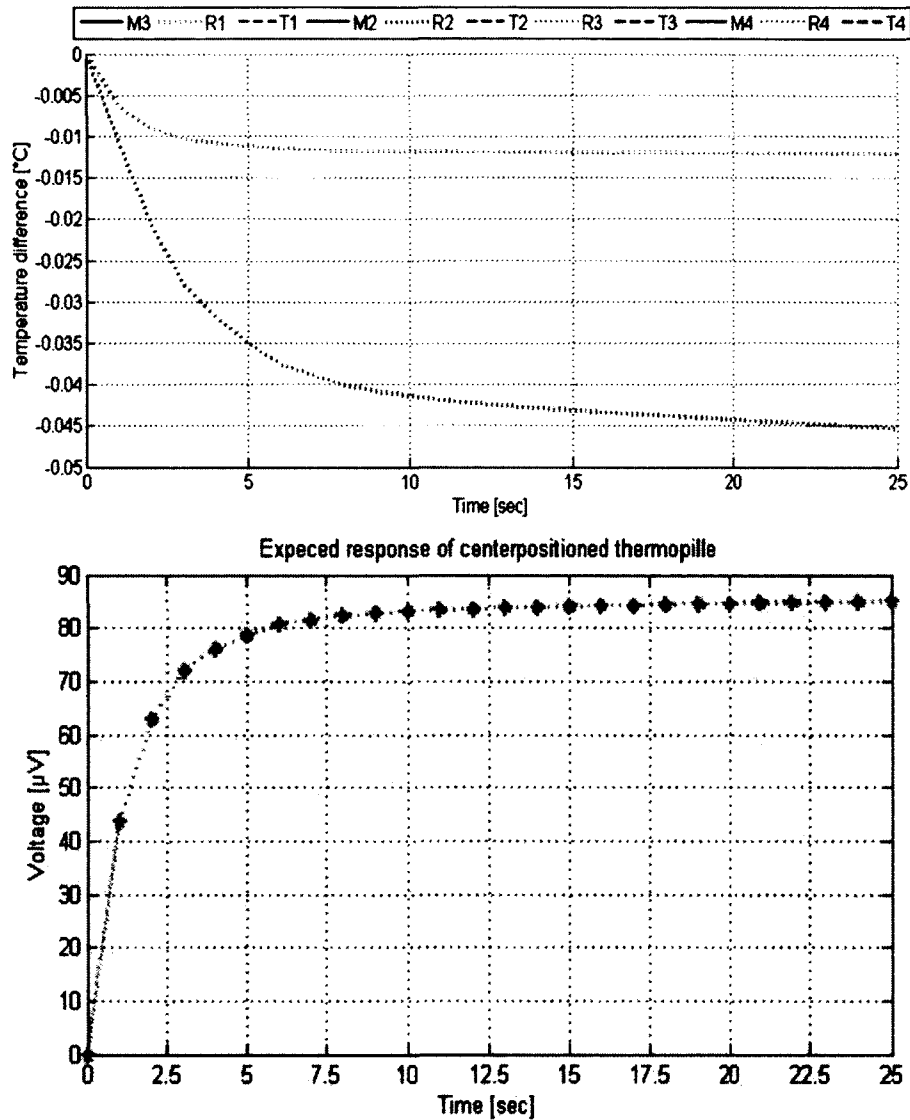


Figure 5-5 The zoomed in analysis of the data shows slight differences between the individual points, that in the selected shown range is maximally 0.5 °C. The temperature difference of two vertical points is of much lesser intensity then the horizontal temperature change. This is understandable since the energy dissipation in the system is provided by the “hanging” surfaces of the microfluidic chip.

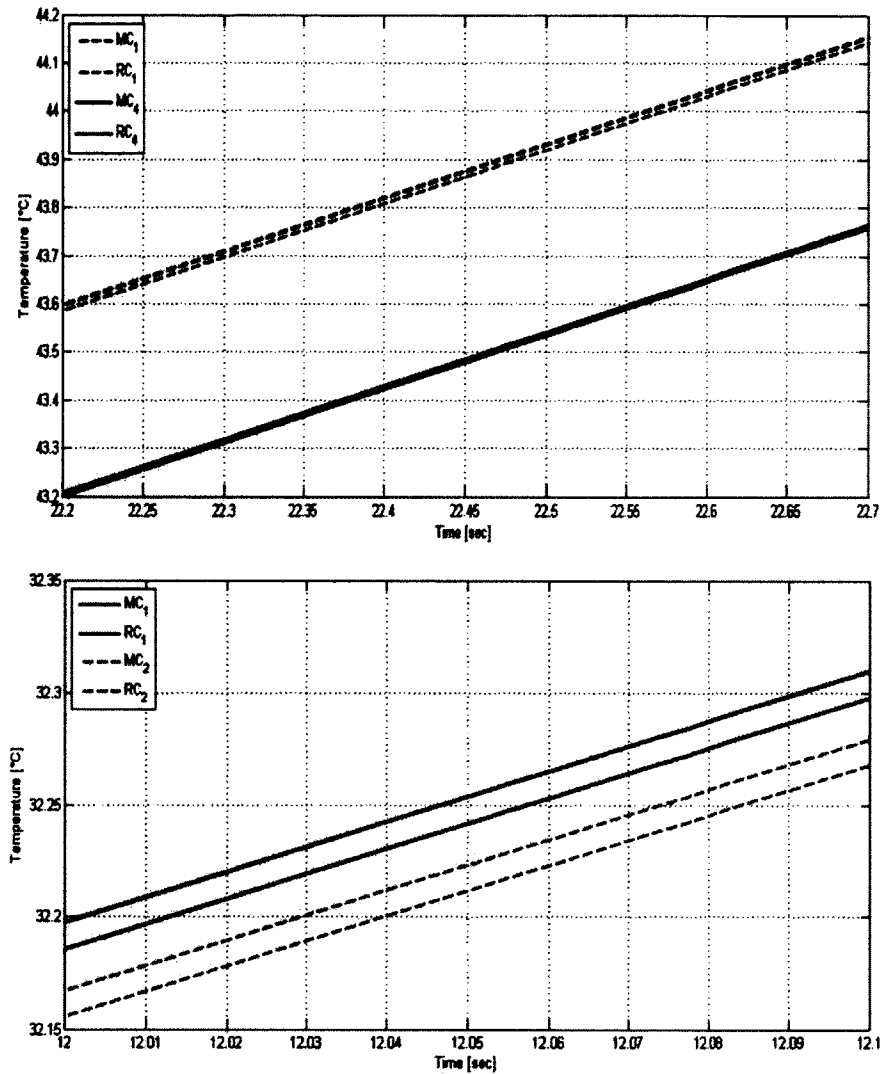


Figure 5-6 The figure illustrates a lateral and horizontal temperature change inside the microfluidic chip. The total horizontal change of temperature for the two most distant points (left) on both the measurement and reference channel are roughly $0.4\text{ }^{\circ}\text{C}$ across a 14 mm distance, resulting in an assumed temperature gradient of $0.0285\text{ }^{\circ}\text{C/mm}$. The temperature difference across the height was $0.01\text{ }^{\circ}\text{C}$ on a 3 mm distance, resulting in a $0.0033\text{ }^{\circ}\text{C/mm}$ temperature gradient. The two closest points in the center of the structure, for both of the measurement channel and the reference channel the horizontal thermal gradient is $0.01\text{ }^{\circ}\text{C/mm}$ and the vertical is $0.0041\text{ }^{\circ}\text{C/mm}$.

5.2.3 2D modeling – isoflux flow in parallel non homogeneous structures

A further 2D analysis of the system is performed in which a planar model is designed that represents one of the cross-sections of a prospective device that includes two microfluidic channels. The reasoning behind this approach is the understanding of heat propagation in two parallel different materials like water and tape. This study although is to a certain extent possible in the actual 3D model; the low resolution mesh makes the obtained results of questionable quality. The 2D model being rectangular was “mapped meshed”, resulting in a total of 20k elements and a minimum of 7 elements across the smallest feature (tape thickness) Figure 5-7.

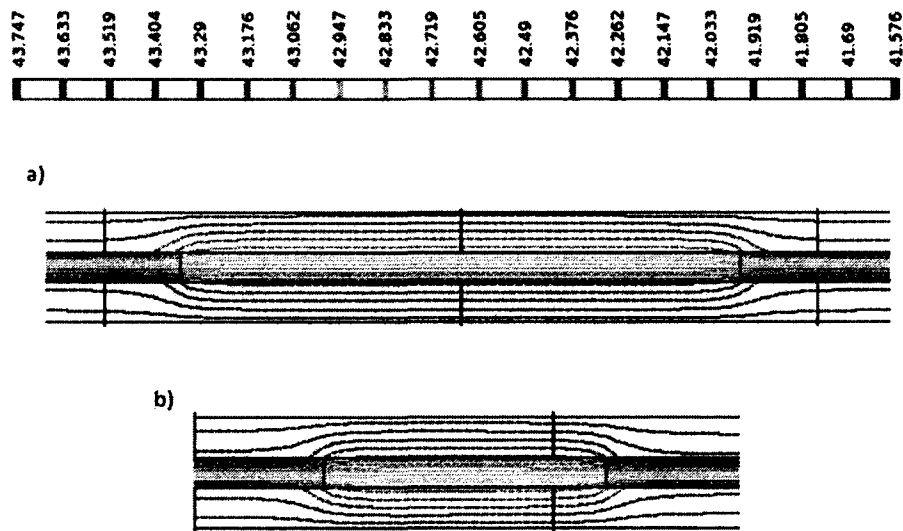


Figure 5-7 The temperature distortions shown in a) the measurement channel and b) the reference channel have their origin in the heterogeneous structure in which water with a conductivity of 0.5 W/mK is positioned just next to a polyimide tape layer with 0.15 W/mK thermal conductivity. The intensity of these effects is small leaving only a local effect on the temperature distribution. The adaptation space needed for the temperature to settle to the new value is roughly equivalent to the glass cover slip's thickness.

The model was loaded with the same heat source and sink as in the previous simulation and the simulation was run for 60 s time intervals with 2 s increments.

One of the questions that will hopefully be answered is the exact location of the maximal thermal distortion due to material thermal properties change. As expected due to different material conductivities a skewed flux is observed around the channels in which the temperature drop across the channels is lesser than the one observed in the polyimide layer. From the images we can observe that there is a lesser number of contour isothermal lines present in the water channels. The deformation of the temperature field is yet to a certain extent alleviated by the width of the channel on top of which the measurement will take place. The contact length between the antimony and the bismuth is approximately 200 μm , which is 5 times less than the reference channel width. We can also observe that the temperature field in the middle of the channels is more stable and uniform than on the edges, giving the notion that the placement of a thermopile in respect to the channel geometry is of great importance Figure 5-8. Also, it can be noticed that the temperature distortion due to the presence of an alternative material affected both sides, the incoming and outgoing flux by decreasing their temperature.

5.3 Experimental Design

In hopes to observe a similar thermal behavior, a thermal systems with two Peltie devices acting as a heater and cooler are mounted on two 50 x 50 mm aluminum plates using double-sided adhesive tapes. The aluminum plates had a twofold reasoning: firstly the high thermal conductivity of aluminum would generate consistent thermal distribution and secondly it would act as a Faraday cage preventing electromagnetic interference with the thermopile sensing. Both plates were grounded to a power source.



Figure 5-8 In the image we see the whole 2D model in which the heat flux is evaluated. The purpose of this is not to evaluate the amount of energy transferred or to quantify the effect but to see if the boundary conditions and the material heterogeneity affect the temperature distribution within the chip. The top chip has a zero heat flux boundary condition on the lateral edges, while the lower image has convective air cooling. The differences are obvious - the image in b) is the actual total heat flux and we can notice that there is a significant shift of heat flux intensity towards the lateral side. In the model the top is the heater side and the bottom the cooler side.

The heater and cooler were assigned each with a thermocouple and a power source through a PID thermal control system. In between the two aluminum plates with the heater/cooler a microscope glass cover slip and a planar sensing element were positioned. Two different options were present: a coverslip with a directly deposited thermopile and a coverslip with a polyimide layer deposited thermopile attached to it. To avoid damage to such a fragile structure a thin PDMS layer was made and positioned in between the aluminum and the coverslip and sensor as shown on Figure 5-9. Also to alleviate thermal resistance due to surface imperfection thermally conductive grease (non-electrically conductive) based on silver particles was uniformly distributed on both sides of the PDMS layers. The PID control system was scavenged from a separate project and was designed by Dr. Bryan Cox under the supervision of Dr. Niel D Crews. The

system had the capability to perform wireless control via Bluetooth from the laptop. The user interface was designed in visual basic and allowed control of the peltie work cycles in a 10 bit mode. The duty cycle was changed by increasing or decreasing the frequency of the work cycle.

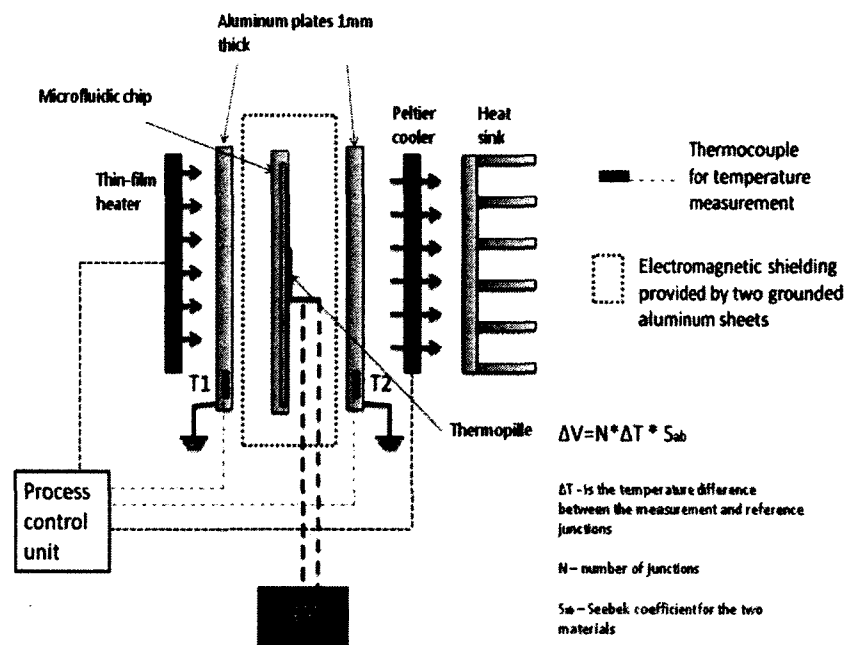


Figure 5-9 This is a schematic of the experimental setup – a thin-film heater is attached to a grounded aluminum plate (left). The glass cover slip in the middle with the thermopile is attached to a voltmeter and in between the two plates. The other plate is attached to the cooling unit which is further attached to a heat sink. The thin layer of PDMS and the coatings are not shown on this image to avoid over complication.

Two thermocouples were following the temperature of each of the elements. Though, due to their size and the importance of a consistent geometry, they were attached on the outer rims of the aluminum plates.

The thermoelectric sensor was developed and designed by Dr. Guilbeau's laboratory. It was an antimony-bismuth composite structure consisting of two rows of thermocouples, resulting in large thermopile. The thermopiles were deposited by metal evaporation under extremely low pressure environments by flowing high currents and inducing heating in the material. The low pressure allowed the material to evaporate and to be deposited on substrates like polyimide tape, due to the relatively low temperatures. Two copper threads with adhesives are merged with the thermopile by the means of a highly conductive silver epoxy that was cured in vacuum. The epoxy was not conductive in liquid form and if not cured properly would result in a sporadic and inconsistent measurement.

5.4 Results

The issue arose that the newly introduced aluminum sheets were in direct contact with the thermopile junctions short circuiting the measurement. Also the pressure that would be applied on the junctions would deform the connections and destroy the sensors connection. To avoid these issues a very thin (approximately 400 μm thick) layer of cured PDMS polymer was set on the side of the device with the thermopile. The polymer flexibility allowed the two rugged surfaces, aluminum sheet and a glass cover slip with a thermopile on top to complement each other.

Due to the relatively primitive setup, the glass cover slip would move in between the aluminum plates even after pressing down with a spring mechanism. Also there were concerns that the aluminum-glass interface on the bottom would not provide sufficient contact, creating parasitic air pocket. The initial trial was to deposit a thin layer of conductive paste on both sides of the thermopile, though it was not anticipated that the

conductive grease solvent could dissolve the silver epoxy connection. Therefore this paste could only be applied on the side of the cover slip without the sensor.

Initially the setup was used to test the thermopiles and their capability to perform under surface pressure at elevated temperatures. With the setup provided two different devices were tested – in the first case a sensor was deposited on a polymer surface and subsequently placed on a cover slip, while the second process was with a sensor directly deposited on the cover slip. A long cycling period was introduced with sporadic heating and cooling of the system.

The system was initiated and a certain amount of time was given to the system to settle and achieve a thermal uniformity. On the Figure 5-11 5-10 it can be seen that initially the voltage is settling and converging until it reaches the red dashed line. The bottom Peltie cooler was turned on, the system was running on 12 V and was consuming roughly 2 A of current. A sudden surge in signal intensity is shown due to thermal inconsistencies within the measurement element. After a peak is reached, the element is slowly returning to a base line. Artifacts in form of jumps were present. By observing the PID system and the power source it was noticed that there are surges in the power consumption. After the convergence was noticed, the system was turned “off” cutting the power to the cooler. A signal of the opposite sign was noticed, where the behavioral pattern is similar to the first process. This signal originates from the thermal energy that crossed the peltie cooler now that it is inactivated. Until this point the peltie cooling system was active as a thermal barrier, simultaneously dumping heat from the sensors immediate environment across it’s surface, the extra heat that is generated by the cooler itself would not stay within the system.

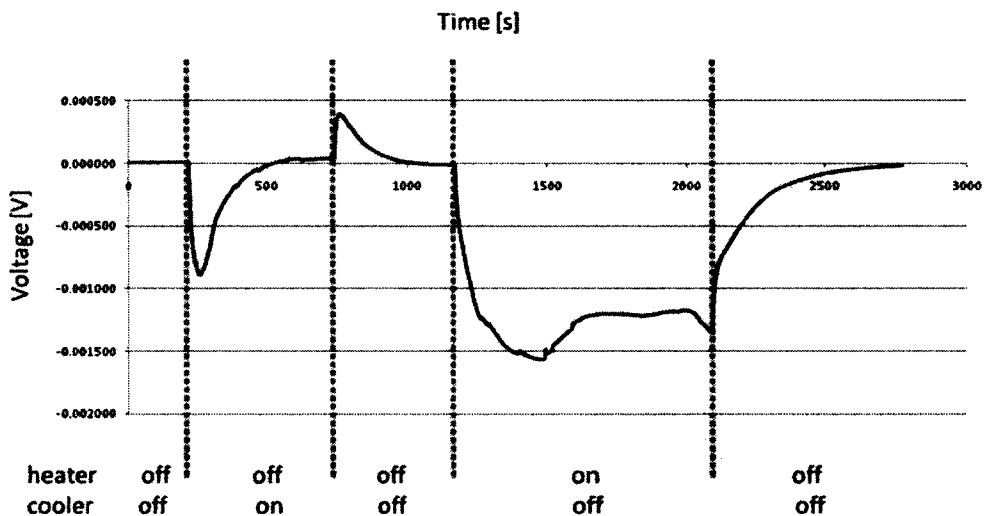
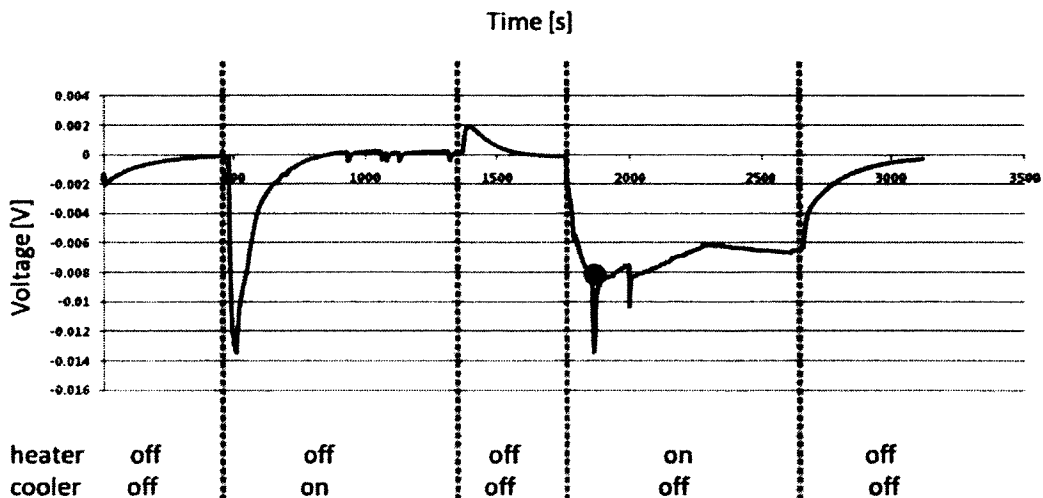


Figure 5-10 Two diagrams are presented in this image. The thermoelectric signal of a thermopile deposited on polyimide tape (top) shows a very strong response in respect to the directly deposited sensor (bottom). Below each of the two diagrams is the switching protocol.

At point of time the cooler was depowered this heat freely traveled across the cooler and heated the sensor. Once convergence was observed again, the heater was initiated. The heater reached 110° C in a relatively short period of time (on the figure it is

marked with a large red circle). Similar to previously observe thermal artifacts were present in form of peaks. The system maintained a voltage and fluctuated. This is assumed to be a lateral thermal gradient caused by ambient cooling of the microscope cover slip. The power was again set on “off” and the signal was allowed to return to its base.

The exact same protocol was used in the second with the same power settings. The major difference is that the sensor is directly deposited on the glass cover slip avoiding the additional medium Figure 5-11. The signal intensity was an order of magnitude less, with little or no artifacts present in the experiment. Even when the system achieved high temperatures the signal stabilized to a certain extent. Of great importance is that the transition stages from room to high temperature are relatively smooth and without great fluctuations. The same temperature was achieved with a brink of the signal intensity in comparison to the previous experiment. Also it has to taken in consideration the presence of a PDMS layer surrounding the coverslip which will slow down the heat propagation creating a more inert system.

5.5 Conclusions and Future Work

From the simulations it can be noticed that a significant thermal flux variation and temperature distribution due to material heterogeneity – ideally for these effects to be reduced to a minimum, a tape with similar conductivity would cause less distortion. Though since the thermopile is positioned at a distance equal to the thickness of the glass-cover slip the distance from the event reduces the variation of the temperature. Thermal dissipation from the lateral surfaces that are exposed to natural heat convection affects the thermal field within the system. It would be expected that with increase of

measurement junction distance from the edge, a decrease in thermal distortion should be observed.

Also, the thermopile apart from being positioned in the center of the system should be also placed in the direction of the microfluidic chip. The reasoning is that the heat dissipation is proportional to the exposed surface and the overhang parts of the chip are acting as cooling fins, creating a “strong” gradient along the chip. The thermopile to have a minimal baseline has to be positioned along the strongest present gradient.

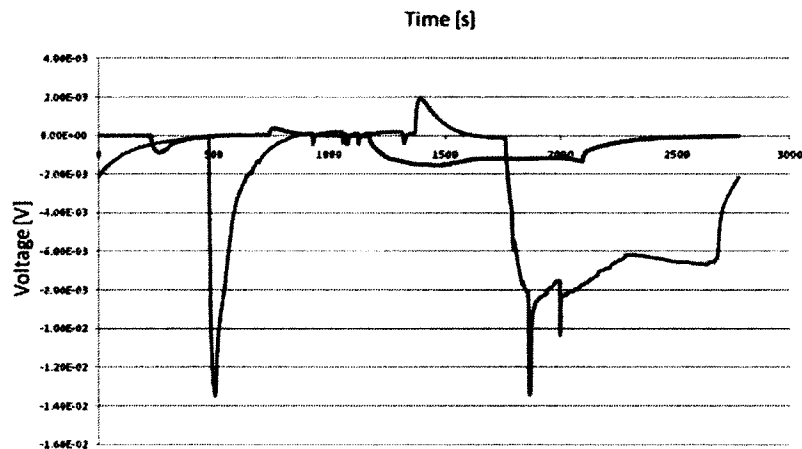


Figure 5-11 The comparison between the two is provided showing a very significant difference between the two and their performance (bottom).

The geometrical constraints of the copper connections onto the thermopile constitute a significant thermal mass in the vicinity of the measurement junctions probably causing thermal disruptions. The presence of PDMS creates a general thermal inertia forcing the system to behave slow. For such subtle thermal changes to be detected, a system of great precision is needed. With the current system it will not be possible to detect these changes although the data looks very promising for future trials.

CHAPTER 6

CONCLUSION

In the field of microfluidics, somewhat more profoundly present in biochemical systems, for a fully functional and reliable system it is of essential value to understand thermo-fluidic interactions. Though even this insight does not guarantee a successful project since the intricate nature of biochemical process requires a wide spectrum of knowledge ranging from optics, surface chemistry, biochemical reaction characteristics, microfabrication etc. To tackle each of the problems in depth would require financial and human effort beyond the scope of our capabilities. That is true, if conventional technologies were to be applied.

The efforts presented in this dissertation⁴ show that low-end technologies are not to be underestimated. Although in their infancy, they represent a powerful tool for iterative design and study of many different aspects. The ease of fabrication and the low cost nature allowed a variety of designs until the final concept was reached.

As examples dental drill-bits were used for glass drilling in conjunction with a hobby tool drill system; deposition of silanes and similar nature chemicals on glass were pipette and then pressed together in a nitrogen glove-box; PDMS was baked in petri dishes with flat polished surfaces, while the central hole was punched out with a biopsy

⁴ Each of the previous chapters has a conclusion addressing the topic individually.

punch; double sided polyimide silicon adhesive tape was used for microfluidic channels as the intermediate composite layer; a conventional CCD camera was used to image the fluorescence signatures with adequate filter sets etc. As minor as these issues might seem, in comparison to existing solutions they show that the usual tendency of scientist is to exaggerate in the size and needed specifications of the equipment. I cannot claim that this approach will always give a better result, though it will shape an individual capable of designing and evaluating systems from its most basic components to sophisticated and intricate systems. It also has the benefit of knowing the device cost and being able to predict project feasibility and cost assessment.

The publications, using these technologies, were submitted to the top journals of the field without a single rejection. The publications represent serious solutions to existing problems as the latest one is a complete microfluidic system for genotyping from saliva.

In conclusion, an institution of importance like Louisiana Tech University shows that any shortfall of any other nature can be overcome with dedication, wisdom and hard work.

REFERENCES

- [1] Pjescic, I., Tranter, C.A., Haywood, J.C., Paidipalli, M., Ganveer, A., Haywood, S.E., Tham, J., and Crews, N.D.: 'Real-time damage monitoring of irradiated DNA,' *Integr Biol (Camb)*, 2011, 3, (9), pp. 937-947.
- [2] Kopp, M.U., de Mello, A.J., and Manz, A.: 'Chemical amplification: continuous-flow PCR on a chip,' *Science*, 1998, 280, (5366), pp. 1046-1048.
- [3] Crews, N., Wittwer, C.T., Palais, R., and Gale, B.: 'Product Differentiation During Continuous-Flow Thermal Gradient PCR,' *Lab on a Chip*, 2008, 8, pp. 919-924.
- [4] Crews, N., Ameel, T., Wittwer, C.T., and Gale, B.: 'Flow Induced Thermal Effects in Spatial DNA Melting,' *Lab on a Chip*, 2008, 8, pp. 1922-1929.
- [5] Pjescic, I., Tranter, C., Hindmarsh, P.L., and Crews, N.D.: 'Glass-composite prototyping for flow PCR with in situ DNA analysis,' *Biomed Microdevices*, 2010, 12, (2), pp. 333-343.
- [6] Pjescic, I., and Crews, N.: 'Genotyping from saliva with a one-step microdevice,' *Lab Chip*, 2012, 12, (14), pp. 2514-2519.
- [7] Crews, N., Wittwer, C.T., and Gale, B.: 'Continuous-Flow Thermal Gradient PCR,' *Biomedical Microdevices*, 2008, 10, (2), pp. 187-195.
- [8] Schaerli, Y., Wootton, R.C., Robinson, T., Stein, V., Dunsby, C., Neil, M.A.A., French, P.M.W., deMello, A.J., Abell, C., and Hollfelder, F.: 'Continuous-Flow Polymerase Chain Reaction of Single-Copy DNA in Microfluidic Microdroplets,' *Analytical Chemistry*, 2008, 81, (1), pp. 302-306.
- [9] Obeid, P.J., Christopoulos, T.K., Crabtree, H.J., and Backhouse, C.J.: 'Microfabricated device for DNA and RNA amplification by continuous-flow polymerase chain reaction and reverse transcription-polymerase chain reaction with cycle number selection,' *Analytical Chemistry*, 2003, 75, (2), pp. 288-295.

- [10] Nakayama, T., Kurosawa, Y., Furui, S., Kerman, K., Kobayashi, M., Rao, S.R., Yonezawa, Y., Nakano, K., Hino, A., Yamamura, S., Takamura, Y., and Tamiya, E.: 'Circumventing air bubbles in microfluidic systems and quantitative continuous-flow PCR applications,' *Analytical and Bioanalytical Chemistry*, 2006, 386, (5), pp. 1327-1333.
- [11] Zhou, L., Myers, A.N., Vandersteen, J.G., Wang, L., and Wittwer, C.T.: 'Closed-Tube Genotyping with Unlabeled Oligonucleotide Probes and a Saturating DNA Dye,' *Clin Chem*, 2004, 50, (8), pp. 1328-1335.
- [12] Crews, N., Wittwer, C.T., Montgomery, J., Pryor, R., and Gale, B.: 'Spatial DNA Melting Analysis for Genotyping and Variant Scanning,' *Analytical Chemistry*, 2009, 81, (6), pp. 2053-2058.
- [13] Schneegass, I., Brautigam, R., and Kohler, J.M.: 'Miniaturized flow-through PCR with different template types in a silicon chip thermocycler,' *Lab on a Chip*, 2001, 1, (1), pp. 42-49.
- [14] Becker, H., and Gartner, C.: 'Polymer microfabrication technologies for microfluidic systems,' *Analytical and Bioanalytical Chemistry*, 2008, 390, (1), pp. 89-111.
- [15] Hashimoto, M., Chen, P.C., Mitchell, M.W., Nikitopoulos, D.E., Soper, S.A., and Murphy, M.C.: 'Rapid PCR in a continuous flow device,' *Lab on a Chip*, 2004, 4, (6), pp. 638-645.
- [16] Bartholomeusz, D.A., Boutte, R.W., and Andrade, J.D.: 'Xurography: Rapid prototyping of microstructures using a cutting plotter,' *Journal of Microelectromechanical Systems*, 2005, 14, (6), pp. 1364-1374.
- [17] Sun, Y., Nguyen, N.-T., and Kwok, Y.C.: 'High-Throughput Polymerase Chain Reaction in Parallel Circular Loops Using Magnetic Actuation,' *Analytical Chemistry*, 2008, 80, (15), pp. 6127-6130.
- [18] Greer, J., Sundberg, S.O., Wittwer, C.T., and Gale, B.K.: 'Comparison of glass etching to xurography prototyping of microfluidic channels for DNA melting analysis,' *Journal of Micromechanics and Microengineering*, 2007, 17, (12), pp. 2407-2413.
- [19] Sundberg, S., Wittwer, C., Greer, J., Pryor, R., Elenitoba-Johnson, O., and Gale, B.: 'Solution-phase DNA mutation scanning and SNP genotyping by nanoliter melting analysis,' *Biomedical Microdevices*, 2007, 9, pp. 159-166.

- [20] Erill, I., Campoy, S., Erill, N., Barbé, J., and Aguiló, J.: 'Biochemical analysis and optimization of inhibition and adsorption phenomena in glass-silicon PCR-chips,' *Sensors and Actuators B: Chemical*, 2003, 96, (3), pp. 685-692.
- [21] Wittwer, C.T., and Hermann, M.G.: 'Rapid Thermal Cycling and PCR Kinetics', in Innis, M.A., Gelfand, D.H., and Sninsky, J.J. (Eds.): 'PCR Applications: Protocols for Functional Genomics,' (Academic Press, 1999, 1 edn.), pp. 211-229.
- [22] Herrmann, M.G., Durtschi, J.D., Bromley, L.K., Wittwer, C.T., and Voelkerding, K.V.: 'Amplicon DNA melting analysis for mutation scanning and genotyping: Cross-platform comparison of instruments and dyes,' *Clinical Chemistry*, 2006, 52, (3), pp. 494-503.
- [23] Njoroge, S., Chen, H., Witek, M., and Soper, S.: 'Integrated Microfluidic Systems for DNA Analysis,' *Topics in current chemistry*, 2011.
- [24] Easley, C.J., Karlinsey, J.M., Bienvenue, J.M., Legendre, L.A., Roper, M.G., Feldman, S.H., Hughes, M.A., Hewlett, E.L., Merkel, T.J., and Ferrance, J.P.: 'A fully integrated microfluidic genetic analysis system with sample-in-answer-out capability,' *Proceedings of the National Academy of Sciences*, 2006, 103, (51), pp. 19972.
- [25] Liu, R.H., Yang, J., Lenigk, R., Bonanno, J., and Grodzinski, P.: 'Self-contained, fully integrated biochip for sample preparation, polymerase chain reaction amplification, and DNA microarray detection,' *Analytical Chemistry*, 2004, 76, (7), pp. 1824-1831.
- [26] Chen, L., Manz, A., and Day, P.J.R.: 'Total nucleic acid analysis integrated on microfluidic devices,' *Lab on a Chip*, 2007, 7, (11), pp. 1413-1423.
- [27] Wen, J., Legendre, L.A., Bienvenue, J.M., and Landers, J.P.: 'Purification of nucleic acids in microfluidic devices,' *Analytical Chemistry*, 2008, 80, (17), pp. 6472-6479.
- [28] Chomczynski, P., and Rymaszewski, M.: 'Alkaline polyethylene glycol-based method for direct PCR from bacteria, eukaryotic tissue samples, and whole blood,' *BioTechniques*, 2006, 40, (4), pp. 454-458.
- [29] Park, S.J., Kim, J.Y., Yang, Y.G., and Lee, S.H.: 'Direct STR Amplification from Whole Blood and Blood- or Saliva-Spotted FTA® without DNA Purification*,' *Journal of Forensic Sciences*, 2008, 53, (2), pp. 335-341.

- [30] Kermekchiev, M.B., Kirilova, L.I., Vail, E.E., and Barnes, W.M.: 'Mutants of Taq DNA polymerase resistant to PCR inhibitors allow DNA amplification from whole blood and crude soil samples,' *Nucl. Acids Res.*, 2009, pp. gkn1055.
- [31] Schlenk, J., Seidl, S., Braunschweiger, G., Betz, P., and Lederer, T.: 'Development of a 13-locus PCR multiplex system for paternity testing,' *International journal of legal medicine*, 2004, 118, (1), pp. 55-61.
- [32] Bahlo, M., Stankovich, J., Danoy, P., Hickey, P.F., Taylor, B.V., Browning, S.R., Australian, T., Consortium, N.Z.M.S.G., Brown, M.A., and Rubio, J.P.: 'Saliva-Derived DNA Performs Well in Large-Scale, High-Density Single-Nucleotide Polymorphism Microarray Studies,' *Cancer Epidemiology Biomarkers & Prevention*, 2010, 19, (3), pp. 794-798.
- [33] Farnaud, S., Kosti, O., Getting, S.J., and Renshaw, D.: 'Saliva: physiology and diagnostic potential in health and disease.' *TheScientificWorldJournal*, 2010, 10, pp. 434.
- [34] Kaufman, E., and Lamster, I.B.: 'The Diagnostic Applications of Saliva— A Review,' *Critical Reviews in Oral Biology & Medicine*, 2002, 13, (2), pp. 197-212.
- [35] French, D., Archard, C., Andersen, M., and McDowell, D.: 'Ultra-rapid DNA analysis using HyBeacon (TM) probes and direct PCR amplification from saliva,' *Molecular and Cellular probes*, 2002, 16, (5), pp. 319-326.
- [36] Jobling, M.A., Pandya, A., and Tyler-Smith, C.: 'The Y chromosome in forensic analysis and paternity testing,' *International journal of legal medicine*, 1997, 110, (3), pp. 118-124.
- [37] Nakahori, Y., Mitani, K., Yamada, M., and Nakagome, Y.: 'A human Y-chromosome specific repeated DNA family (DYZ1) consists of a tandem array of pentanucleotides,' *Nucleic acids research*, 1986, 14, (19), pp. 7569.
- [38] Pješčić, I., Tranter, C., Haywood, J.C., Paidipalli, M., Ganveer, A., Haywood, S.E., Tham, J., and Crews, N.: 'Real-time Damage Monitoring of Irradiated DNA,' *Integrative Biology*, 2011, 3, (9), pp. 937-947.
- [39] Pješčić, I., Tranter, C., Hindmarsh, P., and Crews, N.: 'Glass-composite prototyping for flow PCR with in situ DNA analysis,' *Biomedical Microdevices*, 2010, 12, (2), pp. 333-343.

- [40] Wittwer, C.T., Reed, G.B., and Ririe, K.M.: 'Rapid Cycle DNA Amplification', in Mullis, K.B., Ferre, F., and Gibbs, R. (Eds.): 'The Polymerase Chain Reaction,' (Springer-Verlag, 1994), pp. 174-181.
- [41] Cadet, J., Berger, M., Douki, T., Morin, B., Raoul, S., Ravanat, J.L., and Spinelli, S.: 'Effects of UV and visible radiation on DNA-final base damage,' *Biological chemistry*, 1997, 378, (11), pp. 1275-1286.
- [42] Neuzil, P., Pipper, J., and Hsieh, T.M.: 'Disposable real-time microPCR device: lab-on-a-chip at a low cost,' *Mol Biosyst*, 2006, 2, (6-7), pp. 292-298.
- [43] Man, P.F., Mastrangelo, C.H., Burns, M.A., and Burke, D.T.: 'Microfabricated capillarity-driven stop valve and sample injector,' in 'Microfabricated capillarity-driven stop valve and sample injector,' (1998, edn.), pp. 45-50.
- [44] Christensen, T.B., Pedersen, C.M., Grondahl, K.G., Jensen, T.G., Sekulovic, A., Bang, D.D., and Wolff, A.: 'PCR biocompatibility of lab-on-a-chip and MEMS materials,' *Journal of Micromechanics and Microengineering*, 2007, 17, (8), pp. 1527-1532.
- [45] Lu, C., Xie, Y., Yang, Y., Cheng, M.M.C., Koh, C.-G., Bai, Y., Lee, L.J., and Juang, Y.-J.: 'New valve and bonding designs for microfluidic biochips containing proteins,' *Analytical Chemistry*, 2007, 79, (3), pp. 994-1001.
- [46] Cubaud, T., Ulmanella, U., and Ho, C.-M.: 'Two-phase flow in microchannels with surface modifications,' *Fluid Dynamics Research*, 2006, 38, (11), pp. 772-786.
- [47] Lu, Y., Shi, W., Jiang, L., Qin, J., and Lin, B.: 'Rapid prototyping of paper-based microfluidics with wax for low-cost, portable bioassay,' *Electrophoresis*, 2009, 30, (9), pp. 1497-1500.
- [48] Martinez, A.W., Phillips, S.T., Whitesides, G.M., and Carrilho, E.: 'Diagnostics for the developing world: Microfluidic paper-based analytical devices,' *Analytical Chemistry*, 2010, 82, (1), pp. 3-10.
- [49] Bhattacharya, S., Datta, A., Berg, J.M., and Gangopadhyay, S.: 'Studies on surface wettability of poly(dimethyl) siloxane (PDMS) and glass under oxygen-plasma treatment and correlation with bond strength,' *Journal of Microelectromechanical Systems*, 2005, 14, (3), pp. 590-597.